

FUNDAMENTAL PARAMETERS AND SPECTRAL ENERGY DISTRIBUTIONS OF YOUNG AND FIELD AGE OBJECTS WITH MASSES SPANNING THE STELLAR TO PLANETARY REGIME

JOSEPH C. FILIPPAZZO^{1,2,3}, EMILY L. RICE^{1,2,3}, JACQUELINE FAHERTY^{2,5,6}, KELLE L. CRUZ^{2,3,4}, MOLLIE M. VAN GORDON⁷, DAGNY L. LOOPER⁸

¹Department of Engineering Science and Physics, College of Staten Island, City University of New York, 2800 Victory Blvd, Staten Island, NY 10314, USA

²Department of Astrophysics, American Museum of Natural History, New York, NY 10024, USA

³The Graduate Center, City University of New York, New York, NY 10016, USA

⁴Department of Physics and Astronomy, Hunter College, City University of New York, New York, NY 10065, USA

⁵Department of Terrestrial Magnetism, Carnegie Institution of Washington, DC 20015, USA

⁶Hubble Fellow

⁷Department of Geography, University of California, Berkeley, CA 94720, USA and

⁸Tisch School of the Arts, New York University, New York, NY 10003, USA

Draft version August 10, 2015

ABSTRACT

We combine optical, near-infrared and mid-infrared spectra and photometry to construct expanded spectral energy distributions (SEDs) for 145 field age (>500 Myr) and 53 young (lower age estimate <500 Myr) ultracool dwarfs (M6-T9). This range of spectral types includes very low mass stars, brown dwarfs, and planetary mass objects, providing fundamental parameters across both the hydrogen and deuterium burning minimum masses for the largest sample assembled to date. A subsample of 29 objects have well constrained ages as probable members of a nearby young moving group (NYMG). We use 182 parallaxes and 16 kinematic distances to determine precise bolometric luminosities (L_{bol}) and radius estimates from evolutionary models give semi-empirical effective temperatures (T_{eff}) for the full range of young and field age late-M, L and T dwarfs. We construct age-sensitive relationships of luminosity, temperature and absolute magnitude as functions of spectral type and absolute magnitude to disentangle the effects of degenerate physical parameters such as T_{eff} , surface gravity, and clouds on spectral morphology. We report bolometric corrections in J for both field age and young objects and find differences of up to a magnitude for late-L dwarfs. Our correction in K_s shows a larger dispersion but not necessarily a different relationship for young and field age sequences. We also characterize the NIR-MIR reddening of low gravity L dwarfs and identify a systematically cooler T_{eff} of up to 300K from field age objects of the same spectral type and 400K cooler from field age objects of the same M_H magnitude.

Subject headings: brown dwarfs, stars: low-mass, stars: fundamental parameters

1. INTRODUCTION

Brown dwarfs are unable to sustain nuclear fusion in their cores due to insufficient mass and are thus degenerate across effective temperature, mass, and age. While these objects all contract to about the size of Jupiter within 500 Myr (Baraffe et al. 1998), the extended photospheres of younger objects introduce the radius as yet another elusive observable. Entanglement of these fundamental parameters prohibits precise atmospheric characterization by spectral type and color alone. This necessitates determination of broader physical quantities such as distance, radius, and luminosity. Flux calibrated spectral energy distributions (SEDs) comprised of spectra as well as photometry enable precise empirical determination of L_{bol} which can then be used to estimate additional stellar parameters.

Effective temperatures lower than about 3000K cause the emergent spectra of brown dwarfs to deviate substantially from that of a blackbody due to absorption and scattering from molecules, dust and clouds. Determination of their physical properties is further complicated as these substellar objects age and cool, changing opacity sources and evolving through later spectral types. Though current ultracool dwarf model atmosphere codes (Allard 2013; Saumon & Marley 2008;

Burrows et al. 2011; Barman 2008) account for more complex chemistry and dynamics than ever before, incomplete physics and line lists frequently limit reliable data fits to those brown dwarfs which exhibit the simplest atmospheric conditions. Even for these objects, there are broad regions of the model spectra that have yet to reproduce observations and so must be excluded from the fitting routine (e.g. Cushing et al. 2008; Mann et al. 2015). Consequently, derivation of fundamental parameters with model atmospheres depend heavily on the included wavelength ranges, the resolution of the spectrum, the fitting technique, and the models used.

Rice et al. (2010a) fit model atmospheres to young (<10 Myr) and field age late-M dwarfs and concluded that a combination of medium- and high-resolution NIR spectra is needed to derive fundamental parameters, though this is rarely attempted due to limited available data especially for fainter sources. Patience et al. (2012) fit five model atmosphere grids to NIR spectra of a small sample of 1-50 Myr M8-L5 dwarfs and found T_{eff} discrepant by up to 300K based on the models used. Despite such documented inconsistencies, this remains the most common way to extract atmospheric properties such as effective temperature, surface gravity, sedimentation efficiency, and metallicity (Cushing et al. 2008;

Stephens et al. 2009; Witte et al. 2011; Bonnefoy et al. 2014; Dieterich et al. 2014; Manjavacas et al. 2014). Recent L_{bol} determinations of large samples of M, L and T dwarfs (Stephens et al. 2009; Dupuy & Kraus 2013; Dieterich et al. 2014; Schmidt et al. 2014) have used MIR spectroscopy or photometry but have similarly employed various model atmospheres and fitting routines to estimate flux in areas without spectral coverage. Most other L_{bol} estimates in the literature use bolometric corrections derived from these samples. These techniques are self-consistent in the parameters they predict but suffer from both known and unidentified systematics introduced by imperfect model atmosphere codes. Until the model grids reproduce the variety of our observations and fitting routines become more robust, a strictly empirical sanity check is needed.

Direct integration of flux calibrated SEDs provides L_{bol} as a function of more ubiquitous measurements such as magnitude, color, spectral index, and spectral type. Accurate characterization of these distance-scaled relationships can be powerful tools for inferring the atmospheric properties of additional ultracool dwarfs. Since distance is the dominant source of uncertainty in these calculations, the accumulation of trigonometric parallaxes for a diverse sample of late-M, L and T dwarfs (e.g. Dahn et al. 2002; Tinney et al. 2003; Vrba et al. 2004; Faherty et al. 2009; Dupuy & Liu 2012; Marocco et al. 2013; Dieterich et al. 2014; Tinney et al. 2014) is crucial to providing precise L_{bol} measurements across the entire stellar/brown dwarf/planetary mass sequence. Radius and mass can then be inferred from evolutionary models and T_{eff} can be calculated from the Stefan-Boltzmann Law. This is preferable to deriving L_{bol} from T_{eff} values obtained by model atmosphere fits since the results are not tied to the fidelity of a fitting routine, the complexities of modeled atmospheric conditions, or the quality of the data.

Construction of ultracool dwarf SEDs from nearly complete observational coverage is therefore ideal and timely due to the mid-infrared (MIR) photometry of the Wide-Field Infrared Survey Explorer (WISE; Wright et al. 2010) and the *Spitzer Space Telescope* Infrared Array Camera (IRAC; Fazio et al. 2004), as well as the groundswell of publicly available optical and infrared spectra of recent years (e.g. Cruz et al. 2003, 2009; Burgasser 2014). Calculation of L_{bol} from direct integration of distance-scaled SEDs without the use of model atmosphere grids has been done in the past by Tinney et al. (1993), Leggett et al. (2001), Dahn et al. (2002), Golimowski et al. (2004), and Cushing et al. (2005b) however these samples only had spectral and photometric coverage up to $4.1\mu\text{m}$.

We use $0.3 - 14.5\mu\text{m}$ spectra and photometry, and parallaxes and kinematic distances to create the largest collection of nearly complete flux calibrated ultracool dwarf SEDs assembled to date. In Sections 2 and 3 we describe our sample and observational data used in the analysis. In Section 4 we detail our SED construction procedure. In Section 5 we describe our calculation of L_{bol} for the sample and in Sections 6, 7, and 8 we determine radii, masses, and T_{eff} respectively. In Section 9 we calculate bolometric corrections, construct luminosity-magnitude diagrams, and derive new spectral type- T_{eff} relations in order to investigate the effects of age on the bulk physical

properties of ultracool dwarfs. Conclusions are presented in Section 10.

2. THE SAMPLE

Our goal was to assemble nearly complete SEDs to investigate global trends in the fundamental parameters of substellar objects, which presumably form like stars from the collapse of a shocked cloud of cold gas and dust. To accomplish this we constructed a sample of diskless objects no longer associated with a molecular cloud with masses just above the hydrogen burning minimum mass of about $79M_{\text{Jup}}$ all the way down to just below the deuterium burning minimum mass of about $12M_{\text{Jup}}$ (Burrows et al. 1997; Chabrier et al. 2000). All objects were required to be within 80pc to avoid interstellar extinction effects (Aumer & Binney 2009).

Young objects are distinguished by their very red $J - K_S$ color due to dust and clouds in or above the photosphere (Kirkpatrick et al. 2006;Looper et al. 2008b), though not all very red objects have youth indicators (Faherty et al. 2013). Therefore young dwarfs were identified based on probable membership in a NYMG (Faherty et al. in prep; Reidel et al. in prep; Gagné et al. 2015a). Additional young L0-L5 dwarfs were identified as those with a β or γ spectral type suffix (Kirkpatrick 2005; Kirkpatrick et al. 2006; Cruz et al. 2009; Rice et al. 2010b, Cruz et al. in prep) indicating low surface gravity features in the optical such as weak alkali doublets and weak metal hydride absorption. Late-M and late-L dwarf spectral types have been updated with β/γ suffixes to reflect intermediate and very low surface gravity identified in the NIR (Allers & Liu 2013). In total, the sample contains 29 NYMG members and 24 low gravity dwarfs that were not placed in a NYMG.

We grouped all objects into three subsamples: 1) the core sample of 28 objects with a parallax measurement, optical through MIR photometry, and optical through MIR spectra, 2) the extended sample of 154 objects with the base requirements of a parallax, NIR spectrum, NIR photometry, and MIR photometry, and 3) the kinematic sample of 16 young objects with the same photometric and spectral requirements as the extended sample but with distances constrained by kinematics based on NYMG membership (Faherty et al., in prep). Optical photometry, optical spectra and/or MIR spectra were included for objects in the extended and kinematic samples where available.

Our resulting sample is comprised of 198 ultracool dwarfs with spectral types of M6-T9 listed in Table 3 where we use optical spectral types for M and L dwarfs and IR spectral types for T dwarfs. We excluded Y dwarfs from the analysis due to the still emerging atmospheric complexities and poorly defined benchmarks for objects with $T_{\text{eff}} < 500K$. Fundamental properties of these latest type dwarfs will be addressed in Filippazzo et al., in preparation.

3. THE DATA

3.1. Distances

Trigonometric parallaxes from the Brown Dwarf Kinematics Project (Faherty et al. 2012), the Hawai'i Infrared Parallax Program (Dupuy & Liu 2012), and the literature (Dahn et al. 2002; Monet et al. 2003; Tinney et al. 2003; Dahn et al. 2002; Vrba et al.

Table 1
Discrepant Parallaxes

Name	π	Ref	Alt π	Ref
2M0501-0010	51 ± 3.7	1	76.4 ± 4.8	2
2M0355+1133	109.6 ± 1.3	3	133.7 ± 11.9	4
LP 944-20	155.89 ± 1.03	5	201.4 ± 4.2	6

References. — (1) Zapatero Osorio et al. (2014); (2) Faherty et al. (2012); (3) Liu et al. (2013); (4) Faherty et al. (2013); (5) Dieterich et al. (2014); (6) Tinney (1996).

2004; Ducourant et al. 2008; Shkolnik et al. 2009; Kirkpatrick et al. 2011; Liu et al. 2013; Marocco et al. 2013; Weinberger et al. 2012; Zapatero Osorio et al. 2014) with uncertainties better than 25% were used to calculate distances to the core and extended samples. For objects with multiple parallaxes, the value with the highest precision was used. The distance uncertainties calculated from these 182 parallaxes ranged from 0.3-25% with a mean of about 4%. Parallaxes for the sample discrepant by more than 1σ are shown in Table 1.

Kinematic distances for 15 M and L dwarfs were calculated using the coordinates, proper motion, and radial velocity of the object given probable membership in a NYMG (Riedel et al., in prep; Faherty et al., in prep). A kinematic distance for GU Psc b was obtained from Naud et al. (2014). Uncertainties in these 16 kinematic distances were about 13%.

3.2. Photometry

The primary sources of optical, NIR and MIR photometry were the Sloan Digital Sky Survey (SDSS; York et al. 2000), the Two Micron All Sky Survey (2MASS; Skrutskie et al. 2006), and WISE respectively. Additional magnitudes came from the Deep Near-Infrared Survey of the Southern Sky (DENIS; Epchtein et al. 1997) and the literature using the Mauna Kea Observatory Near-Infrared (MKO-NIR; Simons & Tokunaga 2002; Tokunaga et al. 2002), *Spitzer Space Telescope* IRAC and Johnson-Cousins V(RI)_C filter sets.

A total of 2360 magnitudes were available for 198 sources. Tables 4, 5, and 6 show the optical, NIR, and MIR apparent magnitudes for the sample and the effective wavelength for each filter. We made no uncertainty cut on the data and uncertainties ranged from 0.06-13% with a mean of about 0.9%.

3.3. Published and Publicly Available Spectra

We used 120, 193, and 53 previously published optical, NIR and MIR spectra, respectively, to construct SEDs for our sample. Table 2 shows a summary of the telescopes and instruments of origin along with the wavelength range, resolving power, and number of spectra used in our analysis for each. NIR spectra for about 77% of the sample are low resolution SpeX Prism (Rayner et al. 2003) data from the NASA Infrared Telescope Facility (IRTF), about half of which were obtained from the SpeX Prism Library¹.

¹ <http://www.brownndwarfs.org/spepxism> maintained by Adam Burgasser

The Low Resolution Imaging Spectrometer (LRIS; Oke et al. 1995) instrument on Keck I was the source for 36% of all optical spectra used. All MIR spectra were obtained with the InfraRed Spectrograph (IRS; Houck et al. 2004) onboard the *Spitzer Space Telescope* using the Short wavelength Low resolution (SL) module, 11 of which had Long wavelength Low resolution (LL) orders stitched in as well. Of the previously published IRS spectra, 26 are from the IRS Dim Suns project (Roellig et al. 2004; Cushing et al. 2006; Mainzer et al. 2007) and 26 are from the IRS Enhanced Products Catalog of the Spitzer Heritage Archive ² (PIIDs 2, 29, 51 and 30540 with PI J. Houck; PID 3136 with PI K. Cruz; PID 20409 with PI M. Cushing; PID 50367 with PIs M. Cushing and M. Liu; and PID 50059 with PI A. Burgasser).

More than half of the objects had multiple optical and NIR spectra so we selected one from each regime with the broadest wavelength coverage and highest signal to noise (S/N). These spectra were trimmed of exceptionally noisy edges by truncating the ends up to the first wavelength position with $S/N \geq 20$. To generate an uncertainty array for the 15 optical spectra where one was not available, we used $S/N=5$ for all wavelengths. Even this very conservative estimate had no effect on the resulting fundamental parameters since the uncertainty in the distance dominates after the spectra are flux calibrated.

3.4. New NIR and MIR Spectra

We present new low-resolution SpeX Prism data for 2MASSI J1017075+130839, 2MASS J23224684-3133231, and 2MASS J05012406-0010452 taken on UT 2011 December 08, 2006 August 28, and 2007 October 12, respectively. We took 180s exposures at two nod positions along the slit, which was oriented to the parallactic angle to minimize slit loss and spectral slope variations. The raw images were corrected for non-linearity, pair subtracted, and flat fielded. We obtained spectra of A0 dwarf stars for telluric correction and flux calibration. A set of exposures of internal flat field and argon arc lamps were also taken for flat fielding and wavelength calibration. Data were then reduced with the SpeXtool package (Cushing et al. 2004) using standard settings.

We also present new medium-resolution NIR spectra taken with the TripleSpec (Wilson et al. 2004) instrument on the 200-inch Hale Telescope at Palomar Observatory. LSPM J1658+7027 and 2MASSW J1155395-372735 were observed on 2010 June 03 and 2009 January 28, respectively. We used an ABBA nod sequence with exposures times of about 300s and observed nearby A0 dwarf stars to perform telluric correction and flux calibration. Dome flats were taken to calibrate the pixel-to-pixel response and data were reduced using a version of SpeXtool modified for TripleSpec.

And finally, we present a new MIR spectrum for 2MASS J21392676+0220226 obtained on 2005 May 25 (PID 3136, PI K. Cruz) with the IRS instrument using the SL module in standard staring mode. Target observations consisted of eight 60 second exposures. The raw data was then put through the Basic Calibrated Data (BCD) processing pipeline, which flags and masks hot

² <http://sha.ipac.caltech.edu/>

Table 2
Instrument Summary of Spectra Used to Construct SEDs

Instrument	Telescope	$\lambda(\mu\text{m})$	R	Number	Refs
Optical					
LRIS	Keck I	0.32–1.0	300–5000	43	1
R–C Spec	KPNO 4m	0.6–1.0	300–5000	29	...
R–C Spec	CTIO 4m	0.55–1.0	300–3000	22	...
GoldCam	KPNO 2.1m	0.55–0.93	300–4500	8	...
R–C Spec	CTIO 1.5m	0.6–0.86	300–3000	4	...
FORS	ESO VLT U2	0.33–1.1	260–2600	3	2
MagE	Magellan II Clay	0.32–1.0	~4100	3	3
FOCAS	Subaru	0.37–1.0	250–2000	2	4
LDSS3	Magellan II Clay	0.6–1.0	~1000	1	5
DIS	ARC 3.5m	0.38–1.0	~600	1	...
NIR					
SpeX – Prism	IRTF	0.8–2.5	~150	153	6
SpeX – SXD	IRTF	0.8–2.4	~2000	25	6
SpeX – LXD1.9	IRTF	1.95–4.2	~2500	10	6
GMOS–S	Gemini South	0.36–0.94	670–4400	7	7
FIRE – Echelle	Magellan I Baade	0.82–2.51	~6000	7	8
SpeX – LXD2.3	IRTF	2.25–5.5	~2500	2	6
GMOS–N	Gemini North	0.36–0.94	670–4400	2	7
GNIRS – SXD	Gemini North	0.9–2.5	~1700	2	9
Triplespec	Palomar 200-inch	0.95–2.46	2500–2700	2	10
CGS4	UKIRT	4.5–5.0	~400	2	11
OSIRIS	CTIO 1.5m	0.9–2.4	1400–3500	1	12
SINFONI	ESO VLT U4	1.1–2.45	1500–4000	1	13,14
NIRC	Keck I	0.9–2.5	~100	1	15
IRCS	Gemini North	1.2–2.4	~100	1	16
NIRI	Subaru	1.0–2.5	~500	1	17
STIS	HST	3.0–4.15	~500	1	18
MIR					
IRS – SL	Spitzer	5.1–14.5	60–128	51	19
IRS – LL	Spitzer	14.5–37	60–128	11	19

References. — (1) Oke et al. (1995); (2) Appenzeller et al. (1998); (3) Marshall et al. (2008); (4) Kashikawa et al. (2000); (5) Allington-Smith et al. (1994); (6) Rayner et al. (2003); (7) Allington-Smith et al. (2002); (8) Simcoe et al. (2008); (9) Elias et al. (2006); (10) Wilson et al. (2004); (11) Mountain et al. (1990); (12) Depoy et al. (1993); (13) Eisenhauer et al. (2003); (14) Bonnet et al. (2004); (15) Matthews & Soifer (1994); (16) Kobayashi et al. (2000); (17) Hodapp et al. (2003); (18) Woodgate et al. (1998); (19) Houck et al. (2004).

pixels, performs a droop correction, subtracts a dark sky reference frame, and does a flat-field correction to account for detector irregularities and spectral order discrepancies. The spectrum was extracted from the background subtracted images with SSC’s SPICE program. SPICE extracts a 1D spectrum from the input image using the determined position of the trace and the wavelength-dependent Point Spread-Function (PSF) (SPICE Spitzer IRS Custom Extraction v. 1.4). Because the standard extraction window width resulted in false features and other artifacts in the spectrum, we used a custom extraction window width of 4 pixels at $7\mu\text{m}$ which worked well with our data. After extraction with SPICE, custom IDL scripts were used to co-add the exposures and merge the separate orders.

4. CONSTRUCTION OF SEDS

4.1. Creation of Composite Optical and NIR Spectra

Overlapping optical and NIR spectra were available for 120 of the 198 sample objects. We combined these into a single composite spectrum using the shared red optical wavelength range to maximize the broadband filter coverage for flux calibration. We smoothed the higher resolution spectrum to the lower resolution wavelength

array in the area of overlap and normalized the two components. Since the spectra have different methods of telluric correction or were not telluric corrected at all, the $0.93–0.97\mu\text{m}$ range was excluded from the normalization process to avoid the telluric feature in that region. The composite spectrum was defined as the mean flux value at each resampled point weighted by the inverse of the uncertainty. A new uncertainty array was created for the composite spectrum by summing component uncertainties in quadrature. Cushing et al. (2005b) find that no significant errors are introduced due to the difference in relative flux densities when creating composite spectra as described.

Given the luxury of multiple optical and NIR resolutions for many sources, we tested whether the integrated flux calculated from the optical+NIR composite spectrum was sensitive to our choice of input spectra. For 52 sources we constructed composites with every permutation of available optical and NIR spectra for a total of 304 tests. We integrated under the curve along the longest common wavelength baseline to get the total flux in the area of overlap of each source’s set of SEDs. The total flux for any source in the optical and NIR is effectively resolution independent in the range $75 < R < 5000$, varying

at most by 0.4%. Table 7 shows the final list of spectra used to construct each SED in the sample.

4.2. Flux Calibration of Spectra

As described in Section 3, spectra used in our SEDs were taken on different days with different instruments under different seeing conditions so there is little uniformity of the data. To account for this heterogeneity we flux calibrate all spectra to available SDSS, V(RI)_C, 2MASS, DENIS, IRAC, and WISE photometry. We shifted the apparent magnitudes to absolute magnitudes using parallaxes or kinematic distances and converted to photon flux densities in units $\text{ergs}^{-1}\text{cm}^{-2}\text{\AA}^{-1}$ using

$$f_\lambda = f_{ZP} \cdot 10^{-\frac{M}{2.5}} \quad (1)$$

where M is the absolute magnitude and f_{ZP} is the flux of a Kurucz model of Vega³ at the filter effective wavelength listed in Tables 4, 5, and 6. The SDSS magnitude system (Fukugita et al. 1996) is not quite in the AB magnitude system (Oke & Gunn 1983) so we converted first to AB using the corrections of Holberg & Bergeron (2006) and then to the Vega system using the corrections of Blanton & Roweis (2007). Uncertainties introduced from these corrections were negligible.

To calibrate the spectra to the absolute photometry, we calculated synthetic magnitudes for every band with complete spectrum coverage using

$$m = -2.5 \log \left(\frac{\int f_\lambda S(\lambda) \lambda d\lambda}{\int f_{Vega} S(\lambda) \lambda d\lambda} \right) \quad (2)$$

Here f_λ and f_{Vega} are the photon flux densities of the spectrum and Vega respectively and $S(\lambda)$ is the filter response function.

IRS spectra were converted from F_ν in Jy to F_λ in $\text{ergs}^{-1}\text{cm}^{-2}\text{\AA}^{-1}$ via the relationship $F_\nu\nu = F_\lambda\lambda$. Most IRS spectra in our sample cover the wavelength range $5.25 - 14.5\mu\text{m}$ so we used *Spitzer* IRAC channel 4 centered at $8\mu\text{m}$ (hereafter [8]) and/or WISE W3 centered at $12\mu\text{m}$ to maximize the number of points available for flux calibration. If a source had a magnitude in W3 but the IRS spectrum ended at $14.5\mu\text{m}$, we appended a Rayleigh-Jeans tail from the longest wavelength value out to the end of the W3 filter at $17.26\mu\text{m}$. The uncertainty on the tail was set as a 300K uncertainty in the blackbody curve. Though the flux in the range $14.5 - 17.26\mu\text{m}$ constitutes 28% of the synthetic magnitude in W3, the relative lack of features at $\lambda > 14.5\mu\text{m}$ (Cushing et al. 2006) and our conservative estimate of uncertainty makes this a good approximation. The 11 IRS spectra for our sample with coverage out to $37\mu\text{m}$ (spectral types M6.5, M8, M8.5, M9, L0.5, L1, L3, L3.5, L5, and T7) confirm this estimate. Figure 1 shows the [8] and W3 filter response curves along with a typical IRS SL/LL spectrum and a Rayleigh-Jeans tail appended at $14.5\mu\text{m}$ to cover the entire W3 band for comparison. The W3 synthetic magnitude was then calculated using equation 2.

For each non-contiguous piece of the spectrum, we calculated a normalization constant C by minimizing the ratio of the catalog and synthetic photometry as

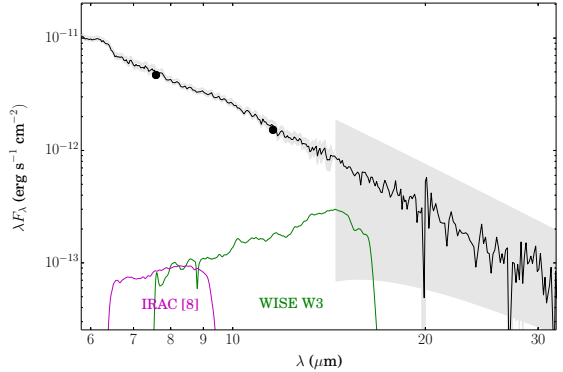


Figure 1. The $5.2 - 37\mu\text{m}$ IRS spectrum of Gliese 752 B (black line) shows that appending a Rayleigh-Jeans tail with a 300K uncertainty in the blackbody temperature (grey shaded region) accounts for all variation in the spectrum long ward of $14.5\mu\text{m}$. While all IRS spectra cover the IRAC [8] passband (magenta curve), we use this approximation to calculate synthetic W3 magnitudes for IRS spectra that do not cover the entire W3 passband (green curve).

$$C = \frac{\sum_i f_i f_{i, \text{syn}} / (\sigma_i^2 + \sigma_{i, \text{syn}}^2)}{\sum_i f_i^2 / (\sigma_i^2 + \sigma_{i, \text{syn}}^2)}, \quad (3)$$

where f_i and $f_{i, \text{syn}}$ are the catalog and synthetic fluxes respectively for the i-th photometric band, and σ_i and $\sigma_{i, \text{syn}}$ are their respective uncertainties. Each spectrum segment was then multiplied by its respective constant C to anchor it to the maximum wavelength baseline of absolute catalog photometry rather than just a single photometric band.

4.3. Filling in the Gaps

To calculate L_{bol} from a complete SED, we filled in the gaps between the non-contiguous flux calibrated spectra and survey photometry, linearly interpolated to zero from the short wavelength limit of our data, and appended a Rayleigh-Jeans tail to the long wavelength limit of our data. The flux in regions with photometry but no spectra were estimated by linearly interpolating between magnitudes. The $1.4, 1.9$ and $2.8\mu\text{m}$ telluric H_2O absorption features were also linearly interpolated across at the flux levels on either side of the gap if necessary.

SDSS ugriz photometry was available for 73 objects, which allowed us to linearly interpolate down to $0.35\mu\text{m}$ before linearly interpolating to zero flux at zero wavelength on the Wein tail of the SED. $V(RI)_C$ photometry for 37 objects was also included. For all other objects, we estimated ugriz photometry based on absolute SDSS-2MASS magnitude-magnitude relations derived from the sample. We fit 3rd-order polynomials to M_z versus M_J , M_H , and M_{Ks} and used the relationship with the smallest dispersion to infer an M_z magnitude. The rms of the polynomial fit was used as the uncertainty on the estimated absolute magnitude. This process was repeated for the other four SDSS bands. M_u , M_g , M_r , M_i , and M_z were estimated for each object based on their value of M_{Ks} , M_J , M_H , M_H , and M_J respectively.

IRAC [3.6], [4.5], [5.8], and [8] photometry was available for 72 objects that also had WISE W1, W2, and

³ <http://kurucz.harvard.edu/stars.html>

W3 photometry, which we used to derive IRAC-WISE magnitude-magnitude relations to better estimate the flux in the MIR. Using the relationship with the smallest rms we estimated $M_{[3.6]}$, $M_{[4.5]}$, $M_{[5.8]}$, and $M_{[8]}$ for each object based on their value of M_{W1} , M_{W2} , M_{W1} , and M_{W1} respectively. For the 7 objects with no W1 photometry, we estimated M_{W1} using $M_{[3.6]}$, $M_{L'}$, or M_{Ks} based upon availability of those magnitudes in that order. M_{W2} was similarly estimated for those seven objects using $M_{[4.5]}$, $M_{L'}$, or M_{Ks} . We estimated M_{W3} for 24 objects in the same way using $M_{[8]}$ or M_{W2} . $M_{L'}$ was estimated using $M_{[3.6]}$ or M_{W1} . Since it is well documented that the colors of ultracool dwarfs are sensitive to age (Kirkpatrick et al. 2006, 2008; Cruz et al. 2009; Faherty et al. 2009; Schmidt et al. 2010; Allers et al. 2010; Bihain et al. 2010; Faherty et al. 2012), we derived one polynomial for the field age objects (M_{FLD}) and a separate one for objects with signatures of low surface gravity, probable membership in a NYMG, or youth indicators of a stellar companion (M_{YNG}). The exceptions were u-, g-, and L'-band, which had either too few magnitudes or too large a scatter about the field sequence to justify distinct FLD and YNG polynomials. All magnitude-magnitude relations mentioned above are presented in Table 10.

Longward of the longest wavelength MIR data point, we appended a Rayleigh-Jeans tail out to $1000\mu m$. If the SED had an IRS spectrum, the tail was flux calibrated to the wavelength range $11 < \lambda < 14.5\mu m$. This was done to avoid the CH_4 ($9.2 < \lambda < 14.5\mu m$) and NH_3 ($10.25 < \lambda < 11\mu m$) absorption features in late-L and T dwarfs (Marley et al. 1996; Burrows et al. 2001; Roellig et al. 2004) and the $9 < \lambda < 11\mu m$ plateau caused by small silicate grains in the upper cloud decks of some L dwarfs (Cushing et al. 2006). If no IRS spectrum was available, the Rayleigh-Jeans tail was flux calibrated to the W3 magnitude, which largely avoids these features as well. The uncertainty on the Rayleigh-Jeans tail was conservatively set as a 300K uncertainty in the black-body temperature, accounting for all variation past W3 band in the 11 SEDs with spectral coverage out to $37\mu m$.

A complete SED is shown in Figure 2 where optical, NIR and MIR spectra are shown in blue, green and magenta respectively. Photometric points are displayed as black markers, the curve integrated under to calculate L_{bol} is the black dashed line, and the grey region is the 1σ uncertainty of the SED.

5. BOLOMETRIC LUMINOSITIES

We calculated L_{bol} for all the sources in our sample by integrating under the absolute flux calibrated SED from $0 - 1000\mu m$. We used

$$L_{bol} = 4\pi d^2 \int_{0\mu m}^{1000\mu m} F_\lambda d\lambda, \quad (4)$$

where F_λ is the absolutely flux calibrated SED and d is the distance in parsecs to the source. All values of L_{bol} in this work are listed in units of $\log(L_{bol}/L_\odot)$ where we use $L_\odot = 3.846 \times 10^{33} \text{ erg s}^{-1}$ (Cox 2000).

We present the first bolometric luminosities for 65 field age and 21 low gravity objects. Table 8 shows the remaining 112 objects with each previously published

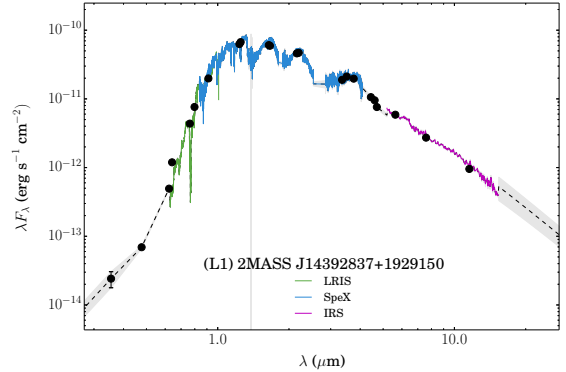


Figure 2. Core sample flux calibrated SED of 2MASS J14392837+1929150 showing the optical (green), NIR (blue) and MIR (magenta) spectra used. Black points are photometry, the dashed black line shows how gaps were filled in regions with no spectra, and the grey shaded region is the uncertainty.

value of L_{bol} , the parallax used in that work, and the L_{bol} value we obtained using our method with the same parallax. Panels a-f in Figure 3 show our values compared with those of Golimowski et al. (2004), Vrba et al. (2004), Cushing et al. (2005b), Dieterich et al. (2014), Zapatero Osorio et al. (2014), and other smaller samples respectively.

Our values of L_{bol} agree with those of Cushing et al. (2005b) (Figure 3c) to within 1σ , which is to be expected since our method of calculation is very similar to the one presented there. However, Cushing et al. append a Rayleigh-Jeans tail longward of L' band at $4.1\mu m$ since the sample predates the MIR capabilities of WISE and Spitzer. While our values of L_{bol} agree very well, our analysis of the precision attainable without MIR data suggests that their uncertainties are slightly underestimated (See Section 9.4). Similarly, Golimowski et al. (2004) assumed a Rayleigh-Jeans tail longward of L' or M'-band for their M and L dwarfs which produces good agreement with our early- to mid-L dwarf luminosities. They use the $0.6 - 4.1\mu m$ SED of the T6.5 dwarf Gl 229B to estimate a correction for their late-T dwarfs and use half that correction for their early-T dwarfs. While this correction results in similar L_{bol} values as our nearly complete late-T SEDs, halving the correction for the early-T dwarfs overestimates the flux longward of $2.5\mu m$ causing all the bright T dwarfs in Figure 3a to fall within the uncertainties but below our distribution.

Vrba et al. (2004) use the K-band bolometric correction derived by Golimowski et al. (2004) to estimate L_{bol} for their sample, causing a larger dispersion and a similar overbrightness in the T dwarfs shown in Figure 3b. We find the slightly blue 2MASS J09373487+2931409 (T6) about 30% brighter and three other T-dwarfs about 20% dimmer. While this bolometric correction in Ks may prove useful for M and L dwarfs, these objects demonstrate the danger of a catch-all correction of late type ultracool dwarfs given their large dispersion in color for objects of the same spectral type.

Dieterich et al. (2014) fit synthetic magnitudes of BT-Settl 2010 model atmospheres to $VRI + JHK + W1W2W3$ photometry to derive L_{bol} for their sample of mid-M to mid-L dwarfs. The good agreement with our empirical results show this method to be fairly robust in

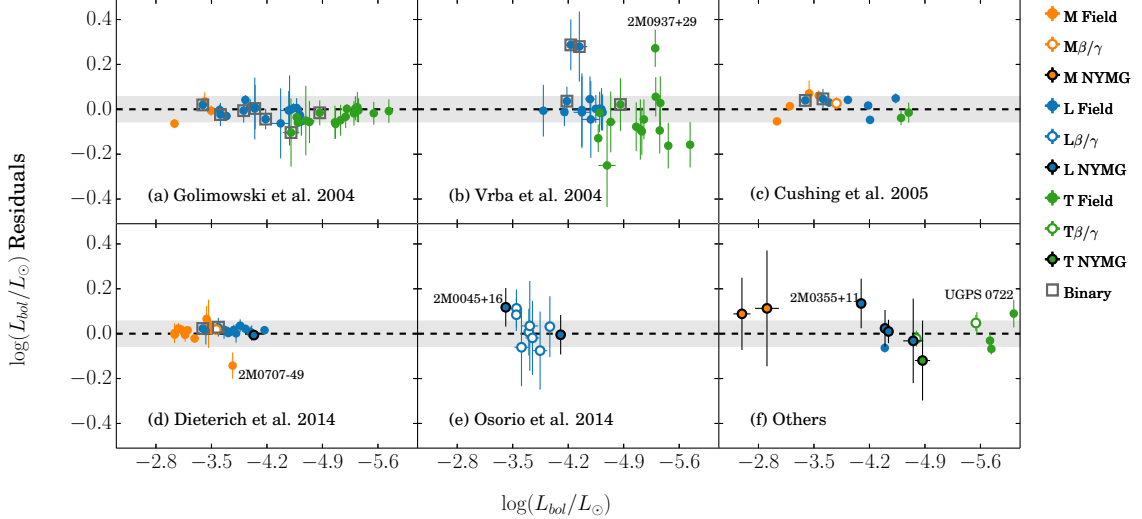


Figure 3. Residuals of L_{bol} calculated in this work compared to the values presented in (a) Glikowski et al. (2004), (b) Vrba et al. (2004), (c) Cushing et al. (2005b), (d) Dieterich et al. (2014), (e) Zapatero Osorio et al. (2014), and (f) smaller samples from the literature. M, L and T dwarfs are shown as orange, blue, and green points, respectively. Field age objects are filled points with no outline, members of a NYMG are filled points with a black border, and objects with signatures of youth or low surface gravity β/γ designations that could not be placed in a NYMG are unfilled points. Binaries are indicated by a grey square.

this range, though the exclusion of late-L and T dwarfs in the Dieterich sample limit its utility to early type brown dwarfs. Though in agreement with the results of this work, most objects systematically lie just above (slightly dimmer than) our findings. Dieterich et al. (2014) acknowledge that their results are about 100K cooler than the effective temperatures derived by Glikowski et al. (2004) using direct integration and evolutionary models, so perhaps this temperature disagreement is due to their method underestimating the total flux. The source of the 12% discrepancy for the outlier 2MASS J07075327-4900503 (M9) is unclear but likely the result of a poor atmospheric model fit to the data in that work.

Zapatero Osorio et al. (2014) have a sample of 10 suspected young L dwarfs for which they determine L_{bol} . They use $BC_{Ks} = 3.40$ of Todorov et al. (2010), derived from three young M9.5-L0 dwarfs, for their four L0-L2 dwarfs. For the six L3-L5 dwarfs in their sample, they use $BC_{Ks} = 3.22$ and $BC_J = 1.16$ determined for G196-3B (L3 β) in Osorio et al. (2010). The disagreement of the three brighter objects in Figure 3e is due to their application of a larger BC_{Ks} for young objects than for field age objects, while we find that low surface gravity results in a larger dispersion and not necessarily an offset from the field age correction (See Section 9.3 for discussion on BCs for young ultracool dwarfs).

Figure 3f shows L_{bol} for a variety of objects in the literature using different methods of calculation. Leggett et al. (2012) use $0.6 - 4.2 \mu\text{m}$ spectral coverage and a bolometric correction derived from model atmospheres for UGPS J072227.51-054031.2, which we find about 10% brighter. For the remarkably red AB Dor member 2MASS J03552337+1133437, Liu et al. (2013) use direct integration of a flux calibrated NIR spectrum coupled with a model atmosphere fit to place this object about 12% dimmer than our result. Just as with the Vrba et al. (2004) and Zapatero Osorio et al. (2014) samples, the use of bolometric corrections for many of

these smaller samples generally greatly increases the uncertainty and scatter of the predicted L_{bol} values.

Distance is by far the largest source of uncertainty in these measurements making large, high-precision parallax programs an imperative for revealing the bulk properties of ultracool dwarfs. Additionally, the large scatter in color due to secondary characteristics such as metallicity, dust, and clouds make values of L_{bol} unreliable when derived using spectrophotometric distances or bolometric corrections insensitive to this diversity. We find that direct integration of patchy flux calibrated SEDs produce the smallest uncertainties in L_{bol} of as little as 2% (See Section 9.4).

6. RADII

Though long-baseline interferometry has been used to measure radii for stars as late as M4 (Boyajian et al. 2012), ultracool dwarfs are as yet too small and dim for this technique. Lacking a significant number of substellar radii measurements, atmospheric and evolutionary models are commonly used instead. One method is to fit a grid of model atmospheres to spectra or photometry and then scale the emitted flux of the best fitting model to the absolute flux calibrated spectrum. A radius can then be estimated from the observed flux if the distance to the object is known via the $(R/d)^2$ scale factor. However, incomplete line lists and poorly reproduced regions such as the H-band peak and $\lambda < 0.9 \mu\text{m}$ result in sometimes highly discrepant best fit parameters (e.g. T_{eff} and surface gravity) and consequently unreliable or unphysical radii estimates (e.g. Bowler et al. 2010; Barman et al. 2011; Dupuy & Kraus 2013; Liu et al. 2013). We derive parameters for our sample using this technique in Filippazzo et al. (in preparation), for comparison with the semi-empirical results of this paper.

The method we employ in this work is to use L_{bol} and the object age to determine the radius from evolutionary models. We assume an age of 0.5-10 Gyr for all field objects in the sample that have no signatures

of youth. Since electron degeneracy pressure limits the size of all field age ultracool dwarfs to about that of Jupiter, the dispersion in radius even over this colossal timespan is predicted to be about $0.1R_{Jup}$. Objects younger than this are likely still undergoing gravitational contraction and are not yet completely electron degenerate, as evidenced by low surface gravity spectral features compared to field age objects. While objects optically typed β/γ exhibit signatures of low surface gravity including weaker absorption and pressure broadening of alkali lines (Cruz et al. 2003), ages cannot yet be accurately inferred solely from a gravity suffix (Cruz et al. 2009; Allers & Liu 2013; Zapatero Osorio et al. 2014, ; Faherty et al. in prep).

Ages of nearby stellar associations have been constrained using a variety of techniques such as dynamical age, Li abundance, $H\alpha$ emission, X-ray emission, and color-magnitude diagrams. Therefore, we have identified 29 objects in our sample that are likely members of NYMGs and adopted the age of the parent association as the age of the object. We use the age ranges and references therein presented by Malo et al. (2012) in their Table 1 of 8-20 Myr for TW Hydrae (TWA), 12-22 Myr for β Pictoris (β Pic), 30-50 Myr for Argus, 50-130 Myr for AB Doradus (AB Dor), and 10-40 Myr for Tucana-Horlogium (Tuc-Hor), Columba, and Carina.

Ages for GL 337CD, Gl 417BC, HN Peg B, HD 3651B, Ross 458C, Luhman 16AB, 2MASS J22344161+404138, and G 196-3B were obtained from the literature using X-ray luminosity, kinematics, chromospheric activity, Li abundance, and/or gyrochronology of a stellar companion (Kirkpatrick et al. 2001b; Burgasser et al. 2005; Luhman et al. 2007; Goldman et al. 2010; Faherty et al. 2014; Shkolnik et al. 2009). For the 17 β/γ objects in our sample that do not have age estimates and could not be placed in NYMGs but are too low-g to be field age, we used an age range of 8-130 Myr to reflect the minimum and maximum ages of the considered NYMGs.

We used the inferred age and calculated L_{bol} for each object to find the range of predicted radii from the solar metallicity, hybrid cloud (SMHC08) evolutionary model isochrones of Saumon & Marley (2008) (Figure 4). We used these model tracks since they do not treat grain sedimentation efficiency (f_{sed}) as a free parameter exhibiting cloudy late-M through L/T transition dwarfs and cloud-free mid- to late-T dwarfs, in agreement with observations.

Differences in gas and condensate chemistry, molecular opacities, cloud modeling, and atmospheric boundary conditions (Saumon & Marley 2008) make radii assumptions heavily tied to the models being used. Thus for M6-T3 dwarfs, we also computed the radii predicted by the evolutionary models of Chabrier et al. (2000) (DUSTY00) and the $f_{sed} = 2$ (SMf208) models of Saumon & Marley (2008). The final radius range for each source was set as the minimum and maximum values of all model predictions for the given L_{bol} and age. The same approach was used for L6-T8 dwarfs using the models of Baraffe et al. (2003) (COND03) and the cloudless (SMNC08) models of Saumon & Marley (2008). None of the models mentioned above extend to sufficiently high luminosity for us to extract radii for our brightest objects. In order to include the most luminous late-M dwarfs of our sample, we used the Dartmouth Magnetic

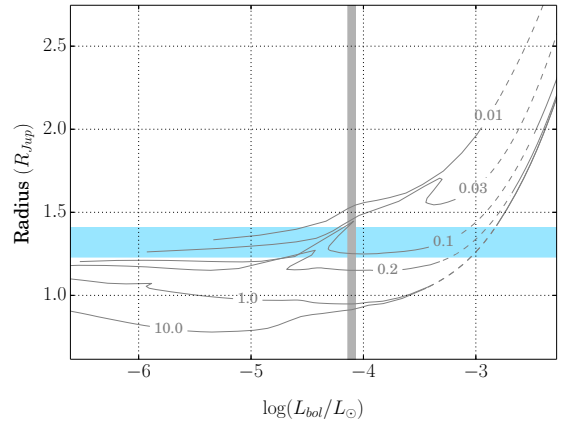


Figure 4. Example of how the radius of 2MASS 0355+1133 was chosen by interpolation between evolutionary model isochrones based on the age of its parent association AB Doradus. The solid grey lines to the left and right of the dashed grey lines show solar metallicity SMHC08 and DMEstar isochrones in Gyrs, respectively. The dashed grey lines show our interpolation used to make the isochrones continuous. The grey vertical bar shows the $1\sigma L_{bol}$ value and the horizontal blue bar shows the resulting radius range.

Evolutionary Stellar Tracks and Relations (DMEstar; Feiden & Chaboyer 2012, 2013) and performed a cubic interpolation across the gaps of each isochrone to make them continuous.

The few directly measured substellar radii have relied upon transit duration and orbital velocity measurements of double-lined eclipsing systems. Unfortunately, none of these objects meet the spectral and photometric requirements to be included in our sample, though we discuss them here for comparison with the predicted values of this work. Excluding M dwarfs and young objects since they are potentially not electron degenerate, we find a range of $0.78 - 1.14R_{Jup}$ for 95 L0-T9 dwarfs with assumed ages of $0.5 - 10Gyr$ and solar metallicity. The directly measured radii of the $0.4 - 12.7Gyr$ brown dwarfs OGLE-TR-122b (Pont et al. 2005), CoRoT-3 b (Deleuil et al. 2008), CoRoT-15b (Bouchy et al. 2010), WASP-30 b (Anderson et al. 2010), LHS 6343 C (Johnson et al. 2011), KELT-1 b (Siverd et al. 2012), KOI-205 b (Díaz et al. 2013), KOI-415 b (Moutou et al. 2013), and SDSS J141126.20+200911.1 (Littlefair et al. 2014) produce a range of $0.66 - 1.19R_{Jup}$. Though in very good agreement, even these few directly measured radii exhibit a range almost 70% larger than that predicted by model isochrones. This is most likely a result of some unaccounted for physical processes in the evolutionary models and/or non-solar metallicity of the objects resulting in a greater size diversity.

7. MASSES

The mass of an ultracool dwarf determines all its other fundamental parameters as a function of time yet it remains an unobservable for single objects. While dynamical masses of visual binaries point to possibly problematic cooling rates of substellar isochrones (Dupuy et al. 2009b,a, 2010; Konopacky et al. 2010), we are only equipped to infer model-derived masses given the data on hand.

We employ the same technique that was used to estimate radii from evolutionary model isochrones in Section

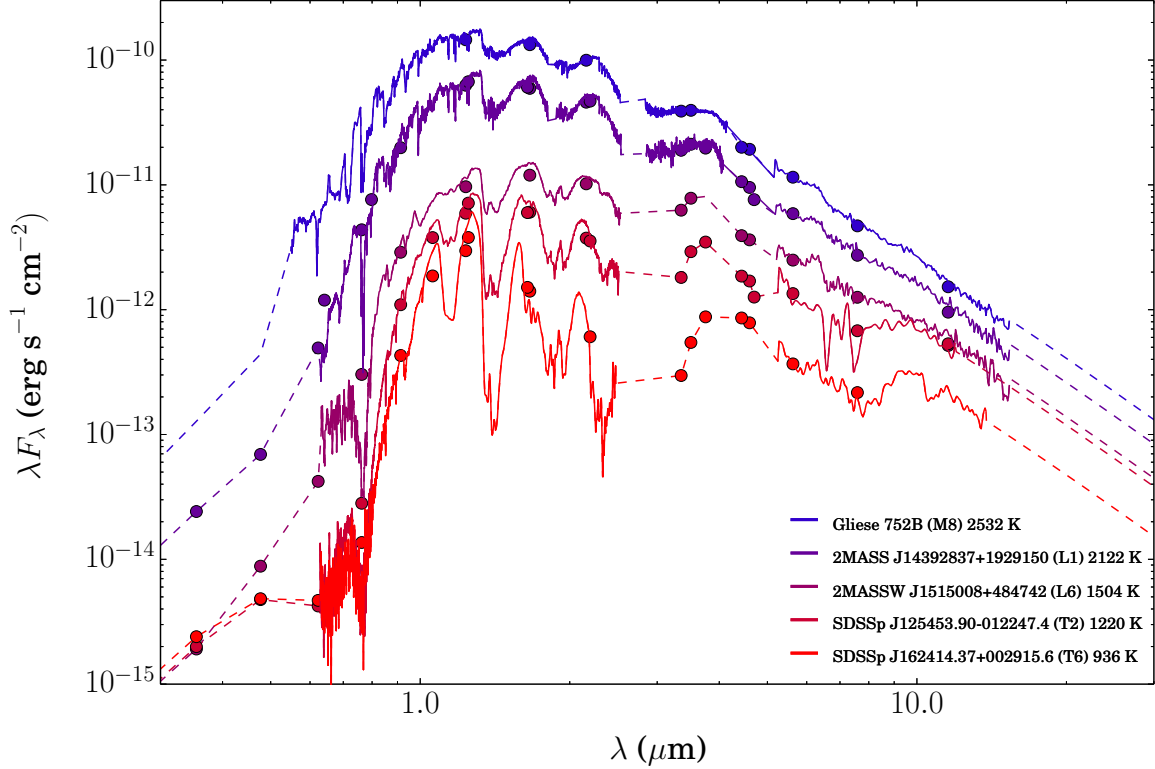


Figure 5. Flux calibrated SEDs of field age dwarfs Gliese 752B (M8), 2MASS J14392837+1929150 (L1), 2MASSW J1515008+484742 (L6), SDSSp J125453.90-012247.4 (T2), and SDSSp J162414.37+002915.6 (T6). Solid lines are observed spectra, points are photometry, and dashed lines show how gaps in the data were filled. Uncertainties were removed for clarity.

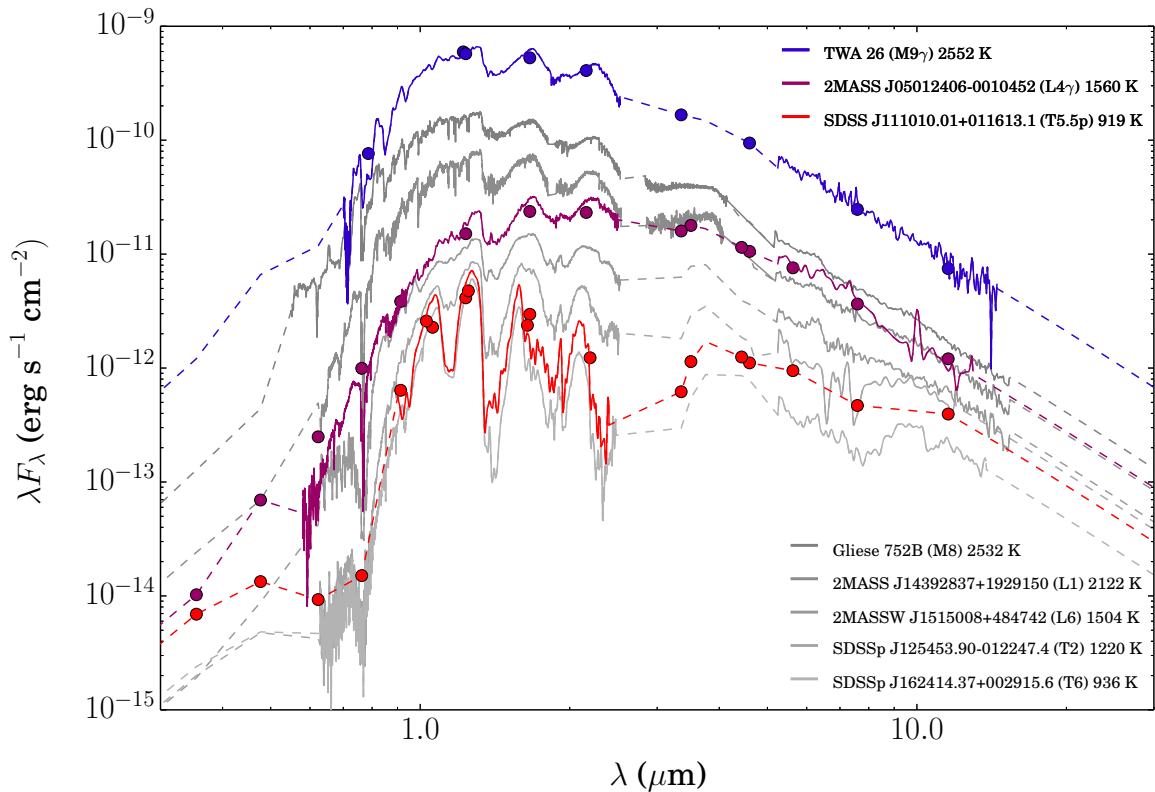


Figure 6. Flux calibrated SEDs of TWA 26 (M9 γ), 2MASS J05012406-001045 (L4 γ), and SDSS J111010.01+011613.1 (T5.5p AB Dor member) plotted with the field age sequence shown in Figure 5. Symbols are the same as in Figure 5.

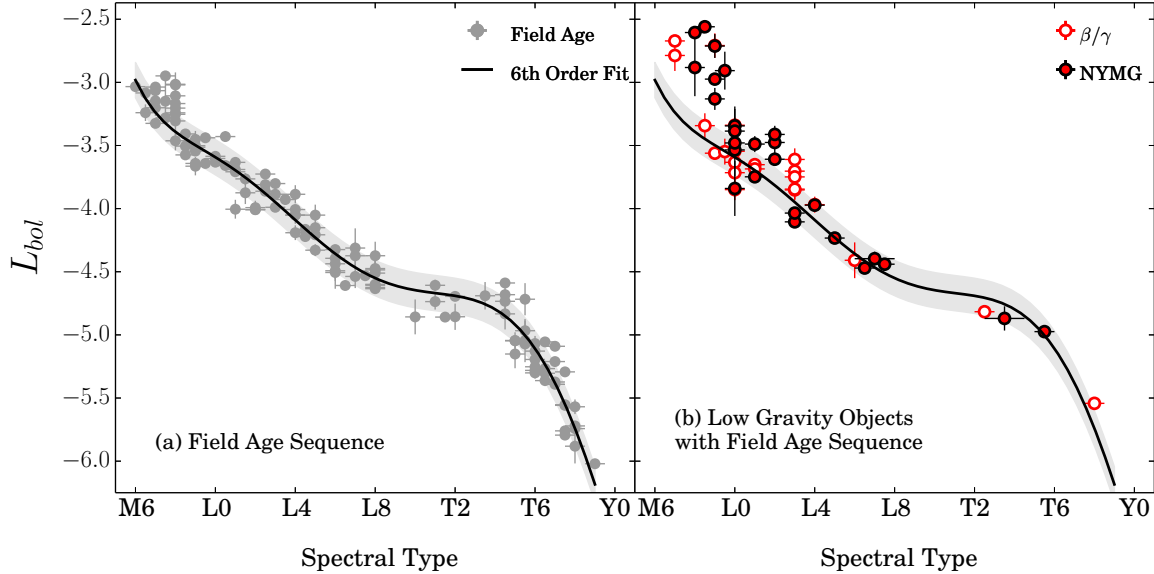


Figure 7. L_{bol} as a function of spectral type for (a) 124 field age objects (grey points) and (b) 48 objects with probable membership in a NYMG (red points with a black border) or signatures of low surface gravity (unfilled points with a red border). A 6th order weighted polynomial fit (solid black line) to the field objects only is shown in both plots.

6 to estimate masses for the sample as well. Just as with the radius, we use our calculated L_{bol} and the maximum and minimum predicted masses of the SMHC08, SMf208, and DUSTY00 tracks for M6-T3 dwarfs and the SMHC08, SMNC08, and COND03 tracks for L6-T8 dwarfs to infer a mass range. We find that the results are highly dependent on the model isochrones and produce uncertainties in mass as low as 3% and as high as 75%. Masses for the sample, which span both the hydrogen burning and deuterium burning limits, are given in Table 9.

8. EFFECTIVE TEMPERATURES

We calculated T_{eff} for each object using our inferred radius R , integrated L_{bol} , and the Stefan-Boltzmann Law

$$T_{\text{eff}} = \left(\frac{L_{\text{bol}}}{4\pi R^2 \sigma_{SB}} \right)^{\frac{1}{4}}, \quad (5)$$

where σ_{SB} is the Stefan-Boltzmann constant. We present fundamental parameters including L_{bol} , radius, mass, surface gravity, and T_{eff} for the entire sample in Table 9.

Uncertainties in T_{eff} are due primarily to the uncertainty in the object distance and radius estimates from evolutionary models. As Dupuy & Kraus (2013) point out, subtle differences in radii do not have a large effect on the calculated temperature since $T_{\text{eff}} \propto R^{-1/2}$. To a lesser degree, our assumptions about the shape and uncertainty of the Wien tail in the optical, linear interpolation between photometry, and flux calibration and uncertainty estimates of the Rayleigh-Jeans tail in the MIR also contributed. Typical uncertainty in T_{eff} for our sample is about 6%.

9. DISCUSSION

9.1. Flux Calibrated SED Sequences

To demonstrate the broad changes in the SED with spectral type, we plot a sequence of flux calibrated field age object SEDs shown in Figure 5. For comparison, Figure 6 shows the same sequence with three young flux calibrated SEDs over plotted. The M9 γ TWA 26 is redder in OPT-NIR color and 80% brighter than the equal temperature M8 Gleise 752B. The L4 γ 2MASS J05012406-0010452 has as much flux in the optical as the equal temperature L6 2MASSW J1515008+484742. However, the young object is as bright in the MIR as the L1 2MASS J14392837+1929150, which is almost 600K hotter. The T5.5p AB Dor member SDSS J111010.01+011613.1 has a very similar SED at all wavelengths and is only 20% brighter than the field age T6 SDSSp J162414.37+002915.6. If this trend holds, young T dwarfs would be almost indistinguishable from field age objects of the same spectral type given the dispersion in L_{bol} of about 15% (Section 9.2).

9.2. L_{bol} -Magnitude-Spectral Type Relations

Figure 7a shows L_{bol} vs. spectral type for 124 field age objects with our weighted 6th-order polynomial fit (Table 10) and rms of 0.14 dex displayed as a solid black line and grey shaded region respectively. Luminosity decreases almost linearly from M6-L7 with a typical scatter in a given spectral type of about 30%. L_{bol} is almost constant through the L/T transition as condensates rain out of the photosphere, quickly evolving through spectral type as deeper and brighter layers are exposed (Marley et al. 2010). The luminosity then drops steeply through the late-T dwarfs.

Figure 7b shows L_{bol} vs. spectral type for 26 probable members of a NYMG and 22 objects with signatures of low surface gravity. The 6th-order polynomial fit to the field age objects is displayed again for comparison, which shows almost all young late-M and L dwarfs lie on or slightly above this sequence due to their still contracting radii. The almost order of magnitude dispersion in our

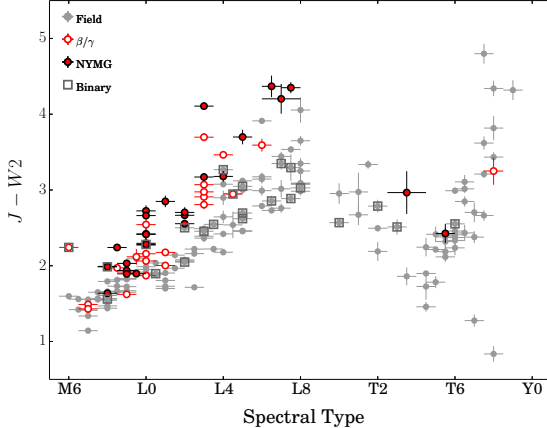


Figure 8. J-W2 color as a function of spectral type for 135 field, 22 low gravity, and 26 NYMG members. NYMG members and low gravity L dwarfs are up to a full magnitude redder than field age objects of the same spectral type. Symbols are the same as in Figure 7.

empirically determined luminosities of young objects at the M/L transition demonstrates the predicted sharp decline in radius for young objects with L_{bol} greater than ~ -3.5 shown in Figure 4. In the most extreme case, the brightest young M9 in the sample (TWA 26) is over three times brighter than the dimmest (LP 944-20). The brightest young L0 (2MASS J01415823-4633574) is 60% brighter than the dimmest (2MASS J02411151-0326587). The three young T dwarfs HN Peg B, GU Psc B, and SDSS J111010.01+011613.1 lie on or below the field age sequence while most young L dwarfs lie on or above it. A larger sample of bona fide young T dwarfs is needed to explore this relationship at later types.

Figure 8 shows how young L dwarfs have J-W2 colors a full magnitude redder than their field age counterparts possibly due to scattering of light in their dusty extended photospheres (Cruz et al. 2009; Gizis et al. 2012; Faherty et al. 2012, 2013). This is in agreement with Zapatero Osorio et al. (2014) who report comparable M_J magnitudes for 10 young L dwarfs with the field age sequence of Dupuy & Liu (2012). Faherty et al. (2012) find 7 young M dwarfs >0.5 mag brighter and 10 young L dwarfs 0.2-1.0 mag dimmer in J-band, though the reddening discussed in that work is in NIR color. With MIR data for our subsample of 42 young objects, we can confirm if this effect is due to an under or over brightness in one of the bands or a true shifting of flux out to longer wavelengths. We find that young objects are 0.5-1.5 mags brighter in M_{W2} than field age objects of the same spectral type (Figure 9a), while their M_J magnitudes range from 2 mags brighter for late-M and 1 mag dimmer for late-L dwarfs, crossing the field age sequence at L0 (Figure 9b).

When compared in terms of L_{bol} , however, low gravity L dwarfs distinguish themselves from normal L dwarfs as systematically dimmer in M_J (Figure 10a,b) and brighter in M_{W2} (Figure 10e,f), corresponding to a redder NIR-MIR color while maintaining about the same bolometric luminosity (Zapatero Osorio et al. 2014).

Figure 11 shows the field age L4 dwarf 2MASS J05002100+0330501 and the redder L4 γ 2MASS J05012406-0010452, which have nearly equal L_{bol} . The

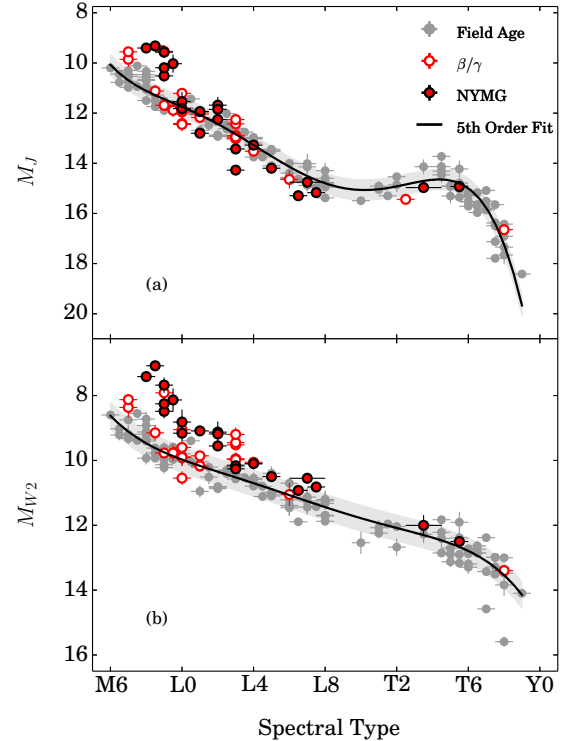


Figure 9. (a) M_J as a function of spectral type shows 12 young late-M dwarfs are up to 2 magnitudes brighter than the 5th order weighted polynomial fit (black line) of 115 field age objects. The 30 young L and T dwarfs have very similar or slightly dimmer M_J magnitudes compared to the field age sequence. (b) M_{W2} as a function of spectral type shows 42 young M, L and T dwarfs to be about 1.5, 0.5 and 0.25 magnitudes brighter than the 4th order weighted polynomial fit of 117 field age objects. The rms of the polynomial fit is shown as the grey shaded region in both plots. Symbols are the same as in Figure 7.

L4 γ however is 0.53 mags brighter in M_{W2} and 0.51 mags dimmer in M_J . The SEDs of these objects suggest the flux pivots around H or Ks band, shifting from $\lambda > 2.5 \mu\text{m}$ to $\lambda < 1.2 \mu\text{m}$ as an L dwarf ages (Faherty et al. 2013). This color mismatch for objects of the same luminosity implies that a bolometric correction (BC) in J or W_2 is different for young and field age objects as suggested by Todorov et al. (2010), Osorio et al. (2010), Luhman (2012), Faherty et al. (2013), Liu et al. (2013) and Zapatero Osorio et al. (2014).

9.3. Bolometric Corrections

Imprecise bolometric corrections are the primary cause of the large scatter of objects in Figures 3b, e, and f, which can propagate into highly inaccurate fundamental parameters for ultracool dwarfs. With strictly empirical L_{bol} values for such a large sample and the routine use of these corrections in the literature, we revisited BC_J and BC_{Ks} for both young and field age objects using $M_{\text{bol}\odot} = +4.74$.

M_{Ks} has an almost linear dependence on L_{bol} for late-M and L dwarfs of all ages in the sample (Figure 10c,d). This makes M_{Ks} an ideal band from which L_{bol} can be determined for late-M and L dwarfs with no age information. We derived $BC_{Ks\text{ FLD}}$ by fitting a 5th order polynomial to 122 field age objects. Figure 12a shows our relation in Ks is in excellent agreement with that of

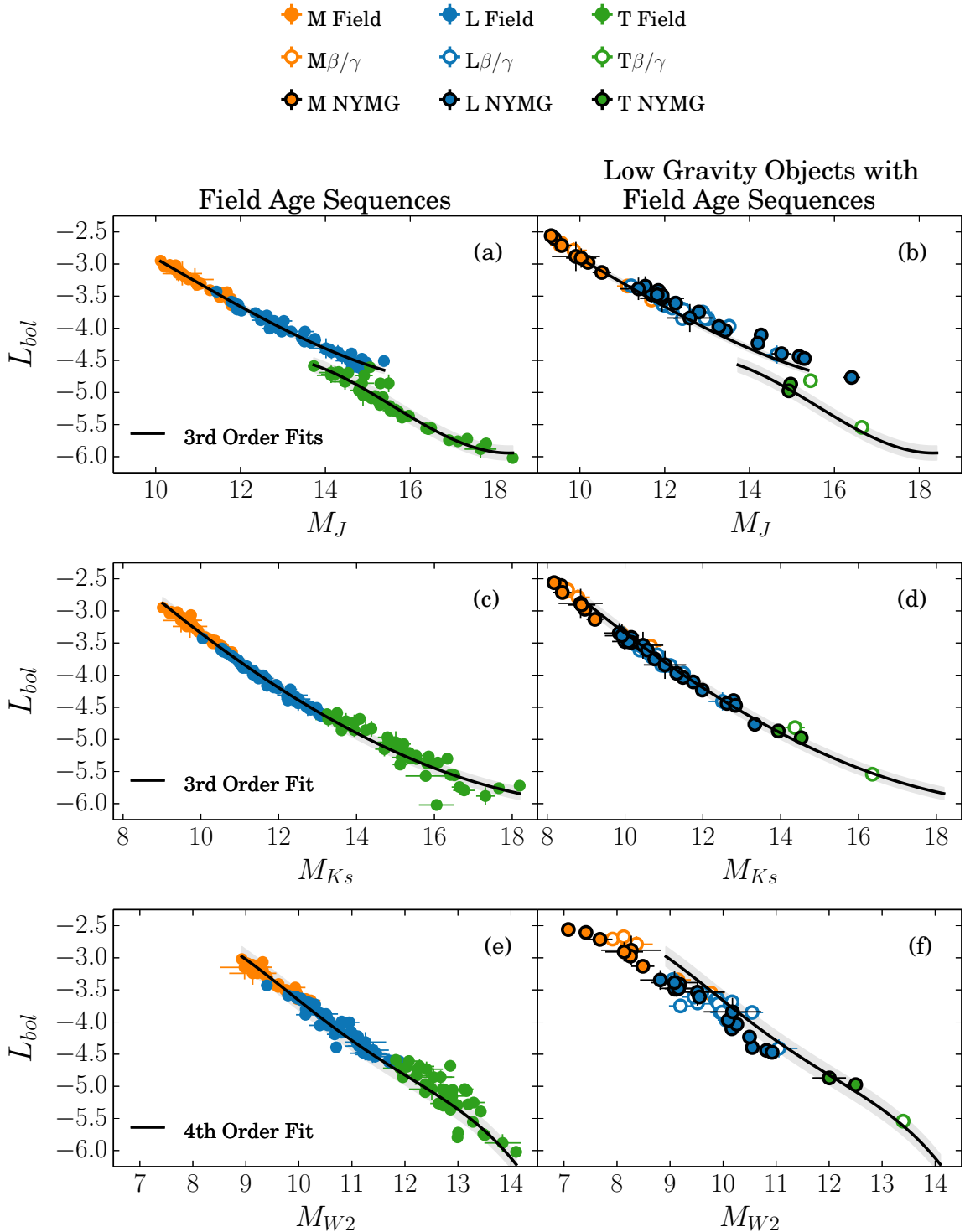


Figure 10. L_{bol} as a function of M_J (top row), M_{Ks} (center row), and M_{W2} (bottom row). Figures a, c, and e show field age objects with 3rd, 3rd, and 4th order polynomial fits, respectively. Figures b, d, and f show those same field sequences with young objects over plotted. Symbols are the same as in Figure 3.

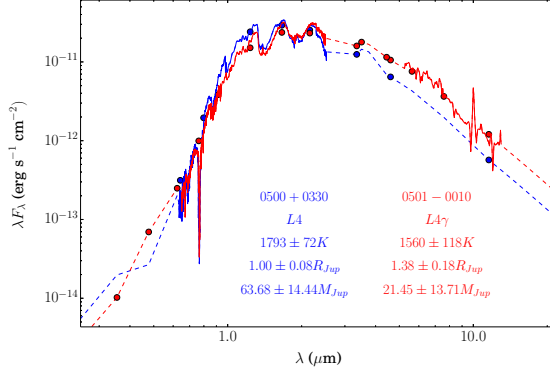


Figure 11. Flux calibrated SEDs of 2MASS J05002100+0330501 (L4; blue) and 2MASS J05012406-0010452 (L4 γ ; red) demonstrate objects with equal luminosities but substantially different colors, radii, temperatures, and masses.

Looper et al. (2008b) (Golimowski et al. 2004, relation excluding binaries; magenta line) for L0-L8 dwarfs but the dispersion of up to 1 mag in mid- to late-T dwarfs causes a mismatch of the polynomials at later types. This may be due to ours being a more complete sample containing twice as many T dwarfs as Looper et al. (2008b) and/or their oversimplification of MIR flux for T dwarfs based solely on the L' and M' spectra of GL 229B.

Todorov et al. (2010) find that BC_{K_s} for three young M9.5/L0 dwarfs is about 0.2 mags larger than that of field age L0 objects and claim that a different BC_{K_s} is needed for young and old objects. While our results agree to within 1σ for the two common sample objects 2MASS J01415823-4633574 and 2MASS J02411151-0326587, we derive BC_{K_s} YNG and find corrections for 8 other young L0 dwarfs only 0.05 mags larger on average than field age objects and well within the uncertainties of the field sequence.

We also derive BC_J FLD and BC_J YNG for the sample as a function of spectral type in Figure 12b and Table 10. The low gravity sequence is remarkably different than the field age sequence, differing by as much as a full magnitude for late-L dwarfs of the same spectral type. The tighter correlation of spectral type with BC_J rather than BC_{K_s} for mid- to late-T dwarfs suggests that the former is actually a more reliable correction to use when estimating late-type luminosities for field age objects. More confirmed young T dwarfs are needed to confirm BC_J YNG at later types.

9.4. Dependence of L_{bol} on Spectral Coverage

Given the sample's varying degrees of spectral coverage, linear interpolation was used between photometric points where no spectra were available. To justify our estimations, we investigated the sensitivity of the apparent bolometric magnitude (m_{bol}) to the amount and quality of data available in order to create a prescription for determining reliable L_{bol} values when certain data are missing.

To perform this test in the optical, we selected the 41 objects with $0.6 < \lambda < 1\mu m$ spectral coverage and ugriz photometry and determined the change in total flux under three different optical data scenarios. Figure 13a shows the difference between m_{bol} measured with optical spectra and m_{bol} measured with linear interpola-

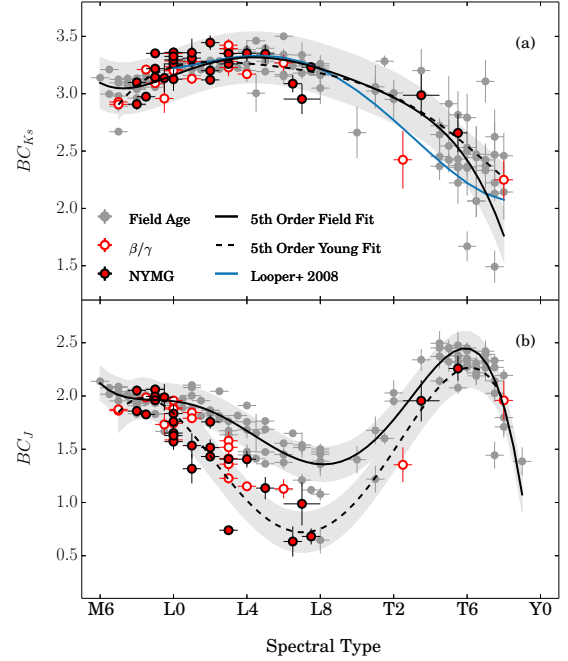


Figure 12. Bolometric corrections for the sample are shown in K_s (a) and J (b) bands for low gravity (dashed line) and field age (solid line) objects as a function of spectral type. The Looper et al. (2008b) relation is shown as the blue line. Symbols are the same as in Figure 7.

tion through SDSS photometry as a function of spectral type. Even though the flux is overestimated when the deep KI doublet and VO bands in the $0.73 < \lambda < 0.8\mu m$ region are washed out, the curve drawn by linear interpolation through SDSS photometry lies below the optical pseudo continuum. This causes a measured m_{bol} about 0.1 mags lower for late-M and L dwarfs. This technique reproduces the total optical flux for T dwarfs very well with an uncertainty of only 0.05 mags.

In the absence of optical spectra and measured ugriz photometry, Figure 13b shows that 2MASS JHKs absolute magnitudes can be used to very accurately reproduce SDSS photometry using the magnitude-magnitude relations presented in Table 10. The almost identical Figures 13a and 13b show that linear interpolation through estimated optical photometry performs just as well as flux calibrated ugriz magnitudes.

Figure 13c shows the difference in m_{bol} between an SED with an optical spectrum and one where linear interpolation was used from $1\mu m$ all the way down to zero flux at zero wavelength. This method overestimates the flux shortward of $1\mu m$ by up to 0.2 mags for late-M and L dwarfs. For late-T dwarfs, however, this can increase m_{bol} by as much as 0.35 mags.

We made the same comparisons with the 27 SEDs having $5.2 < \lambda < 14.5\mu m$ spectral coverage and [3.6], [4.5], [5.8], [8], W1, W2, and W3 photometry in the MIR. Figure 14a shows how linear interpolation through IRAC+WISE photometry in lieu of an IRS spectrum produces m_{bol} values in very good agreement with the true SED for all ultracool dwarfs to within 0.03 mags. While space based MIR spectroscopy missions such as the *James Webb Space Telescope* are still vital to furthering our understanding of the atmospheres of brown

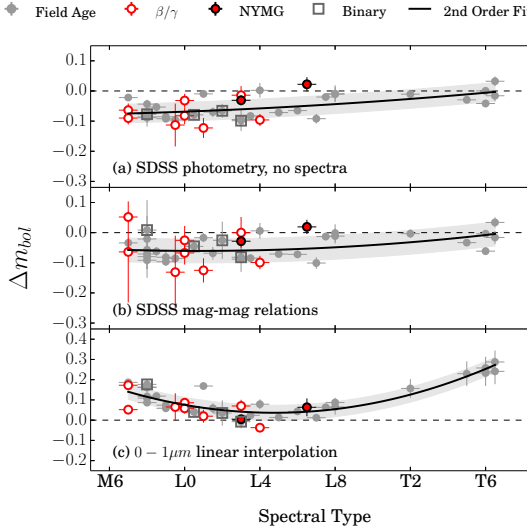


Figure 13. Dependence of m_{bol} on different data coverage scenarios in the optical for 44 field age objects: (a) linear interpolation through SDSS photometry, (b) linear interpolation through photometry estimated from magnitude-magnitude relations, and (c) linear interpolation from $1\mu\text{m}$ down to zero flux at zero wavelength. Symbols are the same as in Figure 7.

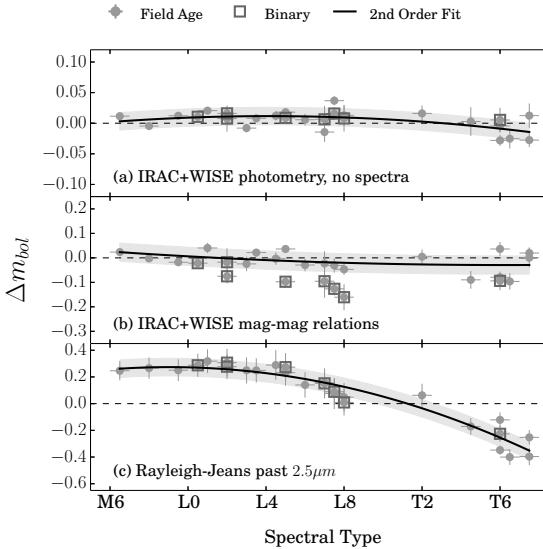


Figure 14. Dependence of m_{bol} on different data coverage scenarios in the MIR for 30 field age objects: (a) linear interpolation through IRAC+WISE photometry, (b) linear interpolation through IRAC+WISE photometry estimated from magnitude-magnitude relations, and (c) appending a Rayleigh-Jeans tail longward of $2.5\mu\text{m}$. Symbols are the same as in Figure 7.

dwarfs, broadband MIR photometry appears to be adequate to reconstruct the shape of ultracool dwarf SEDs at long wavelengths.

Figure 14b shows how the magnitude-magnitude relations listed in Table 10 perform instead of measured IRAC+WISE photometry. A larger scatter of about 0.1 mags is introduced in m_{bol} as a function of spectral type though the 2nd order polynomial fit is in very good agreement with the values produced by the SEDs with MIR spectra and photometry. There are 5 L dwarf binaries that lie up to 0.2 mags below the sequence because bina-

ries were not included in the derivation of the magnitude-magnitude relations presented in Table 10. We also exclude them from the polynomial fits in Figures 13 and 14.

The results of using a Rayleigh-Jeans tail at $\lambda > 2.5\mu\text{m}$ in the event of no available MIR data is shown in Figure 14c. The sequence crosses zero at the L/T transition but this is merely due to a coincidence of equal flux rather than the SED actually resembling a blackbody in the MIR at these spectral types. Due to the relative brightness of the K-band for late-M and L dwarfs, this approximation can overestimate the MIR flux by as much as 0.4 mags. Similarly, the relative faintness of the K-band in late-T dwarfs can underestimate m_{bol} by as much as 0.4 mags.

9.5. Spectral Type as a Proxy for T_{eff}

We use our 172 semi-empirical T_{eff} values to revisit the temperature/spectral type relation for ultracool dwarfs. We demonstrate how most young late-M and L dwarfs lie along a cooler track than their field age counterparts of the same spectral type. This necessitates the inclusion of age and much larger uncertainties when attempting to estimate T_{eff} from spectral type.

We fit a 6th order polynomial weighted by the uncertainties in T_{eff} with rms of 113K (Table 10) to 124 field age objects in our sample (Figure 15a). We find the largest outlier, the very red WISE J164715.57+563208.3 (L9pec; Kirkpatrick et al. 2011) which shows no signatures of youth, to be 450K cooler than the field age sequence. Also, our application of solar metallicity evolutionary models probably overpredicts the radius of the L4 subdwarf 2MASS J16262034+3925190, which would mean an even hotter and more discrepant temperature from our field age sequence. We exclude these objects from our fit due to our lack of understanding for particularly red and blue field L dwarfs.

We also fit 6th order polynomials to 95 and 78 field age objects using their optical and IR spectral types respectively to see how T_{eff} depended on the typing technique used. We find no significant difference in the derived polynomial for L and T dwarfs, though our late-M subsample lacks enough IR spectral types to extend the comparison earlier than M9, so we adopt optical spectral types for our M and L dwarfs and IR spectral types for the T dwarfs.

The relations ofLooper et al. (2008b) (blue line) and Stephens et al. (2009) (green line) are both derived from revised versions of the Golimowski et al. (2004) sample with binaries removed and additional objects added. They use IR spectral types and an assumed age of 3 Gyr with uncertainties corresponding to an age range of 0.1–10 Gyr. The shape of our polynomial for field age objects (solid black line) agrees very well with the Stephens et al. (2009) relation across most of the sequence, though we obtain temperatures about 50K cooler for mid-T dwarfs. In that work, they fit the model atmosphere grid of Saumon & Marley (2008) to SEDs with NIR and MIR spectral coverage.

Marocco et al. (2013) (orange line) perform three types of atmospheric model fits to NIR spectra for their sample and calculate a weighted mean of the best fit model parameters to determine T_{eff} . In comparison to our polynomial, this produces temperatures up to 100K cooler for

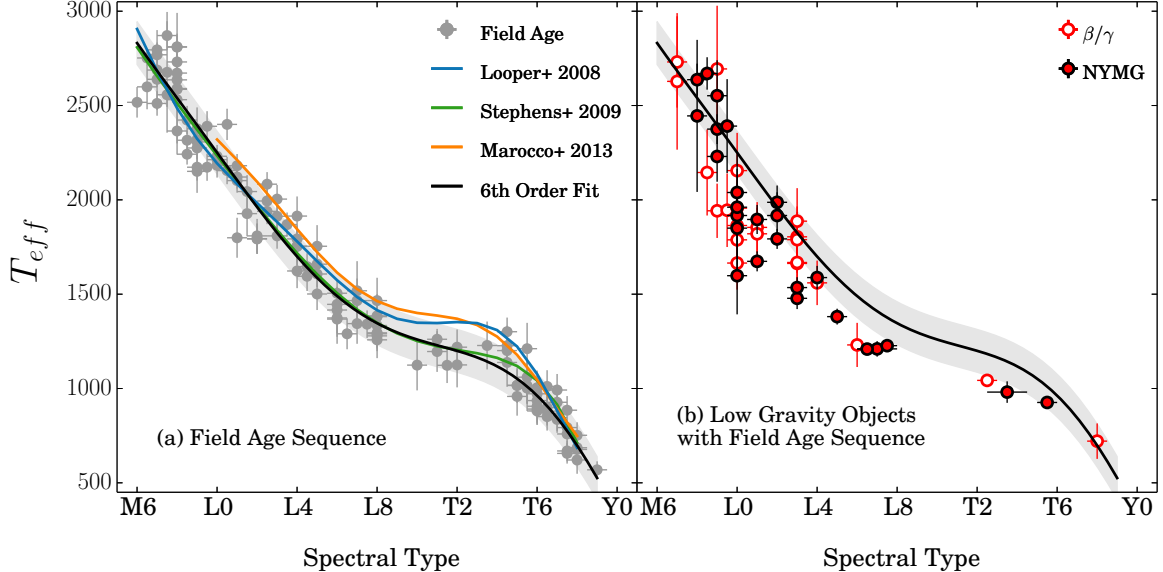


Figure 15. T_{eff} as a function of spectral type for (a) 124 field age objects and (b) 48 objects with signatures of low surface gravity and/or probable membership in a NYMG. A 6th order weighted polynomial fit (solid black line) to the field objects only is shown in both plots. The field age polynomials of Looper et al. (2008b), Stephens et al. (2009) and Marocco et al. (2013) are shown as blue, green, and orange lines, respectively. Symbols are the same as in Figure 7.

M7-L0 dwarfs and about 50K hotter for L3-L8 dwarfs. Their fit through the L/T transition is about 150K hotter than our field age track probably due to their unweighted fitting of only three objects in the L7-T3 range while our relation uses a weighted fit of 20 objects. All four relations agree for types later than T6.5 where the dispersion of the sequence is at a minimum of 200 K. This is most likely due to electron degeneracy putting tight constraints on predicted radii as well as atmospheric models for late-T dwarfs accurately reproducing observations (del Burgo et al. 2009).

Young objects exhibit similar or slightly higher L_{bol} as field age objects of the same spectral type. However, their larger radii mean that young objects must have cooler photospheres than field age objects with the same L_{bol} . Figure 15b shows the same field age polynomial as Figure 15a with only optically typed β/γ dwarfs (unfilled points with red borders) and NYMG members (red points with black borders) plotted. We find that late-M dwarfs with ages below about 25 Myr have similar temperatures as field age M dwarfs, while 25-130 Myr L0-L8 dwarfs have similar luminosities but temperatures up to 300K cooler than their field age counterparts. Also, the sensitivity of radius to the ages of young M8-L0 dwarfs creates a dispersion in T_{eff} of 500-600 K at the M/L transition. HN Peg B (T2.5), GU Psc B (T3.5), and SDSS J111010.01+011613.1 (T5.5pec) lie about 150K below the field age T dwarf track in Figure 15b but more confirmed young objects later than L8 are needed to explore this relationship in the T and Y dwarf regime.

While spectral type is often used as a proxy for effective temperature, we find that the relationship with the smallest dispersion is T_{eff} as a function of M_H (Table 10). Figure 16 shows the 5th order weighted polynomial fit (solid black line) to 115 field age objects (grey points) with an rms of 29K. While cloud clearing exposes deeper and hotter layers causing a brightening in J-band for L/T

transition objects (Tinney et al. 2003; Vrba et al. 2004; Looper et al. 2008a; Faherty et al. 2012), the monotonicity of T_{eff} FLD with decreasing M_H (and M_{K_s} not shown) supports the conclusion that the opacity sources that fall below the photosphere at these spectral types are isolated to J-band (Burgasser et al. 2002a; Knapp et al. 2004; Faherty et al. 2012). We also fit a 4th order weighted polynomial (dashed black line) to 25 NYMG members (red points with black borders) and 21 objects with signatures of low surface gravity (unfilled points with red borders) with an rms of 60K. These sequences show that young late-M to mid-L dwarfs are about 400-500K cooler than field age objects with the same M_H magnitude. Young late-L dwarfs start out about 250K cooler and then come within 50K of the field sequence at the center of the L/T transition probably due to scattering of light from H-band out to longer wavelengths by small dust grains. If a distance is available, M_H can be used to more reliably estimate T_{eff} than spectral type for both young and field age objects.

10. CONCLUSIONS

We constructed flux calibrated $0.3 - 18 \mu\text{m}$ SEDs using optical, NIR, and MIR spectra and photometry for 53 young and 145 field age late-M, L and T dwarfs. Gaps in data were filled by linear interpolation through photometry and newly derived age sensitive absolute magnitude-magnitude relations. These nearly complete SEDs allowed us to create a prescription for estimating systematic uncertainties in m_{bol} of ultracool dwarfs based on the amount and quality of data available. We also presented a flux calibrated sequence of field M, L and T dwarfs for comparison with the SEDs of bona fide NYMG members.

We calculated bolometric luminosities and used evolutionary model isochrones to derive radii, effective temperatures, surface gravities, and masses for the sample, increasing the number of ultracool dwarfs with semi-empirical fundamental parameters by over 40%. We used

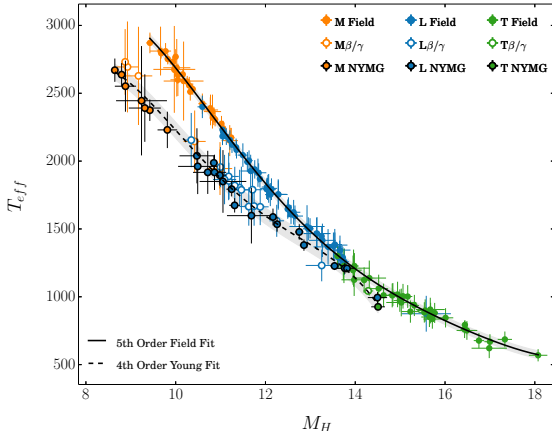


Figure 16. T_{eff} as a function of M_H for the sample. The solid black line shows the 5th order weighted polynomial fit to 115 field age objects and the dashed black line shows the 4th order weighted polynomial fit to 25 NYMG members and 21 objects with signatures of low surface gravity. The rms of each fit is shown as a grey shaded region. Young late-M to mid-L dwarfs are 400–500K cooler than field age objects of the same M_H magnitude. The temperature difference in the sequences reaches a minimum of about 50K around spectral type T0. Symbols are the same as in Figure 3.

these new values to recalculate L_{bol} and T_{eff} versus spectral type relations for field age objects for comparison with young brown dwarfs. These results show that 8–130 Myr L dwarfs are up to 30% more luminous but up to 300K cooler than their field age counterparts. We also present young and field age polynomials of T_{eff} as functions of M_H that can be used estimate temperatures to within 29K and 60K respectively.

We directly compared the empirical results of this work with published L_{bol} values inferred from model fitting and previous bolometric corrections and found disagreements of up to 30%. While we quantified the suspected age dependence of temperature, magnitude, and color as functions of spectral type and luminosity, we found that our newly derived BC_{Ks} is similar for late-M and L dwarfs of all ages. This correction for young objects is on average 0.05 magnitudes greater but within the rather large dispersion of the field age sequence. Our BC_J as a function of spectral type shows two distinct tracks for young and field age objects, differing by up to a full magnitude for late-L dwarfs.

Finally, we characterized the reddening of young L dwarfs as a shifting of flux from J-band out to W2-band, creating a pivot around K-band. Generally, this study has shown that great care must be taken when trying to determine accurate fundamental parameters of ultracool dwarfs given their ever increasing and fascinating natural diversity.

ACKNOWLEDGEMENTS

The authors would like to thank the anonymous referee for many helpful comments which greatly improved the manuscript. The authors would also like to thank P. A. Giorla Godfrey, A. Riedel, and M. C. Cushing for many productive discussions. This material is based upon work supported by the National Science Foundation under Grant No. 1211568 and 1313132. Support for this project was also provided by a PSC-CUNY Award, jointly funded by The Professional Staff Congress

and The City University of New York, and NASA Astrophysics Data Analysis Program (ADAP) award 11-ADAP11-0169. This publication makes use of data products from: the Two Micron All Sky Survey, which is a joint project of the University of Massachusetts and the Infrared Processing and Analysis Center/California Institute of Technology, funded by the National Aeronautics and Space Administration and the National Science Foundation; the Wide-field Infrared Survey Explorer, which is a joint project of the University of California, Los Angeles, and the Jet Propulsion Laboratory/California Institute of Technology, funded by the National Aeronautics and Space Administration; the BDNYC Data Archive, an open access repository of M, L, T and Y dwarf astrometry, photometry and spectra; the SIMBAD database, Aladin, and Vizier, operated at CDS, Strasbourg, France; the M, L, T, and Y dwarf compendium housed at DwarfArchives.org; the SpeX Prism Spectral Libraries, maintained by Adam Burgasser; the Montreal Brown Dwarf and Exoplanet Spectral Library, maintained by Jonathan Gagné; the NASA/ IPAC Infrared Science Archive, which is operated by the Jet Propulsion Laboratory, California Institute of Technology, under contract with the National Aeronautics and Space Administration.

REFERENCES

- Abazajian, K. N., Adelman-McCarthy, J. K., Agüeros, M. A., et al. 2009, ApJS, 182, 543
- Adelman-McCarthy, J. K., Agüeros, M. A., Allam, S. S., et al. 2008, ApJS, 175, 297
- Ahn, C. P., Alexandroff, R., Allende Prieto, C., et al. 2012, ApJS, 203, 21
- Albert, L., Artigau, É., Delorme, P., et al. 2011, The Astronomical Journal, 141, 203
- Allard, F. 2013, Proceedings of the International Astronomical Union, 8, 271
- Allers, K. N., & Liu, M. C. 2013, ApJ, 772, 79
- Allers, K. N., Liu, M. C., Dupuy, T. J., & Cushing, M. C. 2010, ApJ, 715, 561
- Allington-Smith, J., Breare, M., Ellis, R., et al. 1994, PASP, 106, 983
- Allington-Smith, J., Murray, G., Content, R., et al. 2002, PASP, 114, 892
- Anderson, D. R., Cameron, A. C., Hellier, C., et al. 2010, ApJ, 726, L19
- Andrei, A. H., Smart, R. L., Penna, J. L., et al. 2011, AJ, 141, 54
- Appenzeller, I., Fricke, K., Fürtg, W., et al. 1998, The Messenger, 94, 1
- Artigau, É., Radigan, J., Folkes, S., et al. 2010, ApJ, 718, L38
- Aumer, M., & Binney, J. J. 2009, Monthly Notices of the Royal Astronomical Society, 397, 1286
- Baraffe, I., Chabrier, G., Allard, F., & Hauschildt, P. H. 1998, A&A, 337, 403
- Baraffe, I., Chabrier, G., Barman, T. S., Allard, F., & Hauschildt, P. H. 2003, Astronomy and Astrophysics, 402, 701
- Barman, T. S. 2008, in Astronomical Society of the Pacific Conference Series, Vol. 384, 14th Cambridge Workshop on Cool Stars, Stellar Systems, and the Sun, ed. G. van Belle, 133
- Barman, T. S., Macintosh, B., Konopacky, Q. M., & Marois, C. 2011, ApJ, 733, 65
- Becklin, E. E., & Zuckerman, B. 1988, Nature, 336, 656
- Bihain, G., Rebolo, R., Zapatero Osorio, M. R., Béjar, V. J. S., & Caballero, J. A. 2010, A&A, 519, A93
- Blanton, M. R., & Roweis, S. 2007, AJ, 133, 734
- Boffin, H. M. J., Pourbaix, D., Mužić, K., et al. 2013, Astronomy & Astrophysics, 561, L4
- Bonnefoy, M., Chauvin, G., Lagrange, A.-M., et al. 2014, A&A, 562, A127

- Bonnet, H., Abuter, R., Baker, A., et al. 2004, *The Messenger*, 117, 17
- Bouchy, F., Deleuil, M., Guillot, T., et al. 2010, *Astronomy & Astrophysics*, 525, A68
- Bouy, H., Brandner, W., Martn, E. L., et al. 2003, *AJ*, 126, 1526
- Bowler, B. P., Liu, M. C., Dupuy, T. J., & Cushing, M. C. 2010, *ApJ*, 723, 850
- Boyajian, T. S., von Braun, K., van Belle, G., et al. 2012, *ApJ*, 757, 112
- Burgasser, A., Burrows, A., Kirkpatrick, J. D., & Tinney, C. 2005, Metallicity and Gravity Diagnostics in the Coldest Brown Dwarf Spectra, Spitzer Proposal
- Burgasser, A., Cruz, K., Cushing, M., et al. 2008a, Direct Observations of Clouds on Brown Dwarfs: A Spitzer Study of Extreme Cases, Spitzer Proposal
- Burgasser, A. J. 2004, *ApJ*, 614, L73
- Burgasser, A. J. 2007, *ApJ*, 658, 617
- . 2014, International Workshop on Stellar Spectral Libraries ASI Conference Series, 11, 7
- Burgasser, A. J. 2014, in Astronomical Society of India Conference Series, Vol. 11, Astronomical Society of India Conference Series, 7–16
- Burgasser, A. J., Burrows, A., & Kirkpatrick, J. D. 2006, *ApJ*, 639, 1095
- Burgasser, A. J., Cruz, K. L., Cushing, M., et al. 2010a, *ApJ*, 710, 1142
- Burgasser, A. J., Cruz, K. L., & Kirkpatrick, J. D. 2007, *ApJ*, 657, 494
- Burgasser, A. J., Geballe, T. R., Leggett, S. K., Kirkpatrick, J. D., & Goliowski, D. A. 2006a, *ApJ*, 637, 1067
- Burgasser, A. J., Kirkpatrick, J. D., Cruz, K. L., et al. 2006b, *ApJS*, 166, 585
- Burgasser, A. J., Kirkpatrick, J. D., Liebert, J., & Burrows, A. 2003a, *ApJ*, 594, 510
- Burgasser, A. J., Kirkpatrick, J. D., & Lowrance, P. J. 2005, *AJ*, 129, 2849
- Burgasser, A. J., Kirkpatrick, J. D., Reid, I. N., et al. 2000, *AJ*, 120, 473
- Burgasser, A. J., Liu, M. C., Ireland, M. J., Cruz, K. L., & Dupuy, T. J. 2008b, *ApJ*, 681, 579
- Burgasser, A. J.,Looper, D., & Rayner, J. T. 2010b, *AJ*, 139, 2448
- Burgasser, A. J., Marley, M. S., Ackerman, A. S., et al. 2002a, *ApJ*, 571, L151
- Burgasser, A. J., McElwain, M. W., & Kirkpatrick, J. D. 2003b, *AJ*, 126, 2487
- Burgasser, A. J., McElwain, M. W., Kirkpatrick, J. D., et al. 2004, *AJ*, 127, 2856
- Burgasser, A. J., Sheppard, S. S., & Luhman, K. L. 2013, *ApJ*, 772, 129
- Burgasser, A. J., Tinney, C. G., Cushing, M. C., et al. 2008c, *ApJ*, 689, L53
- Burgasser, A. J., Kirkpatrick, J. D., Brown, M. E., et al. 1999, *The Astrophysical Journal*, 522, L65
- Burgasser, A. J., Wilson, J. C., Kirkpatrick, J. D., et al. 2000a, *The Astronomical Journal*, 120, 1100
- Burgasser, A. J., Kirkpatrick, J. D., Cutri, R. M., et al. 2000b, *The Astrophysical Journal*, 531, L57
- Burgasser, A. J., Kirkpatrick, J. D., Brown, M. E., et al. 2002b, *ApJ*, 564, 421
- Burgasser, A. J., Simcoe, R. A., Bochanski, J. J., et al. 2010, *ApJ*, 725, 1405
- Burningham, B., Leggett, S. K., Lucas, P. W., et al. 2010, *MNRAS*, 404, 1952
- Burningham, B., Leggett, S. K., Homeier, D., et al. 2011, *MNRAS*, 414, 3590
- Burrows, A., Heng, K., & Nampaisarn, T. 2011, *ApJ*, 736, 47
- Burrows, A., Hubbard, W., Lunine, J., & Liebert, J. 2001, *Reviews of Modern Physics*, 73, 719
- Burrows, A., Marley, M., Hubbard, W. B., et al. 1997, *ApJ*, 491, 856
- Cesetti, M., Pizzella, A., Ivanov, V. D., et al. 2013, *A&A*, 549, A129
- Chabrier, G., Baraffe, I., Allard, F., & Hauschildt, P. 2000, *ApJ*, 542, 464
- Chauvin, G., Lagrange, A.-M., Dumas, C., et al. 2004, *Astronomy and Astrophysics*, 425, L29
- Chiu, K., Fan, X., Leggett, S. K., et al. 2006, *AJ*, 131, 2722
- Costa, E., Méndez, R. A., Jao, W.-C., et al. 2005, *AJ*, 130, 337
- Costa, E., Méndez, R. A., Jao, W.-C., et al. 2006, *AJ*, 132, 1234
- Cox, A. N. 2000, *Allen's astrophysical quantities*
- Cruz, K., Burrows, A., & Reid, N. 2004a, The Mid-Infrared Spectrophotometric Properties of a Complete Sample of the Nearest L Dwarfs, Spitzer Proposal
- Cruz, K. L., Burgasser, A. J., Reid, I. N., & Liebert, J. 2004b, *ApJ*, 604, L61
- Cruz, K. L., Kirkpatrick, J. D., & Burgasser, A. J. 2009, *AJ*, 137, 3345
- Cruz, K. L., & Reid, I. N. 2002, *The Astronomical Journal*, 123, 2828
- Cruz, K. L., Reid, I. N., Liebert, J., Kirkpatrick, J. D., & Lowrance, P. J. 2003, *AJ*, 126, 2421
- Cruz, K. L., Reid, I. N., Kirkpatrick, J. D., et al. 2007, *AJ*, 133, 439
- Currie, T., Burrows, A., Madhusudhan, N., et al. 2013, *ApJ*, 776, 15
- Cushing, M., Chabrier, G., Hauschildt, P., Liebert, J., & Wehrse, R. 2005a, Probing the Chromospheres of M dwarfs with the IRS, Spitzer Proposal
- Cushing, M., Dupuy, T., Liu, M., Marley, M., & Saumon, D. 2008, Precision Tests of Ultracool Dwarf Atmospheric Models, Spitzer Proposal
- Cushing, M. C.,Looper, D., Burgasser, A. J., et al. 2009, *ApJ*, 696, 986
- Cushing, M. C., Rayner, J. T., & Vacca, W. D. 2005b, *ApJ*, 623, 1115
- Cushing, M. C., Vacca, W. D., & Rayner, J. T. 2004, *Publications of the Astronomical Society of the Pacific*, 116, 362
- Cushing, M. C., Roellig, T. L., Marley, M. S., et al. 2006, *ApJ*, 648, 614
- Cushing, M. C., Marley, M. S., Saumon, D., et al. 2008, *ApJ*, 678, 1372
- Cutri, R. M., & et al. 2012, VizieR Online Data Catalog, 2311, 0
- . 2014, VizieR Online Data Catalog, 2328, 0
- Cutri, R. M., Skrutskie, M. F., van Dyk, S., et al. 2003, 2MASS All Sky Catalog of point sources.
- Dahn, C. C., Harris, H. C., Vrba, F. J., et al. 2002, *The Astronomical Journal*, 124, 1170
- Deacon, N. R., Hambly, N. C., Henry, T. J., et al. 2005, *AJ*, 129, 409
- del Burgo, C., Martín, E. L., Osorio, M. R. Z., & Hauschildt, P. H. 2009, *Astronomy and Astrophysics*, 501, 1059
- Deleuil, M., Deeg, H. J., Alonso, R., et al. 2008, *Astronomy and Astrophysics*, 491, 889
- Delfosse, X., Tinney, C. G., Forveille, T., et al. 1997, *Astronomy and Astrophysics*, 327, 25
- DENIS Consortium. 2003, VizieR Online Data Catalog, 1, 2002
- Depoy, D. L., Atwood, B., Byard, P. L., Frogel, J., & O'Brien, T. P. 1993, in Society of Photo-Optical Instrumentation Engineers (SPIE) Conference Series, Vol. 1946, Infrared Detectors and Instrumentation, ed. A. M. Fowler, 667–672
- Díaz, R. F., Damiani, C., Deleuil, M., et al. 2013, *Astronomy & Astrophysics*, 551, L9
- Dieterich, S. B., Henry, T. J., Jao, W.-C., et al. 2014, *AJ*, 147, 94
- Ducourant, C., Teixeira, R., Chauvin, G., et al. 2008, *Astronomy and Astrophysics*, 477, L1
- Dupuy, T. J., & Kraus, A. L. 2013, *Science*, 341, 1492
- Dupuy, T. J., & Liu, M. C. 2012, *ApJS*, 201, 19
- Dupuy, T. J., Liu, M. C., & Bowler, B. P. 2009a, *ApJ*, 706, 328
- Dupuy, T. J., Liu, M. C., Bowler, B. P., et al. 2010, *ApJ*, 721, 1725
- Dupuy, T. J., Liu, M. C., & Ireland, M. J. 2009b, *ApJ*, 699, 168
- Eisenhauer, F., Abuter, R., Bickert, K., et al. 2003, in Society of Photo-Optical Instrumentation Engineers (SPIE) Conference Series, Vol. 4841, Instrument Design and Performance for Optical/Infrared Ground-based Telescopes, ed. M. Iye & A. F. M. Moorwood, 1548–1561
- Elias, J. H., Joyce, R. R., Liang, M., et al. 2006, in Society of Photo-Optical Instrumentation Engineers (SPIE) Conference Series, Vol. 6269, Society of Photo-Optical Instrumentation Engineers (SPIE) Conference Series, 4
- Epcstein, N., de Batz, B., Capoani, L., et al. 1997, *The Messenger*, 87, 27

- Faherty, J. K., Beletsky, Y., Burgasser, A. J., et al. 2014, *ApJ*, 790, 90
- Faherty, J. K., Burgasser, A. J., Cruz, K. L., et al. 2009, *AJ*, 137, 1
- Faherty, J. K., Rice, E. L., Cruz, K. L., Mamajek, E. E., & Núñez, A. 2013, *AJ*, 145, 2
- Faherty, J. K., Burgasser, A. J., Walter, F. M., et al. 2012, *ApJ*, 752, 56
- Fan, X., Knapp, G. R., Strauss, M. A., et al. 2000, *The Astronomical Journal*, 119, 928
- Fazio, G. G., Hora, J. L., Allen, L. E., et al. 2004, *ApJS*, 154, 10
- Feiden, G. A., & Chaboyer, B. 2012, *ApJ*, 761, 30
- . 2013, *ApJ*, 779, 183
- Fukugita, M., Ichikawa, T., Gunn, J. E., et al. 1996, *AJ*, 111, 1748
- Gagliuffi, D. C. B., Burgasser, A. J., Gelino, C. R., et al. 2014, *ApJ*, 794, 143
- Gagné, J., Burgasser, A. J., Faherty, J. K., et al. 2015a, ArXiv e-prints, arXiv:1506.04195
- . 2015b, ArXiv e-prints, arXiv:1506.04195
- Gagné, J., Faherty, J. K., Cruz, K., et al. 2014, *ApJ*, 785, L14
- Gatewood, G., & Coban, L. 2009, *AJ*, 137, 402
- Geballe, T. R., Saumon, D., Leggett, S. K., et al. 2001, *ApJ*, 556, 373
- Geballe, T. R., Knapp, G. R., Leggett, S. K., et al. 2002, *ApJ*, 564, 466
- Gelino, C. R., Smart, R. L., Marocco, F., et al. 2014, *AJ*, 148, 6
- Giclas, H. L., Burnham, R., & Thomas, N. G. 1961, Lowell Observatory Bulletin, 5, 61
- Giclas, H. L., Slaughter, C. D., & Burnham, R. 1959, Lowell Observatory Bulletin, 4, 136
- Gizis, J. E. 1997, *The Astronomical Journal*, 113, 806
- Gizis, J. E. 2002, *ApJ*, 575, 484
- Gizis, J. E., Allers, K. N., Liu, M. C., et al. 2015, *ApJ*, 799, 203
- Gizis, J. E., Monet, D. G., Reid, I. N., et al. 2000, *The Astronomical Journal*, 120, 1085
- Gizis, J. E., Reid, I. N., Knapp, G. R., et al. 2003, *AJ*, 125, 3302
- Gizis, J. E., Faherty, J. K., Liu, M. C., et al. 2012, *AJ*, 144, 94
- Goldman, B., Marsat, S., Henning, T., Clemens, C., & Greiner, J. 2010, *Monthly Notices of the Royal Astronomical Society*, no Goldman, B., Delfosse, X., Forveille, T., et al. 1999, *Astronomy and Astrophysics*, 351, L5
- Golimowski, D. A., Leggett, S. K., Marley, M. S., et al. 2004, *AJ*, 127, 3516
- Griffith, R. L., Kirkpatrick, J. D., Eisenhardt, P. R. M., et al. 2012, *AJ*, 144, 148
- Hawkins, M. R. S., & Bessell, M. S. 1988, *MNRAS*, 234, 177
- Hawley, S. L., Covey, K. R., Knapp, G. R., et al. 2002, *The Astronomical Journal*, 123, 3409
- Henry, T. J., Jao, W.-C., Subasavage, J. P., et al. 2006, *AJ*, 132, 2360
- Henry, T. J., & Kirkpatrick, J. D. 1990, *ApJL*, 354, L29
- Hewett, P. C., Warren, S. J., Leggett, S. K., & Hodgkin, S. T. 2006, *MNRAS*, 367, 454
- Hodapp, K. W., Jensen, J. B., Irwin, E. M., et al. 2003, *PASP*, 115, 1388
- Holberg, J. B., & Bergeron, P. 2006, *AJ*, 132, 1221
- Houck, J. R., & Roellig, T. 2004a, IRS Observations of the Brown Dwarf L and T Sequence, Spitzer Proposal
- . 2004b, IRS observations of the dwarf M-star sequence, Spitzer Proposal
- Houck, J. R., & Watson, D. 2004, Spectroscopy of protostellar, protoplanetary and debris disks, Spitzer Proposal
- Houck, J. R., Roellig, T. L., Van Cleve, J., et al. 2004, in Society of Photo-Optical Instrumentation Engineers (SPIE) Conference Series, Vol. 5487, Optical, Infrared, and Millimeter Space Telescopes, ed. J. C. Mather, 62–76
- Houck, J. R., Luhman, K., Allen, L., et al. 2006, Disk structure and planet formation around young low-mass stars and brown dwarfs, Spitzer Proposal
- Jayawardhana, R., Ardila, D. R., Stelzer, B., & Haisch, Jr., K. E. 2003, *AJ*, 126, 1515
- Jenkins, J. S., Ramsey, L. W., Jones, H. R. A., et al. 2009, *ApJ*, 704, 975
- Johnson, J. A., Apps, K., Gazak, J. Z., et al. 2011, *ApJ*, 730, 79
- Jones, H. R. A., Longmore, A. J., Allard, F., & Hauschildt, P. H. 1996, *MNRAS*, 280, 77
- Kashikawa, N., Inata, M., Iye, M., et al. 2000, in Society of Photo-Optical Instrumentation Engineers (SPIE) Conference Series, Vol. 4008, Optical and IR Telescope Instrumentation and Detectors, ed. M. Iye & A. F. Moorwood, 104–113
- Kendall, T. R., Delfosse, X., Mart?n, E. L., & Forveille, T. 2004, *Astronomy and Astrophysics*, 416, L17
- Kendall, T. R., Mauron, N., Azzopardi, M., & Gigoyan, K. 2003, *A&A*, 403, 929
- Kirkpatrick, J. D. 2005, *ARA&A*, 43, 195
- Kirkpatrick, J. D., Barman, T. S., Burgasser, A. J., et al. 2006, *ApJ*, 639, 1120
- Kirkpatrick, J. D., Beichman, C. A., & Skrutskie, M. F. 1997, *ApJ*, 476, 311
- Kirkpatrick, J. D., Dahn, C. C., Monet, D. G., et al. 2001a, *The Astronomical Journal*, 121, 3235
- Kirkpatrick, J. D., Henry, T. J., & McCarthy, Jr., D. W. 1991, *ApJS*, 77, 417
- Kirkpatrick, J. D., Henry, T. J., & Simons, D. A. 1995, *The Astronomical Journal*, 109, 797
- Kirkpatrick, J. D., Liebert, J., Cruz, K. L., Gizis, J. E., & Reid, I. N. 2001b, *Publications of the Astronomical Society of the Pacific*, 113, 814
- Kirkpatrick, J. D., McGraw, J. T., Hess, T. R., Liebert, J., & McCarthy, Jr., D. W. 1994, *ApJS*, 94, 749
- Kirkpatrick, J. D., Reid, I. N., Liebert, J., et al. 1999, *ApJ*, 519, 802
- . 2000, *The Astronomical Journal*, 120, 447
- Kirkpatrick, J. D., Cruz, K. L., Barman, T. S., et al. 2008, *Astrophysical Journal*, 689, 1295
- Kirkpatrick, J. D., Looper, D. L., Burgasser, A. J., et al. 2010, *ApJS*, 190, 100
- Kirkpatrick, J. D., Cushing, M. C., Gelino, C. R., et al. 2011, *ApJS*, 197, 19
- Kirkpatrick, J. D., Gelino, C. R., Cushing, M. C., et al. 2012, *ApJ*, 753, 156
- Knapp, G. R., Leggett, S. K., Fan, X., et al. 2004, *AJ*, 127, 3553
- Kobayashi, N., Tokunaga, A. T., Terada, H., et al. 2000, in Society of Photo-Optical Instrumentation Engineers (SPIE) Conference Series, Vol. 4008, Optical and IR Telescope Instrumentation and Detectors, ed. M. Iye & A. F. Moorwood, 1056–1066
- Konopacky, Q. M., Ghez, A. M., Barman, T. S., et al. 2010, *ApJ*, 711, 1087
- Landolt, A. U. 1992, *AJ*, 104, 340
- . 2009, *AJ*, 137, 4186
- Lawrence, A., Warren, S. J., Almaini, O., et al. 2007, *MNRAS*, 379, 1599
- Leggett, S. K., Allard, F., Geballe, T. R., Hauschildt, P. H., & Schweitzer, A. 2001, *ApJ*, 548, 908
- Leggett, S. K., Allard, F., & Hauschildt, P. H. 1998, *ApJ*, 509, 836
- Leggett, S. K., Hauschildt, P. H., Allard, F., Geballe, T. R., & Baron, E. 2002a, *MNRAS*, 332, 78
- Leggett, S. K., Saumon, D., Marley, M. S., et al. 2007, *ApJ*, 655, 1079
- Leggett, S. K., Geballe, T. R., Fan, X., et al. 2000, *The Astrophysical Journal*, 536, L35
- Leggett, S. K., Golimowski, D. A., Fan, X., et al. 2002b, *ApJ*, 564, 452
- Leggett, S. K., Burningham, B., Saumon, D., et al. 2010, *ApJ*, 710, 1627
- Leggett, S. K., Saumon, D., Marley, M. S., et al. 2012, *ApJ*, 748, 74
- Lépine, S., & Shara, M. M. 2005, *AJ*, 129, 1483
- Lépine, S., Shara, M. M., & Rich, R. M. 2002, *AJ*, 124, 1190
- Liebert, J., & Burgasser, A. J. 2007, *ApJ*, 655, 522
- Liebert, J., Dahn, C. C., Gresham, M., & Strittmatter, P. A. 1979, *ApJ*, 233, 226
- Liebert, J., & Gizis, J. E. 2006, *PASP*, 118, 659
- Liebert, J., Kirkpatrick, J. D., Cruz, K. L., et al. 2003, *AJ*, 125, 343
- Liebert, J., Kirkpatrick, J. D., Reid, I. N., & Fisher, M. D. 1999, *ApJ*, 519, 345
- Littlefair, S. P., Casewell, S. L., Parsons, S. G., et al. 2014, *Monthly Notices of the Royal Astronomical Society*, 445, 2106
- Liu, M. C., Magnier, E. A., Deacon, N. R., et al. 2013, *ApJ*, 777, L20

- Liu, M. C., Magnier, E. A., Deacon, N. R., et al. 2013, *ApJ*, 777, L20
- Looper, D. L., Burgasser, A. J., Kirkpatrick, J. D., & Swift, B. J. 2007, *ApJ*, 669, L97
- Looper, D. L., Gelino, C. R., Burgasser, A. J., & Kirkpatrick, J. D. 2008a, *Astrophysical Journal*, 685, 1183
- Looper, D. L., Kirkpatrick, J. D., & Burgasser, A. J. 2007, *AJ*, 134, 1162
- Looper, D. L., Kirkpatrick, J. D., Cutri, R. M., et al. 2008b, *Astrophysical Journal*, 686, 528
- Lucas, P. W., Tinney, C. G., Burningham, B., et al. 2010, *Monthly Notices of the Royal Astronomical Society: Letters*, 408, L56
- Luhman, K. L. 2012, *Annual Review of Astronomy and Astrophysics*, 50, 65
- . 2013, *ApJ*, 767, L1
- Luhman, K. L., Mamajek, E. E., Allen, P. R., & Cruz, K. L. 2009, *ApJ*, 703, 399
- Luhman, K. L., Mamajek, E. E., Allen, P. R., & Cruz, K. L. 2009, *ApJ*, 703, 399
- Luhman, K. L., Patten, B. M., Marengo, M., et al. 2007, *ApJ*, 654, 570
- Lurie, J. C., Henry, T. J., Jao, W.-C., et al. 2014, *AJ*, 148, 91
- Luyten, W. J. 1979a, LHS catalogue. A catalogue of stars with proper motions exceeding 0"5 annually
- . 1979b, New Luyten catalogue of stars with proper motions larger than two tenths of an arcsecond; and first supplement; NLTT. (Minneapolis (1979)); Label 12 = short description; Label 13 = documentation by Warren; Label 14 = catalogue
- Mace, G. N., Kirkpatrick, J. D., Cushing, M. C., et al. 2013, *ApJS*, 205, 6
- Mainzer, A. K., Roellig, T. L., Saumon, D., et al. 2007, *ApJ*, 662, 1245
- Malo, L., Doyon, R., Lafrenière, D., et al. 2012, *ApJ*, 762, 88
- Mamajek, E. E. 2005, *ApJ*, 634, 1385
- Manjavacas, E., Bonnefoy, M., Schlieder, J. E., et al. 2014, *A&A*, 564, A55
- Mann, A. W., Feiden, G. A., Gaidos, E., Boyajian, T., & von Braun, K. 2015, ArXiv e-prints, arXiv:1501.01635
- Marley, M. S., Saumon, D., & Goldblatt, C. 2010, *ApJ*, 723, L117
- Marley, M. S., Saumon, D., Guillot, T., et al. 1996, *Science*, 272, 1919
- Marocco, F., Smart, R. L., Jones, H. R. A., et al. 2010, *A&A*, 524, A38
- Marocco, F., Andrei, A. H., Smart, R. L., et al. 2013, *The Astronomical Journal*, 146, 161
- Marshall, J. L., Burles, S., Thompson, I. B., et al. 2008, in *Society of Photo-Optical Instrumentation Engineers (SPIE) Conference Series*, Vol. 7014, *Society of Photo-Optical Instrumentation Engineers (SPIE) Conference Series*, 54
- Martín, E. L., Delfosse, X., Basri, G., et al. 1999, *The Astronomical Journal*, 118, 2466
- Matthews, K., & Soifer, B. T. 1994, *Experimental Astronomy*, 3, 77
- Metchev, S. A., Kirkpatrick, J. D., Berriman, G. B., &Looper, D. 2008, *ApJ*, 676, 1281
- Mohanty, S., Jayawardhana, R., Huelamo, N., & Mamajek, E. 2007, *ApJ*, 657, 1064
- Monet, D. G., Dahn, C. C., Vrba, F. J., et al. 1992, *AJ*, 103, 638
- Monet, D. G., Levine, S. E., Canzian, B., et al. 2003, *AJ*, 125, 984
- Montes, D., López-Santiago, J., Gálvez, M. C., et al. 2001, *MNRAS*, 328, 45
- Mountain, C. M., Robertson, D. J., Lee, T. J., & Wade, R. 1990, in *Society of Photo-Optical Instrumentation Engineers (SPIE) Conference Series*, Vol. 1235, *Instrumentation in Astronomy VII*, ed. D. L. Crawford, 25–33
- Moutou, C., Bonomo, A. S., Bruno, G., et al. 2013, *Astronomy & Astrophysics*, 558, L6
- Mugrauer, M., Seifahrt, A., Neuhäuser, R., & Mazeh, T. 2006, *MNRAS*, 373, L31
- Nakajima, T., Oppenheimer, B. R., Kulkarni, S. R., et al. 1995, *Nature*, 378, 463
- Naud, M.-E., Artigau, É., Malo, L., et al. 2014, *ApJ*, 787, 5
- Oke, J. B., & Gunn, J. E. 1983, *ApJ*, 266, 713
- Oke, J. B., Cohen, J. G., Carr, M., et al. 1995, *PASP*, 107, 375
- Osorio, M. R. Z., Rebolo, R., Bihain, G., et al. 2010, *ApJ*, 715, 1408
- Patience, J., King, R. R., de Rosa, R. J., & Marois, C. 2010, *A&A*, 517, A76
- Patience, J., King, R. R., De Rosa, R. J., et al. 2012, *A&A*, 540, A85
- Patten, B. M., Stauffer, J. R., Burrows, A., et al. 2006, *ApJ*, 651, 502
- Phan-Bao, N., Crifo, F., Delfosse, X., et al. 2003, *Astronomy and Astrophysics*, 401, 959
- Phan-Bao, N., Bessell, M. S., Martín, E. L., et al. 2006, *MNRAS*, 366, L40
- Phan-Bao, N., Bessell, M. S., Martín, E. L., et al. 2008, *Monthly Notices of the Royal Astronomical Society*, 383, 831
- Pokorný, R. S., Jones, H. R. A., Hambly, N. C., & Pinfield, D. J. 2004, *A&A*, 421, 763
- Pont, F., Melo, C. H. F., Bouchy, F., et al. 2005, *Astronomy and Astrophysics*, 433, L21
- Probst, R. G., & Liebert, J. 1983, *ApJ*, 274, 245
- Rayner, J. T., Cushing, M. C., & Vacca, W. D. 2009, *ApJS*, 185, 289
- Reyner, J. T., Toomey, D. W., Onaka, P. M., et al. 2003, *PASP*, 115, 362
- Rebolo, R. 1998, *Science*, 282, 1309
- Reid, I. N., & Cruz, K. L. 2002, *AJ*, 123, 2806
- Reid, I. N., Cruz, K. L., Kirkpatrick, J. D., et al. 2008, *The Astronomical Journal*, 136, 1290
- Reid, I. N., & Gizis, J. E. 2005, *Publications of the Astronomical Society of the Pacific*, 117, 676
- Reid, I. N., Gizis, J. E., Kirkpatrick, J. D., & Koerner, D. W. 2001, *AJ*, 121, 489
- Reid, I. N., Kirkpatrick, J. D., Gizis, J. E., et al. 2000, *AJ*, 119, 369
- Reid, I. N., Cruz, K. L., Laurie, S. P., et al. 2003, *The Astronomical Journal*, 125, 354
- Reid, I. N., Cruz, K. L., Allen, P., et al. 2003, *AJ*, 126, 3007
- Reid, N. 1987, *Monthly Notices of the Royal Astronomical Society*, 225, 873
- Reylé, C., Delorme, P., Willott, C. J., et al. 2010, *A&A*, 522, A112
- Rice, E. L., Barman, T., McLean, I. S., Prato, L., & Kirkpatrick, J. D. 2010a, *ApJS*, 186, 63
- Rice, E. L., Faherty, J. K., & Cruz, K. L. 2010b, *ApJ*, 715, L165
- Roellig, T. L., Van Cleve, J. E., Sloan, G. C., et al. 2004, *ApJS*, 154, 418
- Ruiz, M. T., Leggett, S. K., & Allard, F. 1997, *The Astrophysical Journal*, 491, L107
- Ruiz, M. T., Takamiya, M. Y., & Roth, M. 1991, *ApJL*, 367, L59
- Ruiz, M. T., Wischnjewsky, M., Rojo, P. M., & Gonzalez, L. E. 2001, *ASTROPHYS J SUPPL S*, 133, 119
- Saumon, D., & Marley, M. S. 2008, *Astrophysical Journal*, 689, 1327
- Saumon, D., Marley, M. S., Leggett, S. K., et al. 2007, *ApJ*, 656, 1136
- Schilbach, E., Röser, S., & Scholz, R.-D. 2009, *A&A*, 493, L27
- Schmidt, S. J., Cruz, K. L., Bongiorno, B. J., Liebert, J., & Reid, I. N. 2007, *AJ*, 133, 2258
- Schmidt, S. J., West, A. A., Bochanski, J. J., Hawley, S. L., & Kiely, C. 2014, *Publications of the Astronomical Society of the Pacific*, 000
- Schmidt, S. J., West, A. A., Hawley, S. L., & Pineda, J. S. 2010, *AJ*, 139, 1808
- Schneider, D. P., Greenstein, J. L., Schmidt, M., & Gunn, J. E. 1991, *The Astronomical Journal*, 102, 1180
- Scholz, R.-D., Bihain, G., Schnurr, O., & Storm, J. 2011, *A&A*, 532, L5
- Scholz, R.-D., Lodieu, N., Ibata, R., et al. 2004, *Monthly Notices of the Royal Astronomical Society*, 347, 685
- Scholz, R.-D., McCaughrean, M. J., Zinnecker, H., & Lodieu, N. 2005, *Astronomy and Astrophysics*, 430, L49
- Scholz, R.-D., Storm, J., Knapp, G. R., & Zinnecker, H. 2009, *A&A*, 494, 949
- Seifahrt, A., Reiners, A., Almaghrbi, K. A. M., & Basri, G. 2010, *Astronomy and Astrophysics*, 512, A37
- Shkolnik, E., Liu, M. C., & Reid, I. N. 2009, *ApJ*, 699, 649

- Simcoe, R. A., Burgasser, A. J., Bernstein, R. A., et al. 2008, in Society of Photo-Optical Instrumentation Engineers (SPIE) Conference Series, Vol. 7014, Society of Photo-Optical Instrumentation Engineers (SPIE) Conference Series, 0
- Simons, D. A., & Tokunaga, A. 2002, PASP, 114, 169
- Siverd, R. J., Beatty, T. G., Pepper, J., et al. 2012, ApJ, 761, 123
- Skrutskie, M. F., Cutri, R. M., Stiening, R., et al. 2006, AJ, 131, 1163
- Smart, R. L., Tinney, C. G., Bucciarelli, B., et al. 2013, MNRAS, 433, 2054
- Stephens, D. C., Leggett, S. K., Cushing, M. C., et al. 2009, ApJ, 702, 154
- Strauss, M. A., Fan, X., Gunn, J. E., et al. 1999, The Astrophysical Journal, 522, L61
- Subasavage, J. P., Jao, W.-C., Henry, T. J., et al. 2009, AJ, 137, 4547
- Teixeira, R., Ducourant, C., Chauvin, G., et al. 2008, A&A, 489, 825
- Thorstensen, J. R., & Kirkpatrick, J. D. 2003, Publications of the Astronomical Society of the Pacific, 115, 1207
- Tinney, C. G. 1993, ApJ, 414, 279
- Tinney, C. G. 1996, Monthly Notices of the Royal Astronomical Society, 281, 644
- Tinney, C. G., Burgasser, A. J., & Kirkpatrick, J. D. 2003, AJ, 126, 975
- Tinney, C. G., Burgasser, A. J., Kirkpatrick, J. D., & McElwain, M. W. 2005, AJ, 130, 2326
- Tinney, C. G., Faherty, J. K., Kirkpatrick, J. D., et al. 2014, ApJ, 796, 39
- Tinney, C. G., Mould, J. R., & Reid, I. N. 1992, ApJ, 396, 173
- . 1993, AJ, 105, 1045
- Tinney, C. G., Reid, I. N., Gizis, J., & Mould, J. R. 1995, AJ, 110, 3014
- Todorov, K., Luhman, K. L., & McLeod, K. K. 2010, ApJ, 714, L84
- Tokunaga, A. T., Simons, D. A., & Vacca, W. D. 2002, PASP, 114, 180
- Tsvetanov, Z. I., Golimowski, D. A., Zheng, W., et al. 2000, The Astrophysical Journal, 531, L61
- Turnbull, M. C., & Tarter, J. C. 2003, ASTROPHYS J SUPPL S, 149, 423
- van Altena, W. F., Lee, J. T., & Hoffleit, E. D. 1995, The general catalogue of trigonometric [stellar] parallaxes
- van Biesbroeck, G. 1961, The Astronomical Journal, 66, 528
- van Leeuwen, F. 2007, A&A, 474, 653
- Vrba, F. J., Henden, A. A., Luginbuhl, C. B., et al. 2004, AJ, 127, 2948
- Weinberger, A. J., Anglada-Escudé, G., & Boss, A. P. 2012, ApJ, 762, 118
- West, A. A., Hawley, S. L., Bochanski, J. J., et al. 2008, The Astronomical Journal, 135, 785
- Wilson, J. C., Kirkpatrick, J. D., Gizis, J. E., et al. 2001, The Astronomical Journal, 122, 1989
- Wilson, J. C., Miller, N. A., Gizis, J. E., et al. 2003, in IAU Symposium, Vol. 211, Brown Dwarfs, ed. E. Martín, 197
- Wilson, J. C., Henderson, C. P., Herter, T. L., et al. 2004, in Ground-based Instrumentation for Astronomy, ed. A. F. M. Moorwood & M. Iye (SPIE-Intl Soc Optical Eng)
- Witte, S., Helling, C., Barman, T., Heidrich, N., & Hauschildt, P. H. 2011, A&A, 529, A44
- Woodgate, B. E., Kimble, R. A., Bowers, C. W., et al. 1998, PASP, 110, 1183
- Wright, E. L., Eisenhardt, P. R. M., Mainzer, A. K., et al. 2010, AJ, 140, 1868
- York, D. G., Adelman, J., Anderson, Jr., J. E., et al. 2000, AJ, 120, 1579
- Zapatero Osorio, M. R., Béjar, V. J. S., Miles-Páez, P. A., et al. 2014, A&A, 568, A6

Table 3
The Sample of Ultracool Dwarfs with Measured SEDs

R.A.	Dec	Designation	Discovery Ref	SpT	SpT Ref
00 00 13.54	+25 54 18.0	SDSS J000013.54+255418.6	1	T4.5	2
00 04 02.88	-64 10 35.8	2MASS J00040288-6410358	3	L1 γ	4
00 04 34.84	-40 44 05.8	LHS 102BC	5	L5	6
00 24 24.63	-01 58 20.1	2MASS J00242463-0158201	7	M9.5	8
00 25 03.65	+47 59 19.1	2MASS J00250365+4759191AB	9	L4	10
00 27 41.97	+05 03 41.7	2MASS J00274197+0503417	11	M9.5 β	8
00 27 55.92	+22 19 32.8	2MASS J00275592+2219328	12	M8	13
00 30 30.13	-14 50 33.3	2MASSW J0030300-145033	14	L7	14
00 33 23.86	-15 21 30.9	2MASS J00332386-1521309	15	L1-L4 β	4,16
00 34 51.57	+05 23 05.0	2MASS J00345157+0523050	17	T6.5	2
00 36 16.17	+18 21 10.4	2MASSW J0036159+182110	18	L3.5	14
00 39 19.10	+21 15 16.4	HD 3651B	19	T7.5	20
00 45 21.43	+16 34 44.6	2MASSW J0045214+1634445	21	L2 β	4
00 47 00.38	+68 03 54.3	WISEP J004701.06+680352.1	22	L7.5p	22
00 50 19.94	-33 22 40.2	2MASS J00501994-3322402	23	T7	24
00 55 39.72	-28 22 42.0	2MASS J00534227-2822410	9	M7.5	9
00 58 42.53	-06 51 23.9	2MASS J00584253-0651239	14	L0 β	14,25
01 02 51.00	-37 37 43.8	LHS 132	26	M8	27
01 03 32.03	+19 35 36.1	2MASSI J0103320+193536	14	L6 β	14
01 07 52.42	-00 41 56.3	SDSSp J010752.33+004156.1	28	L8	29
01 12 35.04	+17 03 55.7	GU Psc b	30	T3.5	31
01 17 47.48	-34 03 25.8	2MASSI J0117474-340325	32	L2:	32
01 41 58.23	-46 33 57.4	2MASS J01415823-4633574	33	L0 γ	4
01 51 41.55	+12 44 30.0	SDSS J015141.69+124429.6	28	T1	2
02 07 42.84	-00 00 56.4	SDSS J020742.48+000056.2	28	T4.5	24
02 10 38.57	-30 15 31.3	2MASS J02103857-3015313	34	L0 γ	35
02 34 00.93	-64 42 06.8	2MASS J02340093-6442068	3	L0 γ	4
02 41 11.51	-03 26 58.7	2MASS J02411151-0326587	9	L0 γ	4
02 43 13.71	-24 53 29.8	2MASSI J0243137-245329	36	T6	24
02 48 41.00	-16 51 21.6	LP 771-21	37	M8	38
02 51 13.27	-00 47 36.4	2MASS J02511327+0047364	39	M8	40
02 53 00.84	+16 52 53.2	2MASS J02530084+1652532	41	M7	42
02 53 59.80	+32 06 37.3	2MASS J02535980+3206373	32	M7 β	43
02 54 09.45	+02 23 59.1	WISEPA J025409.45+022359.1	44	T8	45
02 55 03.57	-47 00 50.9	DENIS-P J0255-4700	46	L8	47
03 18 54.03	-34 21 29.2	2MASS J03185403-3421292	47	L7	47
03 20 59.65	+18 54 23.3	2MASS J03205965+1854233	8	M8	8
03 23 10.02	-46 31 23.7	2MASS J03231002-4631237	48	L0 γ	4
03 25 53.22	+04 25 40.6	SDSS J032553.17+042540.1	49	T5.5	49
03 26 42.25	-21 02 05.7	2MASS J03264225-2102057	15	L5 γ	34
03 28 42.65	+23 02 05.1	2MASSI J0328426+230205	14	L8	14
03 34 12.18	-49 53 32.2	2MASS J03341218-4953322	50	M9	51
03 39 35.22	-35 25 44.0	LP 944-20	37	M9 β	32,16
03 45 43.16	+25 40 23.3	2MASP J0345432+254023	38	L0	52
03 51 00.04	-00 52 45.2	2MASS J03510004-0052452	26	M8	40
03 55 23.37	+11 33 43.7	2MASS J03552337+1133437	48	0355-type γ^a	34
03 57 26.95	-44 17 30.5	DENIS-P J035726.9-441730	53	L0 β	4
04 15 19.54	-09 35 06.6	2MASSI J0415195-093506	36	T8	2
04 23 48.58	-04 14 03.5	SDSSp J042348.57-041403.5	28	L7.5	32
04 28 50.96	-22 53 22.7	2MASS J0428510-225323	54	L0.5	54
04 35 16.13	-16 06 57.5	2MASS J04351612-1606574	37	M7	27
04 36 27.88	-41 14 46.5	2MASS J04362788-4114465	55	M8 $\beta\gamma$	47,16
04 39 01.01	-23 53 08.3	2MASSI J0439010-235308	32	L6.5	32
04 43 37.61	-00 02 05.1	2MASS J04433764+0002040	29	M9 γ	47,16
04 45 53.87	-30 48 20.4	2MASSI J0445538-304820	32	L2	32
04 51 00.93	-34 02 15.0	2MASSI J0451009-340214	32	L0.5	32
05 00 21.00	+03 30 50.1	2MASS J05002100+0330501	48	L4	48
05 01 24.06	-00 10 45.2	2MASS J05012406-0010452	48	L4 γ	4
05 16 09.45	-04 45 49.9	2MASS J05160945-0445499	56	T5.5	24
05 23 38.22	-14 03 02.2	2MASSI J0523382-140302	32	L2.5	32
05 39 52.00	-00 59 01.9	SDSS J053951.99-005902.0	57	L5	57
05 59 19.14	-14 04 48.8	2MASS J05591914-1404488	58	T4.5	2
06 02 30.45	+39 10 59.2	LSR 0602+3910	59	L1 β	35
06 08 52.83	-27 53 58.3	2MASS J06085283-2753583	32	M8.5 γ	60
06 10 34.80	-21 52 00.0	Gl 229B	61	T7p	2
06 11 35.12	-04 10 24.0	WISEP J061135.13-041024.0AB	45	T0	45
06 24 45.95	-45 21 54.8	2MASS J06244595-4521548	48	L5	60
06 41 18.40	-43 22 32.9	2MASS J06411840-4322329	48	L1.5	48
06 52 19.77	-25 34 50.5	DENIS-P J0652197-253450	62	L0	62
07 00 36.64	+31 57 26.6	2MASS J07003664+3157266	63	L3.5:	64
07 07 53.27	-49 00 50.3	2MASS J07075327-4900503	65	M9	65
07 22 27.60	-05 40 38.4	UGPS J072227.51-054031.2	66	T9	66
07 27 18.24	+17 10 01.2	2MASS J0727182+171001	36	T7	2
07 29 00.02	-39 54 04.4	2MASS J07290002-3954043	67	T8pec	67
07 42 01.30	+20 55 19.8	SDSS J074201.41+205520.5	1	T5	24

Table 3
The Sample of Ultracool Dwarfs with Measured SEDs

07 46 42.56	+20 00 32.1	2MASSI J0746425+200032	18	L0.5	14
07 51 16.45	-25 30 43.2	DENIS-P J0751164-253043	62	L2.5	62
07 52 23.90	+16 12 15.7	2MASS J07522390+1612157	37	M7 $\beta\gamma$	68,25
08 17 30.01	-61 55 15.8	DENIS J081730.0-615520	69	T6	69
08 25 19.68	+21 15 52.1	2MASSI J0825196+211552	14	L7.5	14
08 29 49.34	+26 46 33.7	GJ 1111	70	M6.5	71
08 30 08.25	+48 28 48.2	SDSSp J083008.12+482847.4	28	L8	47
08 30 32.56	+09 47 15.4	LHS 2021	26	M6.5	72
08 30 48.78	+01 28 31.1	SDSS J083048.80+012831.1	1	T4.5	24
08 35 42.56	-08 19 23.7	2MASSI J0835425-081923	32	L5	32
08 47 28.72	-15 32 37.2	2MASSI J0847287-153237	32	L2	32
08 53 36.19	-03 29 32.1	2MASS J08533619-0329321	73	M9	74
08 59 25.47	-19 49 26.8	2MASSI J0859254-194926	32	L6	32
09 12 14.69	+14 59 39.6	Gl 337CD	75	L8	75
09 20 12.23	+35 17 42.9	2MASSW J0920122+351742	14	L6.5	14
09 37 34.87	+29 31 40.9	2MASSI J0937347+293142	36	T6p	2
09 39 35.48	-24 48 27.9	2MASS J09393548-2448279	23	T8	24
09 49 08.60	-15 45 48.5	2MASS J09490860-1545485	23	T2	76
10 04 20.66	+50 22 59.6	G 196-3B	77	L3 β	4
10 07 33.69	-45 55 14.7	2MASS J10073369-4555147	67	T5	67
10 10 14.80	-04 06 49.9	2MASSI J1010148-040649	32	L6	32
10 17 07.54	+13 08 39.8	2MASSI J1017075+130839	32	L2:	32
10 21 09.69	-03 04 19.7	SDSS J102109.69-030420.1	78	T3	24
10 22 14.89	+41 14 26.6	HD 89744B	75	L0	75
10 22 48.21	+58 25 45.3	2MASS J10224821+5825453	48	L1 β	4
10 36 53.05	-34 41 38.0	2MASSW J1036530-344138	79	L6	79
10 47 53.85	+21 24 23.4	2MASSI J1047538+212423	80	T6.5	24
10 48 14.64	-39 56 06.2	DENIS-P J1048.0-3956	81	M9	81
10 49 18.91	-53 19 10.0	Luhman 16B	82	T1	83
10 49 18.91	-53 19 10.0	Luhman 16A	82	L8	83
10 56 28.86	+07 00 52.7	2MASS J10562886+0700527	84	M6	74
10 58 47.87	-15 48 17.2	DENIS-P J1058.7-1548	85	L3	52
11 02 09.83	-34 30 35.5	TWA 28	86	M8.5 γ	86
11 10 10.01	+01 16 13.0	SDSS J111010.01+011613.1	28	T5.5p	87
11 12 25.67	+35 48 13.1	Gl 417BC	14	L4.5	14
11 14 51.33	-26 18 23.5	2MASS J11145133-2618235	23	T7.5	24
11 39 51.14	-31 59 21.5	TWA 26	5	M9 γ	60
11 46 34.49	+22 30 52.7	2MASSW J1146345+223053	52	L3	52
11 54 42.23	-34 00 39.0	2MASS J11544223-3400390	53	L0 β	34
11 55 39.52	-37 27 35.0	2MASSW J1155395-372735	79	L2	79
12 07 33.46	-39 32 54.0	TWA 27A	79	M8	88
12 07 33.50	-39 32 54.4	TWA 27	89	M8 γ	79
12 07 48.36	-39 00 04.4	2MASS J12074836-3900043	90	L0 γ	90
12 17 11.10	-03 11 13.1	2MASSI J1217110-031113	80	T7.5	24
12 25 54.32	-27 39 46.6	2MASS J12255432-2739466	80	T6	24
12 28 15.23	-15 47 34.2	DENIS-P J1228.2-1547	85	L5	52
12 37 39.19	+65 26 14.8	2MASS J12373919+6526148	80	T6.5	2
12 39 27.27	+55 15 37.1	2MASSW J1239272+551537	14	L5	14
12 45 14.16	-44 29 07.7	TWA 29	91	M9.5	91
12 54 53.93	-01 22 47.4	SDSSp J125453.90-012247.4	78	T2	2
13 00 41.74	+12 21 14.7	Ross 458C	92	T8	76
13 05 40.19	-25 41 05.9	Kelu-1	93	L2	52
13 20 44.27	+04 09 04.5	2MASS J13204427+0409045	48	L3:	48
13 26 29.81	-00 38 31.4	SDSSp J132629.82-003831.5	57	L8:	57
13 46 46.34	-00 31 50.1	SDSSp J134646.45-003150.4	94	T6.5	24
13 59 55.10	-40 34 58.2	2MASS J13595510-4034582	48	L1	48
14 16 23.94	+13 48 36.3	ULAS J141623.94+134836.3	95	T7.5p	95
14 16 59.86	+50 06 25.8	SDSS J141659.78+500626.4	49	L4.5	49
14 24 39.09	+09 17 10.4	GD 165B	96	L4	52
14 25 27.98	-36 50 22.9	DENIS-P J142527.97-365023.4	97	L3:	48
14 28 43.23	+33 10 39.1	LHS 2924	98	M9	99
14 39 00.31	+18 39 38.5	LHS 377	100	M7sd	101
14 39 28.36	+19 29 14.9	2MASS J14392837+1929150	52	L1	52
14 40 22.93	+13 39 23.0	LSPM J1440+1339	102	M8	27
14 48 25.63	+10 31 59.0	2MASS J14482563+1031590	21	L4:	34
14 56 38.31	-28 09 47.3	LHS 3003	26	M7	8
14 57 14.96	-21 21 47.7	Gliese 570D	103	T7.5	2
15 01 08.18	+22 50 02.0	TVLM 513-46546	104	M8.5	8
15 03 19.61	+25 25 19.6	2MASS J15031961+2525196	105	T5	2
15 04 11.64	+10 27 18.4	CFBDS J150411+102717	49	T7	49
15 06 54.41	+13 21 06.0	2MASSW J1506544+132106	12	L3	12
15 07 47.69	-16 27 38.6	2MASSW J1507476-162738	18	L5	14
15 10 16.85	-02 41 07.8	TVLM 868-110639	104	M9	106
15 11 14.66	+06 07 43.1	SDSS J151114.66+060742.9	49	T2	107
15 15 00.83	+48 47 41.6	2MASSW J1515008+484742	21	L6	9
15 23 22.63	+30 14 56.2	Gl 584C	14	L8	14
15 26 14.05	+20 43 41.4	2MASSI J1526140+204341	14	L7	14

Table 3
The Sample of Ultracool Dwarfs with Measured SEDs

15 39 41.89	-05 20 42.8	DENIS-P J153941.96–052042.4	97	L4	47
15 46 27.19	-33 25 11.2	2MASS J15462718–3325111	36	T5.5	108
15 52 59.06	+29 48 48.5	2MASSW J1552591+294849	21	L0 β	4
15 55 15.73	-09 56 05.5	2MASSW J1555157–095605	79	L1	79
16 15 04.13	+13 40 07.9	2MASS J16150413+1340079	67	T6	67
16 24 14.36	-00 29 15.8	SDSSp J162414.37+002915.6	109	T6	2
16 26 20.34	+39 25 19.0	2MASS J16262034+3925190	110	L4sd	111
16 32 29.11	+19 04 40.7	2MASSW J1632291+190441	52	L8	52
16 47 15.59	+56 32 08.2	WISEPA J164715.59+563208.2	45	L9p	45
16 55 35.29	-08 23 40.1	vB 8	112	M7	99
16 58 03.80	+70 27 01.5	LSPM J1658+7027	12	L1	12
17 26 00.07	+15 38 19.0	2MASSI J1726000+153819	14	L3 β	4
17 28 11.50	+39 48 59.3	2MASSW J1728114+394859	14	L7	14
17 50 32.93	+17 59 04.2	SDSSp J175032.96+175903.9	28	T3.5	2
18 28 35.72	-48 49 04.6	2MASS J18283572–4849046	17	T5.5	108
18 35 37.90	+32 59 54.5	2MASS J18353790+3259545	79	M8.5	113
18 41 08.61	+31 17 27.9	2MASSW J1841086+311727	14	L4p	14
18 43 22.13	+40 40 20.9	2MASS J18432213+4040209	26	M8	9
18 53 21.01	-39 32 54.2	TWA 27B	89	L3VL–G	16
19 16 57.62	+05 09 02.1	Gliese 752 B	112	M8	114
20 00 48.41	-75 23 07.0	2MASS J20004841–7523070	72	M9 γ	35
20 47 49.59	-07 18 18.2	SDSS J204749.61–071818.3	1	T0:	24
20 57 54.09	-02 52 30.2	2MASSI J2057540–025230	32	L1.5	32
21 01 15.44	+17 56 58.6	2MASSW J2101154+175658	14	L7.5	14
21 04 14.91	-10 37 36.9	2MASSI J2104149–103736	32	L2.5	47
21 14 08.02	-22 51 35.8	PSO J318.5338–22.8603	115	L7VL–G	115
21 26 50.40	-81 40 29.3	2MASS J21265040–8140293	48	L3 γ	4
21 27 26.13	-42 15 18.3	HB 2124–4228	116	M7.5	48
21 39 26.77	+02 20 22.7	2MASS J21392676+0220226	48	T1.5	2
21 44 28.46	+14 46 07.8	HN Peg B	20	T2.5	20
21 48 16.33	+40 03 59.4	2MASS J21481628+4003593	117	L6	3
21 50 19.50	-21 19 50.0	2MASS J14112131–2119503	97	M9 β	32,16
22 06 44.98	-42 17 20.8	2MASSW J2206450–421721	14	L4 γ	35
22 08 13.63	+29 21 21.5	2MASSW J2208136+292121	14	L3 γ	4
22 24 43.81	-01 58 52.1	2MASSW J2224438–015852	14	L4.5	14
22 28 28.89	-43 10 26.2	2MASS J22282889–4310262	56	T6	108
22 34 41.62	+40 41 38.8	2MASS J22344161+4041387	32	M6	32
22 37 32.55	+39 22 39.8	2MASS J22373255+3922398	118	M9.5	118
22 44 31.67	+20 43 43.3	2MASSW J2244316+204343	119	L6.5	47
23 06 29.28	-05 02 28.5	2MASS J23062928–0502285	12	M7.5	12
23 22 46.84	-31 33 23.1	2MASS J23224684–3133231	48	L0 β	34,16
23 22 52.99	-61 51 27.5	2MASS J23225299–6151275	48	L2 γ	4
23 51 50.44	-25 37 36.7	2MASS J23515044–2537367	120	M8	121
23 54 09.28	-33 16 26.6	APMPM J2354–3316C	50	M8.5	122
23 56 54.77	-15 53 11.1	2MASSI J2356547–155310	36	T5.5	2

References. — (1) Knapp et al. (2004); (2) Burgasser et al. (2006); (3) Kirkpatrick et al. (2010); (4) Cruz et al. (2009); (5) Goldman et al. (1999); (6) Kirkpatrick et al. (2001a); (7) Cruz & Reid (2002); (8) Kirkpatrick et al. (1995); (9) Cruz et al. (2007); (10) Faherty et al. (2009); (11) Schneider et al. (1991); (12) Gizis et al. (2000); (13) Konopacky et al. (2010); (14) Kirkpatrick et al. (2000); (15) Gizis et al. (2003); (16) Allers & Liu (2013); (17) Burgasser et al. (2004); (18) Reid et al. (2000); (19) Mugrauer et al. (2006); (20) Luhman et al. (2007); (21) Wilson et al. (2003); (22) Gizis et al. (2012); (23) Tinney et al. (2005); (24) Burgasser et al. (2006a); (25) Burgasser (2007); (26) Luyten (1979a); (27) Dieterich et al. (2014); (28) Geballe et al. (2002); (29) Hawley et al. (2002); (30) Naud et al. (2014); (31) Reid et al. (2001); (32) Cruz et al. (2003); (33) Kirkpatrick et al. (2006); (34) Cruz et al. in prep; (35) Faherty et al. in prep; (36) Burgasser et al. (2002b); (37) Luyten (1979b); (38) Kirkpatrick et al. (1997); (39) Metchev et al. (2008); (40) West et al. (2008); (41) Turnbull & Tarter (2003); (42) Henry et al. (2006); (43) Luhman et al. (2009); (44) Scholz et al. (2011); (45) Kirkpatrick et al. (2011); (46) Martín et al. (1999); (47) Kirkpatrick et al. (2008); (48) Reid et al. (2008); (49) Chiu et al. (2006); (50) Pokorny et al. (2004); (51) Phan-Bao et al. (2006); (52) Kirkpatrick et al. (1999); (53) Bouy et al. (2003); (54) Kendall et al. (2003); (55) Phan-Bao et al. (2003); (56) Burgasser et al. (2003b); (57) Fan et al. (2000); (58) Burgasser et al. (2000a); (59) Lépine et al. (2002); (60) Faherty et al. (2012); (61) Nakajima et al. (1995); (62) Phan-Bao et al. (2008); (63) Thorstensen & Kirkpatrick (2003); (64) Kirkpatrick (2005); (65) Ruiz et al. (1991); (66) Lucas et al. (2010); (67)Looper et al. (2007); (68) Reid et al. (2003); (69) Artigau et al. (2010); (70) Giclas et al. (1961); (71) Jenkins et al. (2009); (72) Costa et al. (2006); (73) Reid (1987); (74) Kirkpatrick et al. (1991); (75) Wilson et al. (2001); (76) Burgasser et al. (2010); (77) Rebolo (1998); (78) Leggett et al. (2000); (79) Gizis (2002); (80) Burgasser et al. (1999); (81) Montes et al. (2001); (82) Luhman (2013); (83) Boffin et al. (2013); (84) Giclas et al. (1959); (85) Delfosse et al. (1997); (86) Scholz et al. (2005); (87) Gagné et al. (2015b); (88) Mohanty et al. (2007); (89) Chauvin et al. (2004); (90) Gagné et al. (2014); (91) Liebert et al. (2003); (92) Goldman et al. (2010); (93) Ruiz et al. (1997); (94) Tsvetanov et al. (2000); (95) Burningham et al. (2010); (96) Becklin & Zuckerman (1988); (97) Kendall et al. (2004); (98) Probst & Liebert (1983); (99) Reid & Gizis (2005); (100) Liebert et al. (1979); (101) Gizis (1997); (102) Lépine & Shara (2005); (103) Burgasser et al. (2000b); (104) Tinney et al. (1992); (105) Burgasser et al. (2003a); (106) Kirkpatrick et al. (1994); (107) Albert et al. (2011); (108) Burgasser et al. (2006b); (109) Strauss et al. (1999); (110) Burgasser (2004); (111) Burgasser et al. (2007); (112) van Biesbroeck (1961); (113) Reid et al. (2003); (114) Henry & Kirkpatrick (1990); (115) Liu et al. (2013); (116) Hawkins & Bessell (1988); (117) Looper et al. (2008b); (118) Kirkpatrick et al. (2001b); (119) Dahn et al. (2002); (120) Seifahrt et al. (2010); (121) Schmidt et al. (2007); (122) Scholz et al. (2004).

^a We adopt a type of '0355-type' from Cruz et al. in prep due to this object's spectral uniqueness compared to other M, L and T dwarfs.

Table 4
Optical Photometry for the Sample

Designation	u (0.35 μ m)	g (0.48 μ m)	r (0.62 μ m)	i (0.76 μ m)	z (0.91 μ m)	V (0.54 μ m)	R (0.64 μ m)	I (0.80 μ m)	I_{DENIS} (0.79 μ m)	Refs
0000+2554	24.724 ± 0.927	25.935 ± 0.524	25.613 ± 0.541	22.771 ± 0.441	17.915 ± 0.031	1
0004-4044BC	22.770 ± 0.025	19.238 ± 0.045	16.761 ± 0.012	...	2
0024-0158	21.610 ± 0.304	21.150 ± 0.045	18.517 ± 0.010	15.812 ± 0.005	13.830 ± 0.004	20.010 ± 0.051	17.448 ± 0.016	15.001 ± 0.025	...	1,2
0027+0503	22.421 ± 0.806	22.886 ± 0.181	21.864 ± 0.159	19.849 ± 0.046	17.990 ± 0.045	1
0027+2219	21.273 ± 0.242	19.056 ± 0.010	17.124 ± 0.005	14.017 ± 0.004	12.175 ± 0.004	1
0036+1821	23.778 ± 1.389	22.605 ± 0.137	19.531 ± 0.020	16.810 ± 0.006	14.677 ± 0.005	21.430 ± 0.024	18.318 ± 0.016	15.921 ± 0.022	...	1,2
0045+1634	23.356 ± 1.209	24.047 ± 0.464	20.107 ± 0.031	17.405 ± 0.008	15.248 ± 0.006	1
0047+6803	18.180 ± 0.050	3
0102-3737	18.530 ± 0.021	16.298 ± 0.008	13.881 ± 0.012	13.834 ± 0.030	4,2
0103+1935	24.522 ± 0.967	25.057 ± 0.788	23.855 ± 0.554	21.163 ± 0.097	18.449 ± 0.044	1
0107+0041	23.940 ± 0.857	25.233 ± 0.625	23.869 ± 0.573	20.701 ± 0.081	18.130 ± 0.036	1
0112+1703	21.210 ± 0.070	5
0117-3403	21.038 ± 0.065	18.826 ± 0.028	...	6
0151+1244	23.764 ± 1.035	25.147 ± 0.753	24.254 ± 0.758	22.334 ± 0.324	18.837 ± 0.073	1
0207+0000	25.379 ± 0.474	25.717 ± 0.488	24.337 ± 0.548	24.673 ± 0.484	19.500 ± 0.120	1
0241-0326	23.638 ± 0.818	25.038 ± 0.551	22.382 ± 0.166	20.134 ± 0.046	18.060 ± 0.030	1
0248-1651	24.803 ± 0.809	20.836 ± 0.036	18.842 ± 0.012	15.921 ± 0.005	14.104 ± 0.004	19.970 ± 0.050	17.698 ± 0.015	15.271 ± 0.015	...	1,2
0251+0047	22.784 ± 0.561	22.478 ± 0.093	20.396 ± 0.027	17.296 ± 0.007	15.406 ± 0.007	1
0253+1652	15.140 ± 0.006	13.028 ± 0.004	10.651 ± 0.003	...	2
0253+3206	21.732 ± 0.346	20.870 ± 0.031	18.938 ± 0.014	16.427 ± 0.005	14.926 ± 0.005	1
0320+1854	20.411 ± 0.093	20.021 ± 0.016	17.996 ± 0.007	15.303 ± 0.004	13.448 ± 0.004	1
0325+0425	24.680 ± 1.020	25.330 ± 0.690	25.080 ± 0.690	23.220 ± 0.570	19.210 ± 0.080	7,8
0339-3525	18.700 ± 0.026	16.388 ± 0.007	14.011 ± 0.011	...	2
0351-0052	21.470 ± 0.227	19.083 ± 0.009	17.128 ± 0.005	14.355 ± 0.004	12.743 ± 0.004	18.110 ± 0.053	16.078 ± 0.020	13.801 ± 0.017	...	1,2
0355+1133	23.783 ± 0.844	24.903 ± 0.504	21.605 ± 0.080	18.893 ± 0.015	16.676 ± 0.012	1
0415-0935	23.080 ± 0.090	18.860 ± 0.090	9
0423-0414	24.815 ± 0.576	25.458 ± 0.648	22.604 ± 0.222	19.770 ± 0.080	16.749 ± 0.013	9,1
0428-2253	21.680 ± 0.050	19.178 ± 0.025	16.791 ± 0.017	16.804 ± 0.090	4,2
0435-1606	17.670 ± 0.005	15.488 ± 0.029	13.081 ± 0.030	...	2
0443+0002	24.040 ± 0.678	22.069 ± 0.070	19.598 ± 0.018	16.635 ± 0.006	14.549 ± 0.005	1
0445-3048	16.793 ± 0.100	4
0451-3402	22.110 ± 0.052	19.378 ± 0.015	16.841 ± 0.024	16.873 ± 0.090	4,2
0500+0330	23.010 ± 0.037	19.768 ± 0.026	17.321 ± 0.032	...	2
0501-0010	24.206 ± 0.742	22.903 ± 0.136	20.965 ± 0.048	19.046 ± 0.018	17.226 ± 0.019	1
0523-1403	21.050 ± 0.112	18.708 ± 0.021	16.521 ± 0.012	...	2
0539-0058	23.179 ± 0.918	23.492 ± 0.266	21.236 ± 0.061	18.713 ± 0.015	16.193 ± 0.009	1
0559-1404	20.980 ± 0.090	16.680 ± 0.080	9
0641-4322	16.970 ± 0.080	4
0652-2534	20.770 ± 0.050	18.378 ± 0.005	15.851 ± 0.016	15.963 ± 0.060	4,2
0707-4900	21.090 ± 0.035	18.738 ± 0.023	16.191 ± 0.032	16.374 ± 0.080	4,2
0722-0540	23.950 ± 0.120	19.980 ± 0.100	9
0729-3954	23.810 ± 0.130	19.130 ± 0.090	9
0742+2055	22.986 ± 0.949	24.450 ± 0.539	24.282 ± 0.697	23.634 ± 0.758	18.889 ± 0.089	1
0746+2000	21.173 ± 0.190	21.222 ± 0.037	18.508 ± 0.009	15.742 ± 0.004	13.752 ± 0.004	20.050 ± 0.038	17.418 ± 0.037	14.901 ± 0.038	...	1,2
0751-2530	21.660 ± 0.045	18.858 ± 0.020	16.391 ± 0.005	16.530 ± 0.070	4,2
0752+1612	19.123 ± 0.043	18.041 ± 0.006	16.133 ± 0.004	13.759 ± 0.005	12.218 ± 0.004	1
0825+2115	22.771 ± 0.576	25.134 ± 0.542	23.122 ± 0.309	20.219 ± 0.040	17.272 ± 0.017	6,1
0829+2646	14.940 ± 0.033	12.878 ± 0.005	10.581 ± 0.018	...	2
0830+0128	24.190 ± 1.000	24.810 ± 0.610	25.550 ± 0.510	23.760 ± 0.160	18.880 ± 0.080	9,1
0830+0947	18.881 ± 0.032	19.603 ± 0.012	17.857 ± 0.007	15.354 ± 0.005	13.534 ± 0.005	19.063 ± 0.032	17.158 ± 0.012	14.775 ± 0.003	...	1
0830+4828	24.796 ± 0.689	25.627 ± 0.833	23.354 ± 0.489	20.839 ± 0.085	17.470 ± 0.025	1
0847-1532	21.930 ± 0.068	19.158 ± 0.028	16.861 ± 0.024	...	2
0853-0329	18.940 ± 0.032	16.738 ± 0.015	14.441 ± 0.029	...	2
0920+3517	24.821 ± 1.025	24.591 ± 0.541	23.810 ± 0.593	21.664 ± 0.201	17.813 ± 0.037	1
0937+2931	23.992 ± 1.751	25.478 ± 1.145	23.130 ± 0.644	21.627 ± 0.284	16.961 ± 0.021	1

Filippazzo et al.

Table 4
Optical Photometry for the Sample

Table 4
Optical Photometry for the Sample

1843+4040	19.919 ± 0.067	19.365 ± 0.010	17.359 ± 0.006	14.427 ± 0.004	12.770 ± 0.005	1
2000-7523	21.157 ± 0.008	18.377 ± 0.001	16.120 ± 0.024	15
2047-0718	25.066 ± 0.606	25.386 ± 0.761	23.366 ± 0.455	24.096 ± 0.899	19.160 ± 0.103	16
2057-0252	21.525 ± 0.402	22.857 ± 0.171	20.024 ± 0.029	17.254 ± 0.007	15.213 ± 0.007	1
2101+1756	23.786 ± 0.833	25.093 ± 0.449	24.518 ± 0.658	22.059 ± 0.267	19.145 ± 0.095	1
2104-1037	22.370 ± 0.023	19.458 ± 0.023	17.181 ± 0.021	2
2114-2251	20.260 ± 0.090	17
2126-8140	18.377 ± 0.210	...	4
2139+0220	23.393 ± 0.757	25.235 ± 0.494	24.676 ± 0.470	22.270 ± 0.239	17.651 ± 0.021	1
2208+2921	24.086 ± 0.817	26.042 ± 0.460	23.145 ± 0.342	20.303 ± 0.054	18.265 ± 0.040	1
2224-0158	23.820 ± 0.039	20.258 ± 0.028	17.771 ± 0.022	2
2244+2043	23.631 ± 1.605	25.473 ± 0.756	23.810 ± 0.900	21.208 ± 0.144	18.687 ± 0.072	1
2306-0502	18.798 ± 0.082	16.464 ± 0.065	14.025 ± 0.115	15
2322-3133	16.841 ± 0.120	...	4
2351-2537	15.409 ± 0.050	...	4
2354-3316	16.000 ± 0.060	...	4

References. — (1) Ahn et al. (2012); (2) Dieterich et al. (2014); (3) Gizis et al. (2012); (4) DENIS Consortium (2003); (5) Naud et al. (2014); (6) Liebert & Gizis (2006); (7) Chiu et al. (2006); (8) Abazajian et al. (2009); (9) Leggett et al. (2012); (10) Costa et al. (2005); (11) Boffin et al. (2013); (12) Landolt (2009); (13) Landolt (1992); (14) Reylé et al. (2010); (15) Costa et al. (2006); (16) Adelman-McCarthy et al. (2008); (17) Liu et al. (2013).

Note. — The effective wavelength of each band is given in the table header.

Table 5
NIR Photometry for the Sample

Designation	J ($1.24\mu m$)	H ($1.66\mu m$)	Ks ($2.16\mu m$)	Y_{MKO} ($1.03\mu m$)	J_{MKO} ($1.25\mu m$)	H_{MKO} ($1.64\mu m$)	K_{MKO} ($2.20\mu m$)	Refs
0000+2554	15.063 ± 0.041	14.731 ± 0.074	14.836 ± 0.120	15.810 ± 0.100	14.730 ± 0.030	14.740 ± 0.070	14.820 ± 0.030	1
0003-2822	13.068 ± 0.024	12.376 ± 0.028	11.972 ± 0.025	1
0004-4044BC	13.109 ± 0.024	12.055 ± 0.026	11.396 ± 0.026	1
0004-6410	15.786 ± 0.071	14.831 ± 0.073	14.010 ± 0.045	1
0024-0158	11.992 ± 0.035	11.084 ± 0.022	10.539 ± 0.023	...	11.730 ± 0.030	11.100 ± 0.030	10.530 ± 0.030	1,2
0025+4759	14.840 ± 0.038	13.667 ± 0.031	12.902 ± 0.057	1
0027+0503	16.189 ± 0.093	15.288 ± 0.099	14.964 ± 0.116	1
0027+2219	10.614 ± 0.022	9.967 ± 0.023	9.569 ± 0.017	1
0030-1450	16.278 ± 0.111	15.273 ± 0.100	14.481 ± 0.100	...	16.390 ± 0.030	15.370 ± 0.030	14.490 ± 0.030	3,1
0033-1521	15.286 ± 0.056	14.208 ± 0.051	13.410 ± 0.039	1
0034+0523	15.535 ± 0.045	15.443 ± 0.082	...	16.213 ± 0.007	15.110 ± 0.030	15.550 ± 0.030	15.960 ± 0.030	1
0036+1821	12.466 ± 0.027	11.588 ± 0.030	11.058 ± 0.021	...	12.300 ± 0.030	11.640 ± 0.030	11.040 ± 0.030	1,3
0039+2115	16.595 ± 0.030	16.661 ± 0.030	16.734 ± 0.030	17.220 ± 0.100	16.310 ± 0.030	16.720 ± 0.030	16.860 ± 0.030	4,1
0045+1634	13.059 ± 0.018	12.059 ± 0.034	11.370 ± 0.019	1
0047+6803	15.600 ± 0.070	13.970 ± 0.040	13.050 ± 0.030	1
0050-3322	15.928 ± 0.070	15.838 ± 0.191	15.241 ± 0.185	16.798 ± 0.086	15.650 ± 0.100	16.040 ± 0.100	15.910 ± 0.100	1
0058-0651	14.311 ± 0.026	13.444 ± 0.030	12.904 ± 0.033	1
0102-3737	11.130 ± 0.023	10.479 ± 0.024	10.069 ± 0.021	1
0103+1935	16.288 ± 0.080	14.897 ± 0.056	14.149 ± 0.059	1
0107+0041	15.824 ± 0.058	14.512 ± 0.039	13.709 ± 0.044	...	15.750 ± 0.030	14.560 ± 0.030	13.580 ± 0.030	1,2
0112+1703	19.400 ± 0.050	18.120 ± 0.030	17.700 ± 0.030	17.400 ± 0.030	5
0117-3403	15.178 ± 0.034	14.209 ± 0.038	13.490 ± 0.036	1
0141-4633	14.832 ± 0.041	13.875 ± 0.024	13.100 ± 0.030	1
0151+1244	16.566 ± 0.129	15.603 ± 0.112	15.183 ± 0.189	...	16.250 ± 0.050	15.540 ± 0.050	15.180 ± 0.050	1,2
0207+0000	16.799 ± 0.156	17.940 ± 0.030	16.750 ± 0.010	16.790 ± 0.040	16.710 ± 0.050	1,3
0210-3015	15.066 ± 0.047	14.161 ± 0.044	13.500 ± 0.042	1
0234-6442	15.325 ± 0.062	14.442 ± 0.055	13.850 ± 0.069	1
0241-0326	15.799 ± 0.065	14.811 ± 0.053	14.035 ± 0.050	1
0243-2453	15.381 ± 0.050	15.137 ± 0.109	15.216 ± 0.168	1
0248-1651	12.551 ± 0.022	11.872 ± 0.022	11.422 ± 0.021	...	12.500 ± 0.030	11.810 ± 0.030	11.450 ± 0.030	1,6
0251+0047	13.773 ± 0.026	13.104 ± 0.024	12.681 ± 0.028	1
0253+1652	8.394 ± 0.027	7.883 ± 0.040	7.585 ± 0.046	1
0253+3206	13.616 ± 0.024	12.931 ± 0.022	12.550 ± 0.025	1
0254+0223	16.557 ± 0.156	15.884 ± 0.199	1
0255-4700	13.246 ± 0.027	12.204 ± 0.024	11.558 ± 0.024	1
0318-3421	15.569 ± 0.055	14.346 ± 0.044	13.507 ± 0.039	1
0320+1854	11.759 ± 0.021	11.066 ± 0.022	10.639 ± 0.018	1
0323-4631	15.389 ± 0.069	14.321 ± 0.061	13.700 ± 0.050	1
0325+0425	17.230 ± 0.100	15.900 ± 0.030	16.250 ± 0.030	16.470 ± 0.030	7
0326-2102	16.134 ± 0.094	14.793 ± 0.075	13.922 ± 0.066	1
0328+2302	16.693 ± 0.140	15.547 ± 0.124	14.916 ± 0.113	...	16.350 ± 0.030	15.470 ± 0.030	14.870 ± 0.030	1,2
0334-4953	11.376 ± 0.023	10.823 ± 0.026	10.392 ± 0.022	1
0339-3525	10.725 ± 0.021	10.017 ± 0.021	9.548 ± 0.023	...	10.680 ± 0.030	9.980 ± 0.030	9.530 ± 0.030	1,6
0345+2540	13.997 ± 0.027	13.211 ± 0.030	12.672 ± 0.024	...	13.840 ± 0.050	13.200 ± 0.050	12.660 ± 0.050	1,2
0351-0052	11.302 ± 0.024	10.609 ± 0.022	10.232 ± 0.024	...	11.240 ± 0.030	10.530 ± 0.030	10.150 ± 0.030	1,6
0355+1133	14.050 ± 0.020	12.530 ± 0.029	11.530 ± 0.019	1
0357-4417	14.367 ± 0.029	13.531 ± 0.025	12.910 ± 0.026	1
0415-0935	15.695 ± 0.058	15.537 ± 0.113	15.429 ± 0.201	...	15.320 ± 0.030	15.700 ± 0.030	15.830 ± 0.030	1,3
0423-0414	14.465 ± 0.027	13.463 ± 0.035	12.929 ± 0.034	15.410 ± 0.100	14.300 ± 0.030	...	12.960 ± 0.030	1
0428-2253	13.507 ± 0.023	12.668 ± 0.027	12.118 ± 0.026	1
0435-1606	10.406 ± 0.026	9.779 ± 0.026	9.352 ± 0.021	1
0436-4114	13.097 ± 0.026	12.430 ± 0.022	12.050 ± 0.024	1
0439-2353	14.408 ± 0.029	13.409 ± 0.029	12.816 ± 0.023	1
0443+0002	12.507 ± 0.026	11.804 ± 0.024	11.216 ± 0.021	1
0445-3048	13.393 ± 0.026	12.580 ± 0.024	11.975 ± 0.021	1

Table 5
NIR Photometry for the Sample

0451–3402	13.541 ± 0.023	12.826 ± 0.023	12.294 ± 0.026	1
0500+0330	13.669 ± 0.024	12.683 ± 0.023	12.062 ± 0.024	1
0501–0010	14.982 ± 0.038	13.713 ± 0.034	12.963 ± 0.035	1
0516–0445	15.984 ± 0.079	15.721 ± 0.165	15.486 ± 0.204	15.773 ± 0.011	15.787 ± 0.020	...	1
0523–1403	13.084 ± 0.024	12.220 ± 0.022	11.638 ± 0.027	1
0539–0058	14.033 ± 0.031	13.104 ± 0.026	12.527 ± 0.024	...	13.850 ± 0.030	13.040 ± 0.030	12.400 ± 0.030	1,8
0559–1404	13.802 ± 0.024	13.679 ± 0.044	13.577 ± 0.052	...	13.570 ± 0.030	13.640 ± 0.030	13.730 ± 0.030	1,2
0602+3910	12.300 ± 0.022	11.451 ± 0.021	10.865 ± 0.020	1
0608–2753	13.595 ± 0.028	12.897 ± 0.026	12.371 ± 0.026	1
0610–2152B	15.170 ± 0.100	14.010 ± 0.050	14.360 ± 0.050	14.360 ± 0.050	9,10
0611–0410AB	15.489 ± 0.055	14.645 ± 0.048	14.221 ± 0.070	...	15.398 ± 0.006	14.743 ± 0.005	14.292 ± 0.005	1,11
0619–5803b	16.120 ± 0.100	14.630 ± 0.100	14.080 ± 0.080	12
0624–4521	14.480 ± 0.029	13.335 ± 0.028	12.595 ± 0.026	1
0641–4322	13.751 ± 0.026	12.941 ± 0.034	12.451 ± 0.029	1
0652–2534	12.759 ± 0.023	12.020 ± 0.022	11.516 ± 0.021	1
0700+3157	12.923 ± 0.023	11.947 ± 0.016	11.317 ± 0.023	1
0707–4900	13.228 ± 0.026	12.538 ± 0.030	12.105 ± 0.026	1
0722–0540	16.489 ± 0.128	16.147 ± 0.205	...	17.370 ± 0.020	16.518 ± 0.010	16.896 ± 0.024	17.074 ± 0.078	1
0727+1710	15.600 ± 0.061	15.756 ± 0.171	15.556 ± 0.194	...	15.190 ± 0.030	15.670 ± 0.030	15.690 ± 0.030	1,3
0729–3954	15.920 ± 0.077	15.980 ± 0.180	15.270 ± 0.500	1
0742+2055	16.193 ± 0.091	15.911 ± 0.181	1
0746+2000	11.759 ± 0.020	11.007 ± 0.022	10.468 ± 0.022	1
0751–2530	13.161 ± 0.024	12.495 ± 0.023	11.991 ± 0.024	1
0752+1612	10.879 ± 0.022	10.197 ± 0.022	9.846 ± 0.019	1
0817–6155	13.613 ± 0.024	13.526 ± 0.031	13.520 ± 0.043	1
0825+2115	15.100 ± 0.034	13.792 ± 0.032	13.028 ± 0.026	...	14.890 ± 0.030	13.810 ± 0.030	12.930 ± 0.030	1,2
0829+2646	8.240 ± 0.020	7.620 ± 0.020	7.260 ± 0.020	1
0830+0128	16.290 ± 0.110	16.140 ± 0.213	...	17.203 ± 0.013	16.049 ± 0.009	16.253 ± 0.024	16.350 ± 0.035	1
0830+0947	11.890 ± 0.022	11.165 ± 0.021	10.756 ± 0.023	1
0830+4828	15.444 ± 0.048	14.343 ± 0.037	13.676 ± 0.038	...	15.220 ± 0.030	14.400 ± 0.030	13.680 ± 0.030	1,2
0835–0819	13.169 ± 0.024	11.938 ± 0.024	11.136 ± 0.021	1
0847–1532	13.513 ± 0.026	12.629 ± 0.027	12.061 ± 0.023	1
0853–0329	11.212 ± 0.026	10.469 ± 0.026	9.942 ± 0.024	...	11.180 ± 0.050	10.480 ± 0.050	9.910 ± 0.050	1,13
0859–1949	15.527 ± 0.054	14.436 ± 0.042	13.751 ± 0.058	1
0912+1459	15.512 ± 0.078	14.621 ± 0.081	14.043 ± 0.063	1
0920+3517	15.625 ± 0.063	14.673 ± 0.057	13.979 ± 0.061	1
0937+2931	14.648 ± 0.036	14.703 ± 0.068	15.267 ± 0.130	...	14.290 ± 0.030	14.670 ± 0.030	15.390 ± 0.060	1,3
0939–2448	15.980 ± 0.100	15.970 ± 0.150	16.830 ± 0.090	16.470 ± 0.090	15.610 ± 0.090	15.940 ± 0.090	16.830 ± 0.090	1
0949–1545	16.149 ± 0.117	15.262 ± 0.114	15.227 ± 0.168	1
1004+5022	14.831 ± 0.047	13.648 ± 0.043	12.778 ± 0.034	1
1007–4555	15.653 ± 0.068	15.686 ± 0.122	15.560 ± 0.229	1
1010–0406	15.508 ± 0.059	14.385 ± 0.037	13.619 ± 0.046	1
1017+1308	14.096 ± 0.024	13.284 ± 0.027	12.710 ± 0.023	1
1021–0304	16.253 ± 0.091	15.346 ± 0.101	15.126 ± 0.173	1
1022+4114	14.901 ± 0.037	14.022 ± 0.033	13.608 ± 0.039	1
1022+5825	13.499 ± 0.026	12.642 ± 0.032	12.160 ± 0.025	1
1036–3441	15.620 ± 0.050	14.450 ± 0.040	13.800 ± 0.040	1
1047+2124	15.820 ± 0.060	15.797 ± 0.120	1
1048–3956	9.538 ± 0.022	8.905 ± 0.044	8.447 ± 0.023	1
1049–3519A	11.530 ± 0.040	10.370 ± 0.040	9.440 ± 0.070	14
1049–3519B	11.220 ± 0.040	10.390 ± 0.040	9.730 ± 0.090	14
1056+0700	7.085 ± 0.024	6.482 ± 0.042	6.084 ± 0.017	...	7.030 ± 0.050	6.490 ± 0.050	6.060 ± 0.050	1,2
1058–1548	14.155 ± 0.035	13.226 ± 0.025	12.532 ± 0.029	...	14.120 ± 0.050	13.290 ± 0.050	12.550 ± 0.050	1,2
1102–3430	13.034 ± 0.024	12.356 ± 0.022	11.887 ± 0.024	1
1110+0116	16.343 ± 0.115	15.924 ± 0.144	...	17.338 ± 0.012	16.161 ± 0.008	16.197 ± 0.021	16.051 ± 0.032	1
1112+3548	14.584 ± 0.033	13.499 ± 0.032	12.721 ± 0.028	1
1114–2618	15.858 ± 0.083	15.734 ± 0.123	...	16.440 ± 0.100	15.520 ± 0.050	15.820 ± 0.050	16.540 ± 0.050	1
1139–3159	12.686 ± 0.026	11.996 ± 0.022	11.503 ± 0.023	1

Table 5
NIR Photometry for the Sample

1146+2230	14.165 ± 0.028	13.182 ± 0.026	12.590 ± 0.026	1
1154–3400	14.195 ± 0.033	13.331 ± 0.028	12.850 ± 0.032	1
1155–3727	12.811 ± 0.024	12.040 ± 0.026	11.462 ± 0.021	1
1207–3900	15.500 ± 0.060	14.610 ± 0.050	14.040 ± 0.060	1
1207–3932	12.995 ± 0.026	12.388 ± 0.027	11.945 ± 0.026	1
1207–3932A	13.000 ± 0.030	12.390 ± 0.030	11.950 ± 0.030	1
1207–3932B	20.000 ± 0.200	18.090 ± 0.210	16.930 ± 0.110	15,16
1217–0311	15.860 ± 0.060	15.748 ± 0.119	1
1225–2739	15.260 ± 0.047	15.098 ± 0.081	15.073 ± 0.148	15.840 ± 0.100	14.880 ± 0.030	...	15.280 ± 0.030	...	1
1228–1547	14.378 ± 0.030	13.347 ± 0.032	12.767 ± 0.030	1
1237+6526	16.053 ± 0.087	15.739 ± 0.145	15.560 ± 0.100	15.940 ± 0.100	16.400 ± 0.100	...	1,4
1239+5515	14.711 ± 0.032	13.568 ± 0.033	12.792 ± 0.029	1
1245–4429	14.518 ± 0.032	13.800 ± 0.033	13.369 ± 0.036	1
1254–0122	14.891 ± 0.035	14.090 ± 0.025	13.837 ± 0.054	...	14.660 ± 0.030	14.130 ± 0.030	13.840 ± 0.030	...	1,8
1300+1221	17.715 ± 0.025	16.687 ± 0.015	17.014 ± 0.038	16.903 ± 0.057	...	11
1305–2541	13.414 ± 0.026	12.392 ± 0.025	11.747 ± 0.023	1
1320+0409	15.246 ± 0.046	14.302 ± 0.029	13.621 ± 0.046	1
1326–0038	16.103 ± 0.071	15.050 ± 0.060	14.208 ± 0.067	...	16.210 ± 0.030	15.100 ± 0.030	14.170 ± 0.030	...	3,1
1346–0031	16.000 ± 0.102	15.459 ± 0.118	15.772 ± 0.274	16.630 ± 0.100	15.490 ± 0.050	...	15.730 ± 0.050	...	1
1359–4034	13.645 ± 0.026	13.034 ± 0.028	12.566 ± 0.029	1
1411–2119	12.437 ± 0.022	11.826 ± 0.027	11.330 ± 0.021	1
1416+1348B	18.130 ± 0.020	17.350 ± 0.020	17.620 ± 0.020	18.930 ± 0.170	...	17
1416+5006	16.950 ± 0.171	15.955 ± 0.168	15.597 ± 0.158	...	16.790 ± 0.030	16.030 ± 0.030	15.350 ± 0.030	...	1
1424+0917	15.687 ± 0.078	14.781 ± 0.070	14.169 ± 0.095	17.010 ± 0.100	15.640 ± 0.050	14.750 ± 0.050	14.090 ± 0.050	...	9,2,1
1425–3650	13.747 ± 0.028	12.575 ± 0.022	11.805 ± 0.027	1
1428+3310	11.990 ± 0.020	11.230 ± 0.030	10.740 ± 0.020	1
1439+1839	13.194 ± 0.029	12.733 ± 0.030	12.479 ± 0.025	1,1
1439+1929	12.759 ± 0.019	12.041 ± 0.019	11.546 ± 0.022	...	12.660 ± 0.030	12.050 ± 0.030	11.470 ± 0.030	...	1,2
1440+1339	12.395 ± 0.022	11.710 ± 0.020	11.337 ± 0.020	1
1448+1031	14.556 ± 0.034	13.433 ± 0.033	12.680 ± 0.030	1
1456–2809	9.965 ± 0.026	9.315 ± 0.022	8.928 ± 0.027	...	9.940 ± 0.050	9.430 ± 0.050	8.930 ± 0.050	...	1,2
1457–2121	15.324 ± 0.048	15.268 ± 0.089	15.242 ± 0.156	...	14.820 ± 0.050	15.280 ± 0.050	15.520 ± 0.050	...	1,18
1501+2250	11.866 ± 0.022	11.181 ± 0.030	10.706 ± 0.024	...	11.760 ± 0.050	11.180 ± 0.050	10.690 ± 0.050	...	1,2
1503+2525	13.937 ± 0.024	13.856 ± 0.031	13.963 ± 0.059	...	13.550 ± 0.030	13.900 ± 0.030	13.990 ± 0.030	...	1,3
1504+1027	16.490 ± 0.030	16.920 ± 0.030	17.020 ± 0.030	...	7
1506+1321	13.365 ± 0.023	12.380 ± 0.021	11.741 ± 0.019	1
1507–1627	12.830 ± 0.027	11.895 ± 0.024	11.312 ± 0.026	...	12.700 ± 0.030	11.900 ± 0.030	11.290 ± 0.030	...	1,2
1510–0241	12.614 ± 0.023	11.842 ± 0.022	11.347 ± 0.021	...	12.530 ± 0.030	11.790 ± 0.030	11.340 ± 0.030	...	1,6
1511+0607	16.016 ± 0.079	14.955 ± 0.075	14.544 ± 0.100	...	15.830 ± 0.030	15.160 ± 0.030	14.520 ± 0.030	...	7,1
1515+4847	14.111 ± 0.029	13.099 ± 0.031	12.500 ± 0.024	1
1523+3014	16.056 ± 0.099	14.928 ± 0.081	14.348 ± 0.067	...	15.950 ± 0.050	15.050 ± 0.050	14.350 ± 0.050	...	1,2
1526+2043	15.586 ± 0.055	14.497 ± 0.044	13.922 ± 0.052	1
1539–0520	13.922 ± 0.029	13.060 ± 0.026	12.575 ± 0.029	1
1546–3325	15.631 ± 0.051	15.446 ± 0.092	15.485 ± 0.181	1
1552+2948	13.478 ± 0.026	12.606 ± 0.026	12.022 ± 0.028	1
1555–0956	12.557 ± 0.024	11.984 ± 0.024	11.443 ± 0.019	1
1615+1340	16.350 ± 0.090	16.490 ± 0.250	1
1624+0029	15.494 ± 0.054	15.524 ± 0.100	...	15.200 ± 0.050	15.480 ± 0.050	15.610 ± 0.050	...	1,19	
1626+3925	14.435 ± 0.029	14.533 ± 0.050	14.466 ± 0.074	1
1632+1904	15.867 ± 0.070	14.612 ± 0.038	14.003 ± 0.047	...	15.770 ± 0.050	14.680 ± 0.050	13.970 ± 0.050	...	1,2
1647+5632	16.911 ± 0.180	15.259 ± 0.084	14.611 ± 0.087	1
1655–0823	9.776 ± 0.029	9.201 ± 0.024	8.816 ± 0.023	1
1658+7026	13.288 ± 0.024	12.470 ± 0.032	11.915 ± 0.023	1
1726+1538	15.669 ± 0.065	14.465 ± 0.046	13.659 ± 0.050	1
1728+3948	15.988 ± 0.076	14.756 ± 0.066	13.909 ± 0.048	1
1750+1759	16.340 ± 0.101	15.952 ± 0.132	15.478 ± 0.189	...	16.140 ± 0.050	15.940 ± 0.050	16.020 ± 0.050	...	1,2
1828–4849	15.175 ± 0.056	14.908 ± 0.067	15.181 ± 0.144	1
1835+3259	10.270 ± 0.022	9.617 ± 0.021	9.171 ± 0.018	1

Table 5
NIR Photometry for the Sample

1841+3117	16.158 ± 0.091	14.971 ± 0.066	14.220 ± 0.070	1
1843+4040	11.313 ± 0.022	10.688 ± 0.021	10.308 ± 0.018	...	11.310 ± 0.030	10.700 ± 0.030	10.350 ± 0.030	...	1,6	
1916+0508	9.908 ± 0.025	9.226 ± 0.026	8.765 ± 0.022	1
2000–7523	12.734 ± 0.026	11.967 ± 0.027	11.511 ± 0.026	1
2047–0718	16.700 ± 0.030	15.880 ± 0.030	3	
2057–0252	13.121 ± 0.024	12.268 ± 0.024	11.724 ± 0.025	1
2101+1756	16.853 ± 0.171	15.861 ± 0.182	14.892 ± 0.116	1
2104–1037	13.841 ± 0.029	12.975 ± 0.025	12.369 ± 0.024	1
2114–2251	16.706 ± 0.195	15.720 ± 0.170	14.740 ± 0.118	18.810 ± 0.100	17.150 ± 0.040	15.680 ± 0.020	14.410 ± 0.020	...	1,20	
2126–8140	15.542 ± 0.055	14.405 ± 0.053	13.550 ± 0.041	1
2127–4215	13.321 ± 0.023	12.665 ± 0.025	12.186 ± 0.023	1
2139+0220	15.264 ± 0.049	14.165 ± 0.053	13.582 ± 0.045	1
2144+1446	16.700 ± 0.160	15.550 ± 0.110	15.630 ± 0.250	...	15.860 ± 0.030	15.400 ± 0.030	15.120 ± 0.030	...	1,21	
2148+4003	14.147 ± 0.029	12.783 ± 0.030	11.765 ± 0.023	1
2206–4217	15.555 ± 0.066	14.447 ± 0.061	13.609 ± 0.055	1
2208+2921	15.797 ± 0.085	14.793 ± 0.071	14.148 ± 0.073	1
2224–0158	14.073 ± 0.027	12.818 ± 0.026	12.022 ± 0.023	...	13.890 ± 0.030	12.840 ± 0.030	11.980 ± 0.030	...	1,3	
2228–4310	15.662 ± 0.072	15.363 ± 0.117	15.296 ± 0.206	1
2234+4041	12.573 ± 0.022	11.833 ± 0.021	11.443 ± 0.020	1
2237+3922	13.343 ± 0.022	12.691 ± 0.021	12.178 ± 0.019	1
2244+2043	16.476 ± 0.140	14.999 ± 0.066	14.022 ± 0.073	...	16.330 ± 0.030	15.060 ± 0.030	13.900 ± 0.030	...	1,4	
2306–0502	11.354 ± 0.022	10.718 ± 0.021	10.296 ± 0.023	1
2322–3133	13.577 ± 0.027	12.789 ± 0.023	12.324 ± 0.024	1
2322–6151	15.545 ± 0.062	14.535 ± 0.063	13.860 ± 0.043	1
2351–2537	12.471 ± 0.026	11.725 ± 0.022	11.269 ± 0.026	1
2354–3316	13.051 ± 0.024	12.365 ± 0.027	11.884 ± 0.023	1

References. — (1) Cutri et al. (2003); (2) Leggett et al. (2002b); (3) Knapp et al. (2004); (4) Leggett et al. (2010); (5) Naud et al. (2014); (6) Leggett et al. (1998); (7) Chiu et al. (2006); (8) Leggett et al. (2000); (9) Hewett et al. (2006); (10) Leggett et al. (2002a); (11) Lawrence et al. (2007); (12) Currie et al. (2013); (13) Golimowski et al. (2004); (14) Burgasser et al. (2013); (15) Chauvin et al. (2004); (16) Mohanty et al. (2007); (17) Burningham et al. (2010); (18) Geballe et al. (2001); (19) Strauss et al. (1999); (20) Liu et al. (2013); (21) Luhman et al. (2007).

Note. — The effective wavelength of each band is given in the table header.

Table 6
MIR Photometry for the Sample

Designation	W1 ($3.35\mu m$)	W2 ($4.60\mu m$)	W3 ($11.56\mu m$)	W4 ($22.09\mu m$)	L_{MKO} ($3.75\mu m$)	M_{MKO} ($4.70\mu m$)	[3.6] ($3.51\mu m$)	[4.5] ($4.44\mu m$)	[5.8] ($5.63\mu m$)	[8] ($7.59\mu m$)	Refs
0000+2554	14.211 ± 0.034	13.605 ± 0.050	10.282 ± 0.100	8.831 ± 0.503	13.030 ± 0.030	13.280 ± 0.100	13.720 ± 0.030	13.070 ± 0.030	12.560 ± 0.090	12.500 ± 0.030	1
0003-2822	11.671 ± 0.025	11.502 ± 0.023	10.971 ± 0.099	1
0004-4044BC	10.751 ± 0.023	10.488 ± 0.020	9.868 ± 0.045	10.360 ± 0.010	10.470 ± 0.010	10.140 ± 0.030	10.130 ± 0.020	2,1
0004-6410	13.370 ± 0.025	12.937 ± 0.027	12.178 ± 0.244	1
0024-0158	10.166 ± 0.024	9.900 ± 0.019	9.412 ± 0.039	...	9.780 ± 0.130	...	9.940 ± 0.030	9.910 ± 0.030	9.720 ± 0.010	9.550 ± 0.010	2,3,1
0025+4759	11.740 ± 0.021	11.572 ± 0.020	11.215 ± 0.085	11.485 ± 0.106	4,1
0027+0503	14.618 ± 0.031	14.071 ± 0.045	12.509 ± 0.529	1
0027+2219	9.306 ± 0.022	9.054 ± 0.020	8.789 ± 0.025	8.653 ± 0.371	1
0030-1450	13.657 ± 0.028	13.263 ± 0.034	1
0033-1521	12.801 ± 0.025	12.479 ± 0.027	11.888 ± 0.247	12.540 ± 0.020	12.480 ± 0.020	12.210 ± 0.030	12.040 ± 0.030	5,1
0034+0523	15.061 ± 0.041	12.520 ± 0.028	11.302 ± 0.209	...	13.300 ± 0.040	12.660 ± 0.100	14.100 ± 0.050	12.580 ± 0.030	13.080 ± 0.090	12.250 ± 0.110	1
0036+1821	10.536 ± 0.024	10.245 ± 0.019	9.851 ± 0.054	...	10.080 ± 0.050	10.350 ± 0.070	10.190 ± 0.030	10.240 ± 0.010	10.100 ± 0.020	10.060 ± 0.010	2,6,1
0039+2115	15.380 ± 0.040	13.620 ± 0.020	14.040 ± 0.120	13.450 ± 0.140	7
0045+1634	10.768 ± 0.023	10.393 ± 0.019	9.735 ± 0.040	8.424 ± 0.261	1
0047+6803	11.900 ± 0.020	11.250 ± 0.020	10.140 ± 0.060	1
0050-3322	15.540 ± 0.048	13.550 ± 0.036	11.900 ± 0.213	14.820 ± 0.050	13.570 ± 0.030	13.320 ± 0.170	13.000 ± 0.220	1
0058-0651	12.562 ± 0.025	12.248 ± 0.027	11.692 ± 0.411	1
0102-3737	9.640 ± 0.020	9.620 ± 0.020	9.520 ± 0.020	9.480 ± 0.010	2
0103+1935	13.178 ± 0.024	12.696 ± 0.027	12.234 ± 0.325	1
0107+0041	12.686 ± 0.023	12.174 ± 0.025	11.454 ± 0.202	...	12.060 ± 0.070	6,1
0112+1703	17.170 ± 0.330	15.410 ± 0.220	1
0117-3403	13.028 ± 0.025	12.623 ± 0.026	11.802 ± 0.186	1
0141-4633	12.551 ± 0.024	12.170 ± 0.022	11.921 ± 0.212	12.360 ± 0.020	12.170 ± 0.020	11.950 ± 0.030	11.680 ± 0.030	5,1
0151+1244	14.586 ± 0.031	13.894 ± 0.040	12.476 ± 0.398	...	13.540 ± 0.050	...	14.060 ± 0.020	13.910 ± 0.020	13.620 ± 0.110	13.340 ± 0.180	2,8,1
0207+0000	16.388 ± 0.075	15.073 ± 0.081	15.590 ± 0.060	14.980 ± 0.050	14.670 ± 0.200	14.170 ± 0.190	2,1
0210-3015	13.003 ± 0.026	12.652 ± 0.026	11.934 ± 0.195	1
0234-6442	13.247 ± 0.025	12.905 ± 0.026	12.619 ± 0.279	1
0241-0326	13.638 ± 0.025	13.256 ± 0.029	12.766 ± 0.415	13.390 ± 0.020	13.240 ± 0.020	13.040 ± 0.030	12.770 ± 0.030	5,1
0243-2453	14.670 ± 0.031	12.923 ± 0.027	11.557 ± 0.118	13.900 ± 0.010	12.950 ± 0.030	12.710 ± 0.050	12.270 ± 0.050	2,1
0248-1651	11.171 ± 0.022	10.984 ± 0.021	10.797 ± 0.066	1
0251+0047	12.413 ± 0.023	12.166 ± 0.023	12.141 ± 0.295	1
0253+1652	7.322 ± 0.027	7.057 ± 0.020	6.897 ± 0.017	6.718 ± 0.076	7.120 ± 0.010	7.100 ± 0.020	7.050 ± 0.010	7.020 ± 0.010	2,1
0253+3206	12.324 ± 0.025	12.127 ± 0.024	11.808 ± 0.250	12.170 ± 0.020	12.120 ± 0.020	12.120 ± 0.030	12.010 ± 0.030	5,1
0254+0223	15.760 ± 0.050	12.740 ± 0.030	11.490 ± 0.140	1
0255-4700	10.725 ± 0.022	10.171 ± 0.021	9.163 ± 0.025	8.684 ± 0.276	10.290 ± 0.020	10.200 ± 0.020	9.890 ± 0.010	9.610 ± 0.010	2,1
0318-3421	12.619 ± 0.023	12.126 ± 0.023	11.034 ± 0.067	1
0320+1854	10.347 ± 0.023	10.148 ± 0.020	9.874 ± 0.048	9.087 ± 0.541	1
0323-4631	13.075 ± 0.024	12.665 ± 0.024	11.939 ± 0.160	12.840 ± 0.020	12.680 ± 0.020	12.480 ± 0.030	12.160 ± 0.030	5,1
0325+0425	15.893 ± 0.069	13.783 ± 0.045	12.446 ± 0.443	15.038 ± 0.006	13.776 ± 0.002	1
0326-2102	12.950 ± 0.024	12.435 ± 0.023	12.173 ± 0.203	1
0328+2302	14.152 ± 0.031	13.603 ± 0.041	13.330 ± 0.050	8,1
0334-4953	10.084 ± 0.023	9.726 ± 0.019	9.290 ± 0.032	8.759 ± 0.298	9
0339-3525	9.133 ± 0.022	8.808 ± 0.019	8.272 ± 0.017	7.997 ± 0.110	8.720 ± 0.070	...	8.870 ± 0.030	8.790 ± 0.010	8.590 ± 0.010	8.420 ± 0.010	2,3,1
0345+2540	12.349 ± 0.024	12.093 ± 0.024	12.135 ± 0.440	...	12.010 ± 0.100	1,10
0351-0052	9.968 ± 0.023	9.758 ± 0.021	9.587 ± 0.040	1
0355+1133	10.528 ± 0.023	9.943 ± 0.021	9.294 ± 0.038	9.427 ± 0.017	11,1
0357-4417	12.475 ± 0.023	12.086 ± 0.021	11.600 ± 0.084	12.210 ± 0.020	12.080 ± 0.020	11.860 ± 0.030	11.650 ± 0.030	5,1
0415-0935	15.108 ± 0.041	12.261 ± 0.026	11.132 ± 0.113	...	13.280 ± 0.050	12.820 ± 0.160	14.100 ± 0.030	12.290 ± 0.020	12.870 ± 0.070	12.110 ± 0.050	2,8,1
0423-0414	12.176 ± 0.024	11.578 ± 0.024	10.569 ± 0.079	8.987 ± 0.460	11.450 ± 0.050	11.900 ± 0.070	11.730 ± 0.020	11.580 ± 0.020	11.300 ± 0.010	11.010 ± 0.030	2,1
0428-2253	11.707 ± 0.023	11.470 ± 0.022	11.057 ± 0.099	1
0435-1606	9.081 ± 0.023	8.852 ± 0.021	8.522 ± 0.021	8.443 ± 0.282	1
0436-4114	11.740 ± 0.023	11.460 ± 0.021	11.111 ± 0.082	1
0439-2353	12.039 ± 0.023	11.678 ± 0.023	11.116 ± 0.106	11.276 ± 0.089	12,1
0443+0002	10.826 ± 0.024	10.476 ± 0.021	10.031 ± 0.054	10.550 ± 0.020	10.450 ± 0.020	10.350 ± 0.030	10.220 ± 0.030	5,1
0445-3048	11.573 ± 0.024	11.333 ± 0.023	10.746 ± 0.074	10.983 ± 0.075	12,1

Table 6
MIR Photometry for the Sample

0451–3402	11.920 ± 0.023	11.658 ± 0.022	11.003 ± 0.078	9.047 ± 0.363	11.660 ± 0.040	11.660 ± 0.030	11.520 ± 0.020	11.300 ± 0.040	2,1
0500+0330	11.514 ± 0.022	11.249 ± 0.022	10.962 ± 0.114	1
0501–0010	12.050 ± 0.024	11.518 ± 0.022	10.952 ± 0.107	11.770 ± 0.020	11.520 ± 0.020	11.220 ± 0.030	11.030 ± 0.030	5,1
0516–0445	15.490 ± 0.050	13.665 ± 0.040	11.567 ± 0.161	1
0523–1403	11.156 ± 0.023	10.864 ± 0.020	10.498 ± 0.072	10.698 ± 0.084	12,1
0539–0058	11.869 ± 0.023	11.578 ± 0.021	11.320 ± 0.050	11.870 ± 0.110	11.490 ± 0.020	11.600 ± 0.020	11.350 ± 0.030	11.200 ± 0.040	2,8,6,1
0559–1404	13.386 ± 0.025	11.904 ± 0.023	12.140 ± 0.050	12.150 ± 0.160	12.670 ± 0.030	11.930 ± 0.020	11.730 ± 0.020	11.420 ± 0.020	2,6,1
0602+3910	10.435 ± 0.022	10.124 ± 0.022	9.591 ± 0.040	1
0608–2753	11.976 ± 0.024	11.623 ± 0.021	11.314 ± 0.113	11.750 ± 0.020	11.620 ± 0.020	11.520 ± 0.030	11.440 ± 0.030	5,1
0610–2152B	12.240 ± 0.050	11.740 ± 0.110	8
0611–0410AB	13.559 ± 0.026	12.920 ± 0.027	11.926 ± 0.282	13.069 ± 0.017	12.924 ± 0.017	13,9
0619–5803b	13.220 ± 0.080	14
0624–4521	11.830 ± 0.023	11.478 ± 0.021	10.866 ± 0.067	10.969 ± 0.067	12,1
0641–4322	12.073 ± 0.024	11.784 ± 0.022	11.212 ± 0.086	1
0652–2534	11.120 ± 0.024	10.772 ± 0.021	10.388 ± 0.056	9.314 ± 0.488	1
0700+3157	10.683 ± 0.024	10.377 ± 0.021	9.715 ± 0.042	9.957 ± 0.058	12,1
0707–4900	11.830 ± 0.023	11.558 ± 0.021	11.336 ± 0.102	1
0722–0540	15.147 ± 0.051	12.171 ± 0.026	10.177 ± 0.059	...	13.400 ± 0.300	...	14.280 ± 0.050	12.190 ± 0.040	1
0727+1710	15.000 ± 0.037	14.324 ± 0.054	10.546 ± 0.095	...	13.680 ± 0.050	...	14.410 ± 0.020	13.010 ± 0.010	13.240 ± 0.060	12.640 ± 0.110	2,8,9
0729–3954	14.931 ± 0.034	15.084 ± 0.066	11.555 ± 0.099	9.226 ± 0.324	14.820 ± 0.007	14.808 ± 0.008	1
0742+2055	15.660 ± 0.063	13.778 ± 0.046	11.963 ± 0.278	1
0746+2000	10.125 ± 0.022	9.864 ± 0.021	9.448 ± 0.040	9.860 ± 0.020	9.900 ± 0.040	9.720 ± 0.010	9.570 ± 0.010	2,1
0751–2530	11.670 ± 0.023	11.446 ± 0.023	11.291 ± 0.131	1
0752+1612	9.606 ± 0.023	9.448 ± 0.020	9.256 ± 0.032	8.952 ± 0.460	1
0817–6155	12.960 ± 0.020	11.240 ± 0.020	1
0825+2115	12.083 ± 0.023	11.565 ± 0.021	10.392 ± 0.072	9.027 ± 0.485	11.530 ± 0.030	...	11.700 ± 0.030	11.590 ± 0.010	11.160 ± 0.010	10.930 ± 0.020	2,6,1
0829+2646	7.030 ± 0.031	6.819 ± 0.020	6.630 ± 0.015	6.467 ± 0.058	6.840 ± 0.020	6.840 ± 0.040	6.760 ± 0.050	6.740 ± 0.010	1
0830+0128	15.753 ± 0.062	14.045 ± 0.051	12.583 ± 0.504	1
0830+0947	10.508 ± 0.022	10.331 ± 0.023	10.190 ± 0.098	10.320 ± 0.020	10.350 ± 0.010	10.240 ± 0.010	10.200 ± 0.010	2,1
0830+4828	12.915 ± 0.023	12.461 ± 0.026	11.713 ± 0.206	...	11.980 ± 0.050	12.750 ± 0.150	15,6,1
0835–0819	10.407 ± 0.022	10.048 ± 0.020	9.472 ± 0.039	10.060 ± 0.030	10.060 ± 0.020	9.790 ± 0.010	9.730 ± 0.010	2,1
0847–1532	11.698 ± 0.024	11.453 ± 0.022	11.018 ± 0.092	1
0853–0329	9.624 ± 0.023	9.381 ± 0.020	8.967 ± 0.028	8.756 ± 0.428	9.390 ± 0.070	9.620 ± 0.100	9.410 ± 0.020	9.390 ± 0.030	9.220 ± 0.010	9.130 ± 0.010	2,1,16
0859–1949	12.881 ± 0.024	12.383 ± 0.025	10.990 ± 0.101	9.186 ± 0.501	1
0912+1459	13.225 ± 0.028	12.484 ± 0.028	11.331 ± 0.171	12.500 ± 0.020	12.330 ± 0.020	11.960 ± 0.080	11.950 ± 0.050	2,1
0920+3517	13.207 ± 0.024	12.770 ± 0.026	12.126 ± 0.390	12.210 ± 0.219	17,9
0937+2931	14.073 ± 0.029	11.658 ± 0.022	10.750 ± 0.089	...	12.340 ± 0.050	11.740 ± 0.110	13.100 ± 0.030	11.640 ± 0.040	12.320 ± 0.020	11.730 ± 0.040	2,8,1
0939–2448	15.030 ± 0.040	11.640 ± 0.020	10.714 ± 0.085	13.760 ± 0.040	11.660 ± 0.040	12.950 ± 0.040	11.890 ± 0.040	1,18
0949–1545	14.926 ± 0.035	13.960 ± 0.047	12.480 ± 0.412	1
1004+5022	11.700 ± 0.023	11.134 ± 0.024	10.273 ± 0.068	11.660 ± 0.020	11.470 ± 0.040	11.100 ± 0.060	10.830 ± 0.040	19,9
1007–4555	15.626 ± 0.055	13.870 ± 0.040	12.928 ± 0.502	1
1010–0406	12.891 ± 0.025	12.517 ± 0.029	1
1017+1308	12.288 ± 0.024	12.048 ± 0.025	11.444 ± 0.194	12.030 ± 0.010	12.050 ± 0.030	11.850 ± 0.040	11.700 ± 0.030	2,1
1021–3034	14.736 ± 0.032	13.741 ± 0.040	14.160 ± 0.020	13.800 ± 0.020	13.580 ± 0.120	13.160 ± 0.110	2,1
1022+4114	13.195 ± 0.026	12.949 ± 0.031	1
1022+5825	11.762 ± 0.023	11.496 ± 0.021	11.200 ± 0.109	1
1036–3441	12.965 ± 0.023	12.446 ± 0.025	11.328 ± 0.142	11.892 ± 0.142	17,1
1047+2124	15.428 ± 0.043	12.972 ± 0.032	11.724 ± 0.293	14.390 ± 0.060	12.950 ± 0.040	13.520 ± 0.070	12.910 ± 0.100	2,1
1048–3956	8.103 ± 0.024	7.814 ± 0.021	7.462 ± 0.018	7.226 ± 0.087	1
1049–3519A	8.250 ± 0.040	7.770 ± 0.110	6.940 ± 0.500	1
1049–3519B	9.260 ± 0.100	8.520 ± 0.220	6.960 ± 0.650	1
1056+0700	5.807 ± 0.055	5.487 ± 0.031	5.481 ± 0.015	5.310 ± 0.031	5.710 ± 0.050	5.850 ± 0.060	1,16
1058–1548	12.066 ± 0.025	11.766 ± 0.022	11.417 ± 0.157	...	11.620 ± 0.070	...	11.760 ± 0.020	11.770 ± 0.020	11.600 ± 0.020	11.500 ± 0.020	2,1,10
1102–3430	11.435 ± 0.024	10.793 ± 0.021	9.385 ± 0.033	8.021 ± 0.186	9.920 ± 0.038	20,1
1110+0116	15.531 ± 0.053	13.917 ± 0.047	12.117 ± 0.317	14.710 ± 0.030	13.880 ± 0.020	13.430 ± 0.070	13.210 ± 0.160	2,1
1112+3548	11.968 ± 0.023	11.638 ± 0.022	11.091 ± 0.117	1
1114–2618	15.368 ± 0.051	12.239 ± 0.026	10.973 ± 0.111	14.010 ± 0.030	12.230 ± 0.030	13.220 ± 0.030	12.250 ± 0.040	1
1139–3159	11.155 ± 0.023	10.793 ± 0.020	10.626 ± 0.075	10.607 ± 0.094	21,1

Table 6
MIR Photometry for the Sample

1146+2230	12.014 ± 0.024	11.710 ± 0.023	11.279 ± 0.138	1
1154-3400	12.350 ± 0.023	12.037 ± 0.023	11.369 ± 0.106	1
1155-3727	11.040 ± 0.023	10.733 ± 0.020	10.335 ± 0.056	10.740 ± 0.020	10.750 ± 0.020	10.580 ± 0.010	10.420 ± 0.020	2,1
1207-3900	13.640 ± 0.024	13.204 ± 0.027	12.899 ± 0.506	9
1207-3932	11.556 ± 0.023	11.009 ± 0.020	9.456 ± 0.027	8.029 ± 0.133	11.380 ± 0.100	10.189 ± 0.065	...	22,21,1
1207-3932A	11.556 ± 0.023	11.009 ± 0.020	9.456 ± 0.027	8.029 ± 0.133	11.380 ± 0.100	23,9
1207-3932B	15.280 ± 0.140	23
1217-0311	15.288 ± 0.048	13.197 ± 0.035	11.688 ± 0.243	14.190 ± 0.030	13.230 ± 0.020	13.340 ± 0.070	12.950 ± 0.180	2,1
1225-2739	14.700 ± 0.035	12.707 ± 0.028	11.215 ± 0.118	9.099 ± 0.480	13.220 ± 0.080	13.840 ± 0.020	12.750 ± 0.010	12.840 ± 0.100	12.240 ± 0.020	2,1
1228-1547	12.007 ± 0.022	11.682 ± 0.024	11.171 ± 0.146	1
1237+6526	15.484 ± 0.045	12.946 ± 0.027	12.046 ± 0.235	14.390 ± 0.030	12.930 ± 0.030	13.420 ± 0.060	12.780 ± 0.110	2,1
1239+5515	12.032 ± 0.024	11.663 ± 0.023	11.169 ± 0.093	11.428 ± 0.040	...	1
1245-4429	12.994 ± 0.023	12.623 ± 0.023	1
1254-0122	13.305 ± 0.026	12.396 ± 0.025	10.731 ± 0.091	...	12.250 ± 0.050	12.650 ± 0.210	12.630 ± 0.010	12.390 ± 0.010	11.990 ± 0.050	11.750 ± 0.040	2,6,1
1300+1221	16.009 ± 0.071	13.736 ± 0.040	11.643 ± 0.193	15.365 ± 0.010	13.850 ± 0.004	24,1
1305-2541	11.239 ± 0.024	10.913 ± 0.022	10.376 ± 0.056	10.920 ± 0.050	10.900 ± 0.040	10.730 ± 0.010	10.610 ± 0.020	2,1
1320+0409	13.162 ± 0.026	12.882 ± 0.028	1
1326-0038	13.269 ± 0.024	12.754 ± 0.026	12.364 ± 0.297	1
1346-0031	15.485 ± 0.045	13.567 ± 0.034	12.149 ± 0.257	14.530 ± 0.040	13.600 ± 0.020	13.400 ± 0.110	13.130 ± 0.170	2,1
1359-4034	12.197 ± 0.023	11.916 ± 0.021	11.078 ± 0.079	1
1411-2119	11.077 ± 0.023	10.815 ± 0.022	10.648 ± 0.065	1
1416+1348B	16.118 ± 0.199	12.791 ± 0.038	12.193 ± 0.231	14.690 ± 0.050	12.760 ± 0.030	25,1
1416+5006	14.700 ± 0.028	14.411 ± 0.039	13.194 ± 0.409	1
1424+0917	13.198 ± 0.024	13.042 ± 0.026	12.930 ± 0.070	26,1
1425-3650	10.998 ± 0.022	10.576 ± 0.020	10.010 ± 0.042	10.113 ± 0.053	...	12,1
1428+3310	10.431 ± 0.023	10.168 ± 0.020	9.677 ± 0.030	9.258 ± 0.375	10.160 ± 0.020	10.160 ± 0.010	9.970 ± 0.010	9.810 ± 0.010	2,1
1439+1839	12.298 ± 0.027	12.051 ± 0.025	11.668 ± 0.109	1
1439+1929	11.189 ± 0.023	10.953 ± 0.021	10.529 ± 0.048	...	10.800 ± 0.050	11.130 ± 0.080	10.910 ± 0.020	10.930 ± 0.030	10.820 ± 0.030	10.670 ± 0.020	2,8,6,1
1440+1339	11.092 ± 0.023	10.925 ± 0.020	10.701 ± 0.063	1
1448+1031	11.893 ± 0.022	11.480 ± 0.020	10.849 ± 0.073	11.063 ± 0.076	...	12,1
1456-2809	8.430 ± 0.030	8.470 ± 0.020	8.490 ± 0.010	8.390 ± 0.020	8.360 ± 0.010	2,3
1457-2121	14.824 ± 0.034	12.114 ± 0.023	10.863 ± 0.082	...	12.980 ± 0.050	...	13.800 ± 0.040	12.120 ± 0.020	12.770 ± 0.110	11.970 ± 0.070	27,2,1
1501+2250	10.352 ± 0.022	10.053 ± 0.020	9.618 ± 0.029	9.072 ± 0.338	10.040 ± 0.080	3,1
1503+2525	13.507 ± 0.024	11.723 ± 0.021	10.530 ± 0.049	...	11.910 ± 0.050	11.920 ± 0.040	12.769 ± 0.001	11.757 ± 0.001	11.543 ± 0.040	15,8,24,1
1504+1027	16.215 ± 0.055	14.063 ± 0.039	12.603 ± 0.411	15.440 ± 0.070	14.010 ± 0.050	14.370 ± 0.270	13.760 ± 0.590	7,9
1506+1321	11.176 ± 0.023	10.876 ± 0.021	10.527 ± 0.052	10.860 ± 0.020	10.850 ± 0.060	10.690 ± 0.020	10.580 ± 0.010	2,1
1507-1627	10.670 ± 0.022	10.369 ± 0.021	9.685 ± 0.048	...	9.980 ± 0.030	10.690 ± 0.060	10.270 ± 0.030	10.400 ± 0.020	10.140 ± 0.020	9.990 ± 0.010	2,8,6,9
1510-0241	10.941 ± 0.022	10.674 ± 0.019	10.165 ± 0.053	8.843 ± 0.275	10.680 ± 0.120	3,1
1511+0607	13.676 ± 0.025	13.229 ± 0.029	13.000 ± 0.476	1
1515+4847	11.708 ± 0.023	11.322 ± 0.021	10.515 ± 0.043	11.310 ± 0.020	11.330 ± 0.020	11.070 ± 0.020	10.830 ± 0.020	2,1
1523+3014	13.488 ± 0.024	12.969 ± 0.026	11.793 ± 0.135	...	12.860 ± 0.050	12.205 ± 0.143	...	17,6,1
1526+2043	13.153 ± 0.025	12.826 ± 0.025	12.540 ± 0.267	12.790 ± 0.020	12.870 ± 0.030	12.600 ± 0.110	12.320 ± 0.040	2,1
1539-0520	12.004 ± 0.023	11.744 ± 0.022	11.655 ± 0.230	11.650 ± 0.020	11.750 ± 0.040	11.610 ± 0.050	11.600 ± 0.050	2,1
1546-3325	15.296 ± 0.050	13.445 ± 0.037	11.104 ± 0.127	8.056 ± 0.198	1
1552+2948	11.544 ± 0.023	11.207 ± 0.020	10.664 ± 0.049	1
1555-0956	11.137 ± 0.023	10.857 ± 0.022	10.702 ± 0.106	10.830 ± 0.010	10.880 ± 0.010	10.760 ± 0.020	10.630 ± 0.010	2,1
1615+1340	16.140 ± 0.051	14.114 ± 0.039	9
1624+0029	15.121 ± 0.044	13.085 ± 0.032	12.496 ± 0.446	...	13.600 ± 0.040	...	14.300 ± 0.030	13.080 ± 0.020	13.250 ± 0.080	12.840 ± 0.090	2,6,1
1626+3925	13.461 ± 0.025	13.091 ± 0.028	1
1632+1904	13.124 ± 0.025	12.617 ± 0.025	11.986 ± 0.237	...	12.540 ± 0.050	13.070 ± 0.150	12.700 ± 0.030	12.650 ± 0.020	12.240 ± 0.040	12.000 ± 0.040	2,15,6,1
1647+5632	13.604 ± 0.024	13.086 ± 0.023	12.059 ± 0.094	13.253 ± 0.017	13.128 ± 0.017	28,1
1655-0823	8.588 ± 0.023	8.365 ± 0.021	8.132 ± 0.022	7.857 ± 0.181	8.370 ± 0.020	8.380 ± 0.010	8.280 ± 0.020	8.240 ± 0.020	2,1
1658+7026	11.604 ± 0.023	11.384 ± 0.022	10.829 ± 0.047	11.095 ± 0.061	...	17,1
1726+1538	13.071 ± 0.025	12.694 ± 0.026	11.556 ± 0.157	12.760 ± 0.020	12.640 ± 0.020	12.410 ± 0.030	12.200 ± 0.030	5,1
1728+3948	13.107 ± 0.024	12.639 ± 0.024	11.865 ± 0.125	12.720 ± 0.020	12.660 ± 0.010	12.290 ± 0.040	12.130 ± 0.030	2,1
1750+1759	15.801 ± 0.058	14.480 ± 0.060	14.950 ± 0.030	14.460 ± 0.020	14.150 ± 0.230	13.930 ± 0.230	2,1
1828-4849	14.508 ± 0.036	12.773 ± 0.029	11.408 ± 0.162	1
1835+3259	8.803 ± 0.022	8.539 ± 0.019	8.160 ± 0.019	7.886 ± 0.132	8.550 ± 0.020	8.550 ± 0.010	8.390 ± 0.010	8.290 ± 0.010	2,1

Table 6
MIR Photometry for the Sample

1841+3117	13.596 ± 0.029	13.261 ± 0.029	12.121 ± 0.193	1
1843+4040	10.072 ± 0.022	9.874 ± 0.018	9.618 ± 0.029	9.332 ± 0.434	9.780 ± 0.040	3,1
1916+0508	8.465 ± 0.023	8.249 ± 0.020	8.080 ± 0.022	8.290 ± 0.020	8.300 ± 0.030	8.150 ± 0.010	8.140 ± 0.010	2,1
2000–7523	11.108 ± 0.023	10.797 ± 0.020	10.550 ± 0.069	1
2047–0718	14.481 ± 0.035	14.048 ± 0.051	13.800 ± 0.050	8,1
2057–0252	11.261 ± 0.022	10.981 ± 0.020	10.431 ± 0.079	10.647 ± 0.082	...	12,1
2101+1756	14.099 ± 0.033	13.558 ± 0.037	12.616 ± 0.455	1
2104–1037	11.915 ± 0.023	11.681 ± 0.023	10.445 ± 0.232	11.550 ± 0.030	11.620 ± 0.010	11.440 ± 0.030	11.290 ± 0.040	2,1
2114–2251	13.237 ± 0.024	12.503 ± 0.027	11.946 ± 0.413	1
2126–8140	12.910 ± 0.024	12.472 ± 0.023	11.885 ± 0.161	1
2127–4215	11.905 ± 0.024	11.671 ± 0.021	11.361 ± 0.155	1
2139+0220	12.718 ± 0.023	11.928 ± 0.024	10.665 ± 0.105	1
2144+1446	13.720 ± 0.040	13.390 ± 0.020	13.080 ± 0.100	12.580 ± 0.110	29
2148+4003	10.739 ± 0.023	10.235 ± 0.021	9.657 ± 0.037	9.200 ± 0.439	1
2206–4217	12.823 ± 0.024	12.376 ± 0.025	11.887 ± 0.222	1
2208+2921	13.354 ± 0.027	12.888 ± 0.027	12.584 ± 0.391	13.080 ± 0.020	12.890 ± 0.020	12.620 ± 0.030	12.330 ± 0.030	5,1
2224–0158	11.361 ± 0.023	11.121 ± 0.022	10.648 ± 0.093	...	10.900 ± 0.050	11.320 ± 0.050	11.050 ± 0.020	11.140 ± 0.020	10.850 ± 0.010	10.810 ± 0.020	2,8,1
2228–4310	15.274 ± 0.050	13.328 ± 0.035	11.964 ± 0.244	1
2234+4041	10.916 ± 0.024	10.331 ± 0.021	8.358 ± 0.037	5.685 ± 0.059	1
2237+3922	11.708 ± 0.024	11.426 ± 0.021	11.012 ± 0.091	1
2244+2043	12.777 ± 0.024	12.108 ± 0.024	11.136 ± 0.115	...	12.110 ± 0.030	11.900 ± 0.030	12.350 ± 0.030	12.110 ± 0.030	11.590 ± 0.030	7,1	
2306–0502	10.042 ± 0.023	9.799 ± 0.020	9.528 ± 0.041	1
2322–3133	11.974 ± 0.023	11.707 ± 0.023	11.253 ± 0.128	9
2322–6151	13.243 ± 0.026	12.841 ± 0.029	12.679 ± 0.391	1
2351–2537	10.934 ± 0.022	10.678 ± 0.022	10.303 ± 0.065	10.514 ± 0.071	...	12,1
2354–3316	11.613 ± 0.023	11.387 ± 0.021	11.213 ± 0.153	1

References. — (1) Cutri & et al. (2012); (2) Patten et al. (2006); (3) Leggett et al. (1998); (4) Cushing et al. (2008); (5) Luhman et al. (2009); (6) Leggett et al. (2002b); (7) Leggett et al. (2010); (8) Golimowski et al. (2004); (9) Cutri & et al. (2014); (10) Leggett et al. (2001); (11) Burgasser et al. (2008a); (12) Cruz et al. (2004a); (13) Kirkpatrick et al. (2011); (14) Currie et al. (2013); (15) Leggett et al. (2007); (16) Reid & Cruz (2002); (17) Houck & Roellig (2004a); (18) Burgasser et al. (2008c); (19) Osorio et al. (2010); (20) Houck et al. (2006); (21) Houck & Watson (2004); (22) Jayawardhana et al. (2003); (23) Chauvin et al. (2004); (24) Griffith et al. (2012); (25) Birmingham et al. (2010); (26) Jones et al. (1996); (27) Geballe et al. (2001); (28) Dupuy & Liu (2012); (29) Luhman et al. (2007).

Note. — The effective wavelength of each band is given in the table header.

Table 7
Optical, NIR and MIR Spectra Used to Construct SEDs

Designation	OPT	OPT Refs	NIR	NIR Refs	MIR	MIR Refs
0000+2554	SpeX – Prism	1	IRS	2
0003–2822	KPNO 4m – R–C Spec	3	SpeX – Prism	4
0004–4044BC	LRIS	5	SpeX – Prism	6	IRS	7
0004–6410	FIRE	8
0024–0158	KPNO 4m – R–C Spec	3	SpeX – SXD/LXD1.9	9,10	IRS	11
0025+4759	SpeX – Prism	4	IRS	12
0027+0503	LRIS	13	SpeX – Prism	4
0027+2219	KPNO 4m – R–C Spec	14	SpeX – Prism	4
0030–1450	LRIS	5	SpeX – Prism	15
0033–1521	GMOS–S	4	SpeX – Prism	4
0034+0523	SpeX – Prism	16
0036+1821	KPNO 4m – R–C Spec	4	SpeX – SXD	9	IRS	11
0039+2115	SpeX – Prism	17
0045+1634	KPNO 4m – R–C Spec	18	SpeX – Prism	4
0047+6803	SpeX – Prism	19
0050–3322	SpeX – Prism	20
0058–0651	SpeX – 1/2/3/4/5/6/7	21
0102–3737	CTIO 1.5m – R–C Spec	3	SpeX – Prism	21
0103+1935	SpeX – Prism	4
0107+0041	FORS	22	SpeX – Prism	15
0112+1703	GNIRS	23
0117–3403	LRIS	4	SpeX – Prism	4
0141–4633	GMOS–S	18	SpeX – Prism	24
0151+1244	SpeX – Prism	16
0207+0000	SpeX – Prism	1
0210–3015	LRIS	4	SpeX – Prism	4
0234–6442	FIRE	8
0241–0326	GMOS–S	25	SpeX – Prism	4
0243–2453	SpeX – Prism	16
0248–1651	LRIS	26	SpeX – Prism	4
0251+0047	KPNO 4m – R–C Spec	27	SpeX – Prism	21
0253+1652	SpeX – Prism	28
0253+3206	KPNO 4m – R–C Spec	14	SpeX – SXD	4
0254+0223	SpeX – Prism	29
0255–4700	LRIS	30	SpeX – SXD	9	IRS	11
0318–3421	GMOS–S	25	SpeX – Prism	25
0320+1854	GoldCam	14	SpeX – SXD/LXD1.9	9
0323–4631	GMOS–S	31	SpeX – Prism	4
0325+0425	SpeX – Prism	32
0326–2102	CTIO 4m – R–C Spec	14	SpeX – Prism	4
0328+2302	SpeX – Prism	33
0334–4953	SpeX – Prism	4
0339–3525	LRIS	34	SpeX – SXD/LXD1.9	9,10
0345+2540	LRIS	35	SpeX – Prism	4
0351–0052	KPNO 4m – R–C Spec	4	SpeX – Prism	4
0355+1133	GMOS–N	18	SpeX – SXD	4	IRS	36
0357–4417	LRIS	30	SpeX – Prism	4
0415–0935	LRIS	37	SpeX – Prism	16
0423–0414	SpeX – Prism	38	IRS	11
0428–2253	KPNO 4m – R–C Spec	39	SpeX – Prism	21
0435–1606	GoldCam	40	SpeX – Prism	4
0436–4114	CTIO 4m – R–C Spec	41	SpeX – Prism	4
0439–2353	CTIO 4m – R–C Spec	4	SpeX – Prism	4	IRS	42
0443+0002	CTIO 1.5m – R–C Spec	4	SpeX – Prism	4
0445–3048	CTIO 4m – R–C Spec	4	SpeX – Prism	4	IRS	42
0451–3402	CTIO 4m – R–C Spec	14	SpeX – Prism	21
0500+0330	KPNO 4m – R–C Spec	31	SpeX – Prism	21
0501–0010	LRIS	4	SpeX – Prism	43	IRS	36
0516–0445	SpeX – Prism	28
0523–1403	CTIO 4m – R–C Spec	14	SpeX – Prism	4	IRS	42
0539–0058	DIS	44	SpeX – SXD	10	IRS	11
0559–1404	LRIS	37	SpeX – Prism	1	IRS	11
0602+3910	SpeX – Prism	21
0608–2753	CTIO 4m – R–C Spec	14	SpeX – SXD	4
0610–2152B	STIS/CGS4/NIRC	45
0611–0410AB	SpeX – Prism	46
0619–5803b	SINFONI	47
0624–4521	LDSS3	4	SpeX – Prism	4	IRS	42
0641–4322	CTIO 4m – R–C Spec	48	SpeX – Prism	21
0652–2534	SpeX – Prism	4
0700+3157	KPNO 4m – R–C Spec	31	SpeX – Prism	4	IRS	42
0707–4900	SpeX – Prism	21
0722–0540	SpeX – Prism	29
0727+1710	LRIS	37	SpeX – Prism	1
0729–3954	SpeX – Prism	49

Table 7
Optical, NIR and MIR Spectra Used to Construct SEDs

0742+2055	SpeX – Prism	50
0746+2000	KPNO 4m – R–C Spec	14	SpeX – SXD/LXD1.9	9	IRS	7
0751–2530	SpeX – Prism	4
0752+1612	KPNO 4m – R–C Spec	40	SpeX – Prism	51
0817–6155	OSIRIS	52
0825+2115	LRIS	5	SpeX – SXD	9	IRS	11
0829+2646	SpeX – SXD/LXD2.3	9	IRS	53
0830+0128	SpeX – Prism	50
0830+0947	KPNO 4m – R–C Spec	3	SpeX – Prism	21
0830+4828	LRIS	30	SpeX – Prism	4
0835–0819	CTIO 4m – R–C Spec	14	SpeX – Prism	4
0847–1532	KPNO 4m – R–C Spec	14	SpeX – Prism	4
0853–0329	CTIO 4m – R–C Spec	31	SpeX – SXD	9
0859–1949	CTIO 4m – R–C Spec	4	SpeX – Prism	4
0912+1459	LRIS	54	SpeX – Prism	50	IRS	11
0920+3517	SpeX – Prism	55
0937+2931	LRIS	37	SpeX – Prism	1	IRS	11
0939–2448	SpeX – Prism	1	IRS	56
0949–1545	SpeX – Prism	1
1004+5022	SpeX – Prism	4
1007–4555	SpeX – Prism	49
1010–0406	CTIO 4m – R–C Spec	4	SpeX – Prism	4
1017+1308	KPNO 4m – R–C Spec	4	SpeX – Prism	43	IRS	12
1021–0304	SpeX – Prism	1	IRS	11
1022+4114	SpeX – Prism	28
1022+5825	KPNO 4m – R–C Spec	18	SpeX – Prism	4
1036–3441	SpeX – 1/2/3/4/5/6/7	50	IRS	7
1047+2124	LRIS	37	SpeX – Prism	28
1048–3956	CTIO 1.5m – R–C Spec	31	SpeX – SXD/LXD1.9	9
1049–3519A	MagE	57	FIRE	57
1049–3519B	MagE	57	FIRE	57
1056+0700	KPNO 4m – R–C Spec	31	SpeX – SXD/LXD2.3	9,10
1058–1548	LRIS	35	SpeX – Prism	4
1102–3430	SpeX – Prism	51	IRS	58
1110+0116	SpeX – Prism	20
1112+3548	SpeX – Prism	59
1114–2618	SpeX – Prism	20
1139–3159	CTIO 4m – R–C Spec	31	SpeX – Prism	49	IRS	60
1146+2230	LRIS	35	SpeX – Prism	50
1154–3400	LRIS	30	SpeX – Prism	4
1155–3727	CTIO 4m – R–C Spec	31	TripleSpec	43
1207–3900	MagE	61	SpeX – Prism	61
1207–3932	SpeX – SXD	51	IRS	60
1207–3932A	SINFONI	47
1207–3932B	SINFONI	62
1217–0311	SpeX – Prism	20	IRS	11
1225–2739	LRIS	37	SpeX – Prism	16	IRS	11
1228–1547	LRIS	35	SpeX – Prism	15
1237+6526	LRIS	63	SpeX – Prism	64	IRS	11
1239+5515	SpeX – Prism	50	IRS	7
1245–4429	SpeX – Prism	65
1254–0122	LRIS	37	SpeX – Prism	16	IRS	11
1300+1221	IRCS/NIRI	66
1305–2541	LRIS	35	SpeX – SXD/LXD1.9	9	IRS	11
1320+0409	SpeX – Prism	21
1326–0038	SpeX – Prism	4
1346–0031	LRIS	63	SpeX – Prism	20
1359–4034	CTIO 4m – R–C Spec	31	SpeX – Prism	21
1411–2119	CTIO 4m – R–C Spec	14	FIRE	8
1416+1348B	SpeX – Prism	67
1416+5006	SpeX – Prism	32
1424+0917	SpeX – Prism	21
1425–3650	CTIO 4m – R–C Spec	31	SpeX – Prism	21	IRS	42
1428+3310	KPNO 4m – R–C Spec	31	SpeX – SXD	9,10
1439+1839	SpeX – Prism	16
1439+1929	LRIS	35	SpeX – SXD	9	IRS	11
1440+1339	GoldCam	14	SpeX – Prism	21
1448+1031	CTIO 4m – R–C Spec	31	SpeX – Prism	4	IRS	42
1456–2809	GoldCam	14	SpeX – Prism	21	IRS	11
1457–2121	LRIS	37	SpeX – Prism	16	IRS	11
1501+2250	KPNO 4m – R–C Spec	3	SpeX – Prism	21
1503+2525	LRIS	37	SpeX – Prism	16	IRS	7
1504+1027	CGS4/UIST	32
1506+1321	LRIS	68	SpeX – SXD/LXD1.9	10	IRS	11
1507–1627	LRIS	69	SpeX – SXD/LXD1.9	9	IRS	11
1510–0241	GoldCam	14	SpeX – Prism	21
1511+0607	SpeX – Prism	50

Table 7
Optical, NIR and MIR Spectra Used to Construct SEDs

1515+4847	KPNO 4m – R–C Spec	25	SpeX – Prism	4	IRS	11
1523+3014	LRIS	70	SpeX – Prism	50	IRS	11
1526+2043	LRIS	5	SpeX – Prism	16	IRS	11
1539–0520	KPNO 4m – R–C Spec	31	SpeX – Prism	21
1546–3325	SpeX – Prism	49
1552+2948	KPNO 4m – R–C Spec	31	SpeX – Prism	4
1555–0956	SpeX – Prism	21
1615+1340	SpeX – Prism	49
1624+0029	LRIS	63	SpeX – Prism	1	IRS	11
1626+3925	SpeX – Prism	16
1632+1904	SpeX – Prism	4
1647+5632	SpeX – Prism	46
1655–0823	KPNO 4m – R–C Spec	3	SpeX – SXD/LXD1.9	9,10
1658+7026	GoldCam	3	TripleSpec	43	IRS	7
1726+1538	LRIS	5	SpeX – Prism	4
1728+3948	LRIS	5	SpeX – Prism	4	IRS	11
1750+1759	SpeX – Prism	16
1828–4849	SpeX – Prism	16
1835+3259	KPNO 4m – R–C Spec	4	SpeX – Prism	4
1841+3117	LRIS	5	SpeX – Prism	4
1843+4040	GoldCam	71	SpeX – Prism	4
1916+0508	KPNO 4m – R–C Spec	3	SpeX – Prism/SXD	9,10	IRS	72
2000–7523	CTIO 4m – R–C Spec	31	FIRE	8
2047–0718	SpeX – Prism	50
2057–0252	KPNO 4m – R–C Spec	4	SpeX – Prism	4	IRS	42
2101+1756	SpeX – Prism	50
2104–1037	KPNO 4m – R–C Spec	14	SpeX – Prism	4
2114–2251	GNIRS	23
2126–8140	GMOS–S	31	ISAAC	73
2127–4215	CTIO 4m – R–C Spec	3	SpeX – Prism	21
2139+0220	SpeX – Prism	4	IRS	43
2144+1446	SpeX – Prism	74
2148+4003	SpeX/FOCAS/IRS	75
2206–4217	LRIS	5	SpeX – Prism	4
2208+2921	FOCAS	18	SpeX – Prism	4
2224–0158	LRIS	5	SpeX – Prism	4	IRS	11
2228–4310	SpeX – Prism	16
2234+4041	GoldCam	14	SpeX – SXD	4
2237+3922	SpeX – Prism	4
2244+2043	LRIS	30	SpeX – Prism	76
2306–0502	KPNO 4m – R–C Spec	3	SpeX – Prism	4
2322–3133	CTIO 4m – R–C Spec	31	SpeX – Prism	43
2322–6151	GMOS–S	31	ISAAC	73
2351–2537	SpeX – Prism	4	IRS	42
2354–3316	CTIO 4m – R–C Spec	31	SpeX – Prism	33

References. — (1) Burgasser et al. (2006a); (2) Stephens et al. (2009); (3) Cruz et al. (2007); (4) Cruz et al. in prep; (5) Kirkpatrick et al. (2000); (6) Burgasser et al. (2007); (7) Houck & Roellig (2004a); (8) Faherty et al. in prep; (9) Rayner et al. (2009); (10) Cushing et al. (2005b); (11) Cushing et al. (2006); (12) Cushing et al. (2008); (13) Liebert et al. (1999); (14) Cruz et al. (2003); (15) Burgasser et al. (2010); (16) Burgasser (2004); (17) Burgasser (2007); (18) Cruz et al. (2009); (19) Gizis et al. (2012); (20) Burgasser et al. (2006); (21) Gagliuffi et al. (2014); (22) Scholz et al. (2009); (23) Liu et al. (2013); (24) Kirkpatrick et al. (2006); (25) Cushing et al. (2009); (26) Kirkpatrick et al. (1997); (27) Tinney (1993); (28) Burgasser et al. (2008b); (29) Mace et al. (2013); (30) Kirkpatrick et al. (2008); (31) Reid et al. (2008); (32) Chiu et al. (2006); (33) Burgasser et al. (2008c); (34) Kirkpatrick et al. (2010); (35) Kirkpatrick et al. (1999); (36) Burgasser et al. (2008a); (37) Burgasser et al. (2003a); (38) Cruz et al. (2004b); (39) Kendall et al. (2003); (40) Luyten (1979b); (41) Phan-Bao et al. (2003); (42) Cruz et al. (2004a); (43) This work; (44) Fan et al. (2000); (45) Golimowski et al. (2004); (46) Kirkpatrick et al. (2011); (47) Bonnefoy et al. (2014); (48) Deacon et al. (2005); (49)Looper et al. (2007); (50) Burgasser et al. (2010a); (51) Allers & Liu (2013); (52) Artigau et al. (2010); (53) Cushing et al. (2005a); (54) Wilson et al. (2001); (55) Ruiz et al. (2001); (56) Burgasser et al. (2005); (57) Faherty et al. (2014); (58) Houck et al. (2006); (59) Patience et al. (2012); (60) Houck & Watson (2004); (61) Gagné et al. (2014); (62) Patience et al. (2010); (63) Burgasser et al. (2000); (64) Liebert & Burgasser (2007); (65) Looper et al. (2007); (66) Burningham et al. (2011); (67) Burgasser et al. (2010b); (68) Gizis et al. (2000); (69) Reid et al. (2000); (70) Kirkpatrick et al. (2001a); (71) Luyten (1979a); (72) Houck & Roellig (2004b); (73) Manjavacas et al. (2014); (74) Luhman et al. (2007); (75) Looper et al. (2008a); (76) Looper et al. (2008b).

Table 8
Comparison of L_{bol} Values with the Literature

Designation	π (mas)	$\log(L_*/L_\odot)$	$\log(L_{*,Lit}/L_\odot)$	Refs
0004–4044BC	104.7 ± 11.4	-4.046 ± 0.095	-4.05 ± 0.1	1,2
0024–0158	86.6 ± 4	-3.439 ± 0.040	-3.505 ± 0.042	3,4
...	86.6 ± 4	-3.439 ± 0.040	-3.51 ± 0.04	3,5
0024–0158	84.2 ± 2.6	-3.415 ± 0.027	-3.45 ± 0.03	1,2
0030–1450	37.42 ± 4.5	-4.373 ± 0.106	-4.36 ± 0.12	6,6
0033–1521	24.8 ± 2.5	-3.611 ± 0.088	-3.55 ± 0.15	7,7
0036+1821	114.2 ± 0.8	-3.928 ± 0.006	-3.97 ± 0.02	8,2
...	114.2 ± 0.8	-3.928 ± 0.006	-3.97 ± 0.01	8,5
0036+1821	114.2 ± 0.8	-3.928 ± 0.006	-3.95 ± 0.011	8,4
0039+2115	90.09 ± 0.81	-5.555 ± 0.012	-5.6 ± 0.05	9,9
0045+1634	57.3 ± 2	-3.412 ± 0.031	-3.53 ± 0.08	7,7
0047+6803	82 ± 3	-4.440 ± 0.034	-4.45 ± 0.04	10,10
0107+0041	64.13 ± 4.51	-4.475 ± 0.062	-4.47 ± 0.06	6,2
...	64.13 ± 4.51	-4.475 ± 0.062	-4.52 ± 0.08	6,6
0112+1703	20.83 ± 2.17	-4.870 ± 0.096	-4.75 ± 0.15	11,11
0151+1244	46.73 ± 3.37	-4.736 ± 0.063	-4.68 ± 0.12	6,6
...	46.73 ± 3.37	-4.736 ± 0.063	-4.68 ± 0.07	6,2
0207+0000	34.85 ± 9.87	-4.885 ± 0.246	-4.82 ± 0.25	6,2
...	34.85 ± 9.87	-4.885 ± 0.246	-4.76 ± 0.26	6,6
0241–0326	21.4 ± 2.6	-3.715 ± 0.106	-3.75 ± 0.17	7,7
0243–2453	93.62 ± 3.63	-5.129 ± 0.034	-5.03 ± 0.1	6,6
...	93.62 ± 3.63	-5.129 ± 0.034	-5.08 ± 0.06	6,2
0248–1651	61.6 ± 5.4	-3.463 ± 0.076	-3.507 ± 0.076	12,4
0253+1652	259.41 ± 0.89	-3.118 ± 0.003	-3.137 ± 0.013	13,14,4
0328+2302	33.13 ± 4.2	-4.373 ± 0.111	-4.37 ± 0.12	6,6
...	33.13 ± 4.2	-4.373 ± 0.111	-4.31 ± 0.11	6,2
0339–3525	201.4 ± 4.2	-3.783 ± 0.018	-3.81 ± 0.02	8,5
...	155.89 ± 1.03	-3.561 ± 0.006	-3.579 ± 0.01	4,4
0345+2540	37.1 ± 0.5	-3.603 ± 0.013	-3.6 ± 0.02	8,2
0355+1133	110.8 ± 4.6	-4.105 ± 0.036	-4.1 ± 0.08	7,7
...	109.6 ± 1.3	-4.095 ± 0.011	-4.23 ± 0.11	15,15
0415–0935	174.34 ± 2.79	-5.738 ± 0.015	-5.73 ± 0.05	2,2
...	174.34 ± 2.76	-5.738 ± 0.015	-5.67 ± 0.02	16,16
0415–0935	174.34 ± 2.76	-5.738 ± 0.015	-5.58 ± 0.1	6,6
0423–0414	65.93 ± 1.7	-4.184 ± 0.023	-4.14 ± 0.04	6,2
...	65.93 ± 1.7	-4.184 ± 0.023	-4.22 ± 0.06	6,6
0428–2253	38.48 ± 1.85	-3.429 ± 0.043	-3.441 ± 0.042	4,4
0435–1606	95.35 ± 1.06	-3.037 ± 0.010	-3.033 ± 0.012	4,4
0451–3402	47.46 ± 1.51	-3.659 ± 0.028	-3.676 ± 0.029	4,4
0500+0330	73.85 ± 1.98	-4.007 ± 0.024	-4.01 ± 0.024	4,4
0501–0010	51 ± 3.7	-3.969 ± 0.063	-4.0 ± 0.12	7,7
0523–1403	80.95 ± 1.76	-3.862 ± 0.019	-3.898 ± 0.021	4,4
0559–1404	95.53 ± 1.44	-4.579 ± 0.013	-4.45 ± 0.06	6,6
...	97.7 ± 1.3	-4.599 ± 0.012	-4.56 ± 0.03	8,5
0559–1404	96.73 ± 0.96	-4.590 ± 0.009	-4.53 ± 0.05	17,18,2
0610–2152B	173.17 ± 1.1	-5.208 ± 0.007	-5.21 ± 0.02	1,2
0652–2534	63.76 ± 0.94	-3.586 ± 0.014	-3.6 ± 0.015	4,4
0707–4900	60.93 ± 3.02	-3.767 ± 0.043	-3.625 ± 0.039	1,4
0722–0540	242.8 ± 2.4	-6.020 ± 0.015	-6.11 ± 0.06	19,19
0727+1710	110.14 ± 2.34	-5.355 ± 0.019	-5.26 ± 0.1	6,6
...	110.14 ± 2.34	-5.355 ± 0.019	-5.35 ± 0.05	6,2
0746+2000	81.9 ± 0.3	-3.391 ± 0.003	-3.41 ± 0.02	8,2
...	81.9 ± 0.3	-3.391 ± 0.003	-3.43 ± 0.01	8,5
0746+2000	81.84 ± 0.3	-3.390 ± 0.003	-3.413 ± 0.009	8,4
0751–2530	59.15 ± 0.84	-3.726 ± 0.013	-3.732 ± 0.013	4,4
0825+2115	94.22 ± 0.88	-4.535 ± 0.008	-4.54 ± 0.02	17,18,2
...	95.64 ± 1.84	-4.548 ± 0.017	-4.55 ± 0.06	6,6
0825+2115	93.8 ± 1	-4.531 ± 0.009	-4.58 ± 0.02	8,5
0829+2646	275.8 ± 3	-3.084 ± 0.009	-3.107 ± 0.022	1,4
0830+4828	76.42 ± 3.43	-4.634 ± 0.040	-4.58 ± 0.05	6,2
...	76.42 ± 3.43	-4.634 ± 0.040	-4.62 ± 0.07	6,6
0847–1532	58.96 ± 0.99	-3.781 ± 0.015	-3.798 ± 0.017	4,4
0853–0329	117.3 ± 1.5	-3.496 ± 0.011	-3.49 ± 0.02	1,2
...	117.98 ± 0.76	-3.501 ± 0.006	-3.516 ± 0.01	4,4
0937+2931	162.84 ± 3.88	-5.298 ± 0.021	-5.28 ± 0.05	6,2
...	162.84 ± 3.88	-5.298 ± 0.021	-5.57 ± 0.08	6,6
0939–2448	187.3 ± 4.6	-5.721 ± 0.022	-5.69 ± 0.03	20,20
1004+5022	41 ± 4.1	-3.749 ± 0.087	-3.73 ± 0.14	7,7
1021–0304	40.78 ± 11	-4.628 ± 0.234	-4.48 ± 0.25	6,6
...	35.35 ± 4.24	-4.504 ± 0.104	-4.4 ± 0.11	18,21,2
1022+5825	46.3 ± 1.3	-3.547 ± 0.027	-3.66 ± 0.08	7,7
1047+2124	94.73 ± 3.81	-5.304 ± 0.035	-5.36 ± 0.08	6,6
...	98.75 ± 3.3	-5.340 ± 0.029	-5.35 ± 0.06	18,21,2
1049–3519A	495 ± 4.6	-4.478 ± 0.009	-4.67 ± 0.04	22,22
1049–3519B	495 ± 4.6	-4.575 ± 0.009	-4.71 ± 0.01	22,22

Table 8
Comparison of L_{bol} Values with the Literature

1056+0700	419.1 ± 2.1	-3.034 ± 0.004	-2.98 ± 0.01	1,5
...	419.1 ± 2.1	-3.034 ± 0.004	-3.036 ± 0.044	1,4
1056+0700	419.1 ± 2.1	-3.034 ± 0.004	-2.97 ± 0.02	1,2
1058-1548	57.7 ± 1	-3.989 ± 0.015	-3.997 ± 0.019	8,4
...	57.7 ± 1	-3.989 ± 0.015	-4.0 ± 0.03	8,2
1207-3932A	18.8 ± 2.3	-2.592 ± 0.107	-2.68 ± 0.12	23,23
1207-3932B	18.8 ± 2.3	-4.752 ± 0.126	-4.72 ± 0.14	23,23
1217-0311	93.2 ± 2.06	-5.316 ± 0.020	-5.32 ± 0.05	18,21,2
...	110.36 ± 5.88	-5.462 ± 0.047	-5.3 ± 0.09	6,6
1225-2739	74.2 ± 3.47	-4.859 ± 0.041	-4.88 ± 0.11	6,6
...	74.79 ± 2.03	-4.866 ± 0.024	-4.85 ± 0.05	18,21,2
1228-1547	49.4 ± 1.9	-3.906 ± 0.035	-3.9 ± 0.04	8,2
1237+6526	96.07 ± 4.78	-5.362 ± 0.043	-5.39 ± 0.11	6,6
1245-4429	12.66 ± 2.07	-2.907 ± 0.150	-3.02 ± 0.21	24,24
1254-0122	73.96 ± 1.59	-4.575 ± 0.019	-4.54 ± 0.04	18,21,2
...	84.9 ± 1.9	-4.695 ± 0.020	-4.68 ± 0.04	8,5
1254-0122	75.71 ± 2.88	-4.595 ± 0.033	-4.58 ± 0.08	6,6
1300+1221	85.54 ± 1.53	-5.542 ± 0.020	-5.59 ± 0.03	25,25
1305-2541	52 ± 1.54	-3.587 ± 0.026	-3.616 ± 0.033	8,4
...	53.6 ± 2	-3.613 ± 0.032	-3.66 ± 0.03	8,5
1305-2541	53.6 ± 2	-3.613 ± 0.032	-3.59 ± 0.04	8,2
1326-0038	49.98 ± 6.33	-4.485 ± 0.111	-4.44 ± 0.13	6,6
...	49.98 ± 6.33	-4.485 ± 0.111	-4.48 ± 0.11	6,2
1346-0031	72.74 ± 5.02	-5.110 ± 0.060	-5.02 ± 0.12	6,6
...	69.07 ± 2.09	-5.065 ± 0.027	-5.0 ± 0.06	18,21,2
1424+0917	31.7 ± 2.5	-4.050 ± 0.070	-4.06 ± 0.07	1,2
1425-3650	86.45 ± 0.83	-4.035 ± 0.010	-4.029 ± 0.009	4,4
1428+3310	92.4 ± 1.3	-3.559 ± 0.012	-3.62 ± 0.02	1,5
1439+1929	69.6 ± 0.5	-3.690 ± 0.006	-3.703 ± 0.01	8,4
...	69.6 ± 0.5	-3.690 ± 0.006	-3.72 ± 0.01	8,5
1439+1929	69.6 ± 0.5	-3.690 ± 0.006	-3.66 ± 0.02	8,2
1440+1339	45 ± 1.11	-3.168 ± 0.022	-3.163 ± 0.022	4,4
1456-2809	152.49 ± 2.02	-3.287 ± 0.012	-3.266 ± 0.013	1,4
1457-2121	170.16 ± 1.45	-5.548 ± 0.008	-5.53 ± 0.05	1,26
1501+2250	94.4 ± 0.6	-3.575 ± 0.006	-3.602 ± 0.009	8,4
1507-1627	136.4 ± 0.6	-4.207 ± 0.004	-4.16 ± 0.01	8,5
1523+3014	54.37 ± 1.14	-4.574 ± 0.019	-4.58 ± 0.04	27,18,2
...	57.3 ± 3.27	-4.620 ± 0.050	-4.62 ± 0.08	6,6
1539-0520	61.25 ± 1.26	-4.007 ± 0.018	-4.006 ± 0.019	4,4
1552+2948	47.7 ± 0.9	-3.546 ± 0.018	-3.63 ± 0.07	7,7
1555-0956	74.53 ± 1.21	-3.708 ± 0.014	-3.712 ± 0.015	4,4
1624+0029	90.73 ± 1.03	-5.193 ± 0.010	-5.16 ± 0.05	17,18,21,2
...	86.85 ± 3.85	-5.155 ± 0.039	-5.11 ± 0.08	6,6
1632+1904	65.02 ± 1.77	-4.616 ± 0.024	-4.59 ± 0.03	8,2
...	63.58 ± 3.32	-4.597 ± 0.045	-4.6 ± 0.06	6,6
1655-0823	154.96 ± 0.52	-3.199 ± 0.004	-3.214 ± 0.007	28,4
...	154.5 ± 0.7	-3.196 ± 0.005	-3.21 ± 0.01	29,5
1726+1538	28.6 ± 2.9	-3.845 ± 0.088	-3.77 ± 0.15	7,7
1728+3948	41.49 ± 3.26	-4.233 ± 0.069	-4.52 ± 0.09	6,6
1750+1759	36.24 ± 4.53	-4.690 ± 0.109	-4.64 ± 0.11	6,2
...	36.24 ± 4.53	-4.690 ± 0.109	-4.44 ± 0.15	6,6
1841+3117	23.57 ± 1.89	-3.886 ± 0.072	-3.88 ± 0.09	6,6
2101+1756	30.14 ± 3.42	-4.341 ± 0.100	-4.62 ± 0.12	6,6
2104-1037	53 ± 1.71	-3.810 ± 0.028	-3.812 ± 0.03	4,4
2114-2251	40.7 ± 2.4	-4.396 ± 0.056	-4.42 ± 0.06	15,15
2144+1446	54.35 ± 0.89	-4.792 ± 0.019	-4.77 ± 0.03	9,9
2148+4003	124.07 ± 0.55	-4.394 ± 0.004	-4.33 ± 0.02	10,10
2208+2921	21.2 ± 0.7	-3.703 ± 0.030	-3.71 ± 0.1	7,7
2224-0158	88.1 ± 0.1	-4.183 ± 0.003	-4.2 ± 0.01	8,5
...	86.7 ± 0.69	-4.169 ± 0.007	-4.185 ± 0.013	8,4
2224-0158	85.01 ± 1.5	-4.152 ± 0.016	-4.14 ± 0.06	6,6
2356-1553	68.97 ± 3.42	-5.058 ± 0.043	-5.0 ± 0.06	6,2

References. — (1) van Altena et al. (1995); (2) Goliowski et al. (2004); (3) Tinney et al. (1995); (4) Dieterich et al. (2014); (5) Cushing et al. (2005b); (6) Vrba et al. (2004); (7) Zapatero Osorio et al. (2014); (8) Dahn et al. (2002); (9) Luhman et al. (2007); (10) Gizis et al. (2015); (11) Naud et al. (2014); (12) Tinney (1996); (13) Henry et al. (2006); (14) Gatewood & Coban (2009); (15) Liu et al. (2013); (16) Saumon et al. (2007); (17) Dahn et al. (2002); (18) Vrba et al. (2004); (19) Leggett et al. (2012); (20) Burgasser et al. (2008c); (21) Tinney et al. (2003); (22) Faherty et al. (2014); (23) Mamajek (2005); (24) Manjavacas et al. (2014); (25) Burningham et al. (2011); (26) Geballe et al. (2001); (27) van Altena et al. (1995); (28) van Leeuwen (2007); (29) Monet et al. (1992).

Table 9
Fundamental Parameters of the Sample

Designation	π (mas)	π Ref	$\log(L_*/L_\odot)$	Age ^a (Gyr)	Radius (R_{Jup})	$\log(g)$ (dex)	T_{eff} (K)	Mass (M_{Jup})
0000+2554	70.8 ± 1.9	1	-4.68 ± 0.02	0.500–10.00	0.99 ± 0.15	5.02 ± 0.47	1227 ± 95	47.56 ± 26.76
0003–2822	25.7 ± 0.93	2	-2.95 ± 0.03	0.500–10.00	1.32 ± 0.05	5.18 ± 0.05	2871 ± 76	106.97 ± 9.15
0004–4044BC	77.02 ± 2.07	3	-3.78 ± 0.02	0.500–10.00
0004–6410	17 ± 1 ^b	4	-3.49 ± 0.06	0.010–0.040	1.63 ± 0.06	4.25 ± 0.18	1896 ± 77	19.18 ± 6.41
0024–0158	86.6 ± 4	5	-3.44 ± 0.04	0.500–10.00	1.09 ± 0.05	5.22 ± 0.10	2390 ± 80	79.27 ± 11.13
0025+4759	22.8 ± 0.9	2	-3.33 ± 0.04	0.500–10.00
0027+0503	13.8 ± 1.6	6	-3.55 ± 0.10	0.010–0.150	1.44 ± 0.23	4.48 ± 0.43	1945 ± 195	31.35 ± 19.44
0027+2219	69.6 ± 0.9	1	-2.83 ± 0.01	0.500–10.00
0030–1450	37.42 ± 4.5	7	-4.37 ± 0.11	0.500–10.00	0.98 ± 0.10	5.10 ± 0.31	1466 ± 117	53.55 ± 21.14
0033–1521	24.8 ± 2.5	8	-3.61 ± 0.09	0.010–0.150	1.43 ± 0.22	4.47 ± 0.42	1887 ± 175	29.05 ± 18.53
0034+0523	105.4 ± 7.5	9	-5.27 ± 0.06	0.500–10.00	0.94 ± 0.16	4.97 ± 0.49	899 ± 82	42.13 ± 26.46
0036+1821	114.2 ± 0.8	6	-3.93 ± 0.01	0.500–10.00	1.01 ± 0.07	5.21 ± 0.17	1869 ± 64	66.07 ± 12.98
0039+2115	90.42 ± 0.32	1	-5.56 ± 0.01	4.000–10.00	0.86 ± 0.07	5.16 ± 0.24	793 ± 35	46.96 ± 14.34
0045+1634	57.3 ± 2	8	-3.41 ± 0.03	0.030–0.050	1.62 ± 0.06	4.35 ± 0.22	1987 ± 53	22.71 ± 7.95
0047+6803	82 ± 3	10	-4.44 ± 0.03	0.050–0.120	1.30 ± 0.04	4.24 ± 0.13	1227 ± 30	12.13 ± 2.97
0050–3322	94.6 ± 2.4	11	-5.39 ± 0.02	0.500–10.00	0.94 ± 0.16	4.95 ± 0.49	836 ± 71	40.34 ± 25.54
0058–0651	33.8 ± 4	12	-3.63 ± 0.10	0.010–0.150	1.43 ± 0.22	4.46 ± 0.43	1864 ± 182	29.23 ± 18.09
0102–3737	81.95 ± 2.73	13	-3.20 ± 0.03	0.500–10.00	1.17 ± 0.04	5.22 ± 0.07	2636 ± 67	90.28 ± 9.22
0103+1935	46.9 ± 7.6	9	-4.41 ± 0.14	0.010–0.150	1.34 ± 0.13	4.18 ± 0.45	1231 ± 117	15.07 ± 10.69
0107+0041	64.13 ± 4.51	7	-4.47 ± 0.06	0.500–10.00	0.98 ± 0.11	5.11 ± 0.37	1385 ± 89	52.41 ± 23.34
0112+1703	20.83 ± 2.17 ^b	14	-4.87 ± 0.10	0.050–0.120	1.24 ± 0.04	4.17 ± 0.17	981 ± 57	9.84 ± 2.99
0117–3403	20 ± 3 ^b	4	-3.48 ± 0.13	0.010–0.040	1.62 ± 0.11	4.26 ± 0.20	1917 ± 159	19.85 ± 7.54
0141–4633	25 ± 3 ^b	4	-3.48 ± 0.10	0.010–0.040	1.61 ± 0.10	4.25 ± 0.19	1917 ± 130	19.57 ± 7.04
0151+1244	46.73 ± 3.37	7	-4.74 ± 0.06	0.500–10.00	0.97 ± 0.16	5.02 ± 0.48	1196 ± 108	47.11 ± 27.12
0207+0000	29.3 ± 4	15	-4.73 ± 0.12	0.500–10.00	0.97 ± 0.17	5.02 ± 0.48	1201 ± 132	47.08 ± 27.48
0210–3015	32 ± 8 ^b	4	-3.84 ± 0.22	0.010–0.040	1.53 ± 0.09	4.16 ± 0.22	1598 ± 205	14.59 ± 7.03
0234–6442	21 ± 5 ^b	4	-3.54 ± 0.21	0.010–0.040	1.62 ± 0.11	4.25 ± 0.22	1850 ± 231	19.56 ± 8.49
0241–0326	21.4 ± 2.6	8	-3.72 ± 0.11	0.010–0.150	1.41 ± 0.21	4.44 ± 0.43	1788 ± 171	27.35 ± 17.05
0243–2453	93.6 ± 3.63	7	-5.13 ± 0.03	0.500–10.00	0.94 ± 0.16	4.99 ± 0.47	972 ± 83	43.59 ± 26.41
0248–1651	61.6 ± 5.4	16	-3.46 ± 0.08	0.500–10.00	1.08 ± 0.06	5.22 ± 0.11	2365 ± 125	78.26 ± 12.51
0251+0047	20.5 ± 2.2	17	-3.02 ± 0.09	0.500–10.00	1.28 ± 0.09	5.20 ± 0.06	2811 ± 180	102.13 ± 13.54
0253+1652	268 ± 37	18	-3.15 ± 0.12	0.500–10.00	1.20 ± 0.09	5.22 ± 0.07	2688 ± 212	93.64 ± 14.47
0253+3206	17.7 ± 2.5	4	-2.79 ± 0.12	0.010–0.150	1.90 ± 0.45	4.49 ± 0.52	2628 ± 362	65.10 ± 47.55
0254+0223	166 ± 26	19	-5.88 ± 0.14	0.500–10.00	0.97 ± 0.17	4.75 ± 0.59	621 ± 73	31.22 ± 23.15
0255–4700	201.37 ± 3.89	20	-4.61 ± 0.02	0.500–10.00	0.97 ± 0.12	5.09 ± 0.40	1290 ± 78	49.92 ± 24.80
0318–3421	72.9 ± 7.7	9	-4.54 ± 0.09	0.500–10.00	0.97 ± 0.12	5.05 ± 0.36	1344 ± 107	48.98 ± 24.02
0320+1854	68.9 ± 0.6	6	-3.25 ± 0.01	0.500–10.00	1.15 ± 0.04	5.22 ± 0.07	2586 ± 42	87.60 ± 8.11
0323–4631	17 ± 3 ^b	4	-3.34 ± 0.15	0.010–0.040	1.66 ± 0.15	4.29 ± 0.24	2039 ± 203	23.11 ± 9.97
0325+0425	55.55 ± 10.93	9	-5.04 ± 0.17	0.500–10.00	0.95 ± 0.17	5.00 ± 0.50	1015 ± 134	44.61 ± 27.91
0326–2102	41 ± 1 ^b	4	-4.23 ± 0.03	0.050–0.120	1.30 ± 0.07	4.39 ± 0.21	1381 ± 42	18.40 ± 6.46
0328+2302	33.13 ± 4.2	7	-4.37 ± 0.11	0.500–10.00	0.98 ± 0.10	5.13 ± 0.35	1466 ± 121	54.42 ± 22.25
0334–4953	120.6 ± 3.6	9	-3.64 ± 0.03	0.500–10.00	1.04 ± 0.06	5.22 ± 0.13	2173 ± 71	72.89 ± 11.87
0339–3525	155.89 ± 1.03	3	-3.56 ± 0.01	0.010–0.150	1.43 ± 0.21	4.48 ± 0.41	1942 ± 144	29.53 ± 16.87
0345+2540	37.1 ± 0.5	6	-3.60 ± 0.01	0.500–10.00	1.05 ± 0.05	5.22 ± 0.12	2213 ± 60	74.14 ± 11.27
0351–0052	68.1 ± 1.9	21	-3.02 ± 0.02	0.500–10.00	1.27 ± 0.04	5.19 ± 0.05	2810 ± 60	101.58 ± 8.57
0355+1133	110.8 ± 4.3	8	-4.10 ± 0.03	0.050–0.120	1.32 ± 0.09	4.45 ± 0.21	1478 ± 57	19.98 ± 7.76
0357–4417	18 ± 5 ^b	4	-3.09 ± 0.24	0.010–0.040
0415–0935	175.2 ± 1.7	11	-5.74 ± 0.01	0.500–10.00	0.95 ± 0.16	4.83 ± 0.51	677 ± 56	32.99 ± 21.87
0423–0414	65.9 ± 1.7	18	-4.18 ± 0.02	0.500–10.00
0428–2253	38.48 ± 1.85	3	-3.43 ± 0.04	0.500–10.00	1.09 ± 0.05	5.22 ± 0.10	2400 ± 83	79.61 ± 11.15
0435–1606	95.35 ± 1.06	3	-3.04 ± 0.01	0.500–10.00	1.26 ± 0.03	5.19 ± 0.05	2795 ± 39	100.44 ± 7.63
0436–4114	23 ± 6 ^b	4	-2.88 ± 0.23	0.010–0.040	1.97 ± 0.39	4.30 ± 0.33	2445 ± 403	39.00 ± 23.17
0439–2353	110.4 ± 4	9	-4.61 ± 0.03	0.500–10.00	0.97 ± 0.12	5.04 ± 0.37	1290 ± 82	48.01 ± 23.41
0443+0002	40 ± 4 ^b	4	-3.13 ± 0.09	0.012–0.022	1.78 ± 0.12	4.19 ± 0.13	2230 ± 134	21.99 ± 5.76
0445–3048	78.5 ± 4.9	9	-3.99 ± 0.05	0.500–10.00	1.00 ± 0.08	5.19 ± 0.20	1809 ± 90	63.80 ± 15.00
0451–3402	47.46 ± 1.51	3	-3.66 ± 0.03	0.500–10.00	1.04 ± 0.06	5.22 ± 0.13	2155 ± 72	72.38 ± 12.00
0500+0330	73.85 ± 1.98	3	-4.01 ± 0.02	0.500–10.00	1.00 ± 0.08	5.20 ± 0.19	1793 ± 72	63.68 ± 14.44
0501–0010	51 ± 3.7	8	-3.97 ± 0.06	0.010–0.150	1.38 ± 0.18	4.36 ± 0.41	1560 ± 118	21.44 ± 13.70
0516–0445	44.5 ± 6.5	9	-4.72 ± 0.13	0.500–10.00	0.97 ± 0.17	5.02 ± 0.48	1211 ± 137	47.18 ± 27.53
0523–1403	80.95 ± 1.76	3	-3.86 ± 0.02	0.500–10.00	1.01 ± 0.07	5.21 ± 0.16	1939 ± 68	67.54 ± 12.79
0539–0058	76.12 ± 2.17	7	-4.15 ± 0.02	0.500–10.00	0.99 ± 0.08	5.18 ± 0.22	1659 ± 74	60.74 ± 15.43
0559–1404	96.6 ± 1	1	-4.59 ± 0.01	0.500–10.00	0.97 ± 0.11	5.09 ± 0.39	1301 ± 75	50.44 ± 24.33
0602+3910	88.5 ± 1.6	4	-3.65 ± 0.02	0.010–0.150	1.41 ± 0.20	4.46 ± 0.41	1854 ± 134	27.61 ± 15.84
0608–2753	32 ± 3.6	9	-3.34 ± 0.10	0.010–0.150	1.51 ± 0.27	4.51 ± 0.46	2145 ± 228	37.80 ± 24.23
0610–2152B	173.81 ± 0.99	2	-5.21 ± 0.01	0.500–10.00	0.94 ± 0.15	4.98 ± 0.48	927 ± 77	42.64 ± 25.95
0611–0410AB	47.25 ± 3.22	22	-4.38 ± 0.06	0.500–10.00
0619–5803b	21.71 ± 0.69	2	-3.75 ± 0.05	0.010–0.040	1.55 ± 0.05	4.19 ± 0.17	1674 ± 53	15.31 ± 4.70
0624–4521	83.9 ± 4.5	9	-4.33 ± 0.05	0.500–10.00	0.99 ± 0.10	5.14 ± 0.27	1501 ± 85	56.04 ± 18.52
0641–4322	55.7 ± 5.7	23	-3.87 ± 0.09	0.500–10.00	1.01 ± 0.07	5.20 ± 0.18	1927 ± 120	66.67 ± 14.68
0652–2534	63.76 ± 0.94	3	-3.59 ± 0.01	0.500–10.00	1.05 ± 0.05	5.22 ± 0.12	2231 ± 60	74.67 ± 11.18
0700+3157	82 ± 2	24	-3.79 ± 0.02	0.500–10.00
0707–4900	54.1 ± 4.5	16	-3.66 ± 0.07	0.500–10.00	1.03 ± 0.07	5.22 ± 0.14	2151 ± 114	72.07 ± 13.30
0722–0540	242.8 ± 2.4	25	-6.02 ± 0.02	0.500–10.00	0.98 ± 0.16	4.68 ± 0.53	569 ± 45	26.11 ± 18.14

Table 9
Fundamental Parameters of the Sample

0727+1710	112.5 ± 0.9	1	-5.37 ± 0.01	0.500–10.00	0.94 ± 0.16	4.95 ± 0.49	845 ± 71	40.55 ± 25.40
0729–3954	126.3 ± 8.3	9	-5.57 ± 0.06	0.500–10.00	0.94 ± 0.16	4.89 ± 0.52	752 ± 69	37.44 ± 24.97
0742+2055	66.5 ± 8.6	9	-5.15 ± 0.11	0.500–10.00	0.94 ± 0.16	4.98 ± 0.49	958 ± 102	43.43 ± 27.17
0746+2000	81.84 ± 0.3	3	-3.39 ± 0.00	0.500–10.00
0751–2530	59.15 ± 0.84	3	-3.73 ± 0.01	0.500–10.00	1.03 ± 0.06	5.22 ± 0.14	2083 ± 64	70.69 ± 12.01
0752+1612	54.37 ± 1	26	-2.67 ± 0.02	0.010–0.150	2.01 ± 0.35	4.48 ± 0.51	2731 ± 242	67.67 ± 46.32
0817–6155	203 ± 13	27	-5.07 ± 0.06	0.500–10.00	0.94 ± 0.16	5.00 ± 0.48	1004 ± 91	44.20 ± 26.71
0825+2115	93.8 ± 1	6	-4.53 ± 0.01	0.500–10.00	0.98 ± 0.11	5.11 ± 0.37	1341 ± 73	51.98 ± 23.13
0829+2646	275.8 ± 3	17	-3.08 ± 0.01	0.500–10.00	1.23 ± 0.03	5.20 ± 0.05	2752 ± 39	97.35 ± 7.72
0830+0128	43.1 ± 6.1	9	-4.83 ± 0.12	0.500–10.00	0.96 ± 0.17	5.02 ± 0.48	1138 ± 129	46.42 ± 27.59
0830+0947	59.81 ± 4.52	20	-3.24 ± 0.07	0.500–10.00	1.15 ± 0.06	5.22 ± 0.08	2599 ± 119	88.22 ± 11.28
0830+4828	76.42 ± 3.43	7	-4.63 ± 0.04	0.500–10.00	0.99 ± 0.15	5.02 ± 0.47	1258 ± 97	48.00 ± 26.69
0835–0819	117.3 ± 11.2	23	-4.05 ± 0.08	0.500–10.00	1.00 ± 0.08	5.19 ± 0.21	1754 ± 112	62.47 ± 15.86
0847–1532	76.5 ± 3.5	9	-4.01 ± 0.04	0.500–10.00	1.00 ± 0.08	5.19 ± 0.20	1794 ± 81	63.55 ± 14.79
0853–0329	117.98 ± 0.76	3	-3.50 ± 0.01	0.500–10.00	1.07 ± 0.05	5.22 ± 0.11	2320 ± 52	77.36 ± 10.41
0859–1949	65.4 ± 6.1	9	-4.49 ± 0.08	0.500–10.00	0.98 ± 0.11	5.06 ± 0.35	1374 ± 100	50.29 ± 23.10
0912+1459	48.8 ± 0.92	18	-4.32 ± 0.02	0.600–3.400
0920+3517	34.4 ± 0.8	1	-4.08 ± 0.02	0.500–10.00
0937+2931	163.39 ± 1.76	28	-5.30 ± 0.01	0.500–10.00	0.94 ± 0.16	4.97 ± 0.48	881 ± 74	41.56 ± 25.72
0939–2448	187.3 ± 4.6	29	-5.72 ± 0.02	0.500–10.00	0.95 ± 0.16	4.84 ± 0.52	686 ± 58	33.67 ± 22.45
0949–1545	55.3 ± 6.6	9	-4.86 ± 0.10	0.500–10.00	0.96 ± 0.17	5.01 ± 0.49	1125 ± 119	46.29 ± 27.48
1004+5022	41 ± 4.1	8	-3.75 ± 0.09	0.025–0.300	1.36 ± 0.23	4.54 ± 0.46	1789 ± 176	32.41 ± 20.79
1007–4555	71 ± 5.2	9	-5.04 ± 0.06	0.500–10.00	0.94 ± 0.16	5.01 ± 0.48	1017 ± 94	44.44 ± 26.77
1010–0406	59.8 ± 8.1	9	-4.44 ± 0.12	0.500–10.00	0.98 ± 0.11	5.07 ± 0.34	1416 ± 123	51.16 ± 23.06
1017+1308	30.2 ± 1.4	11	-3.44 ± 0.04	0.500–10.00
1021–0304	34.4 ± 4.6	30	-4.48 ± 0.12	0.500–10.00
1022+4114	25.36 ± 0.31	2	-3.63 ± 0.02	0.500–10.00	1.04 ± 0.06	5.22 ± 0.13	2183 ± 65	73.21 ± 11.58
1022+5825	54.3 ± 2.5	4	-3.69 ± 0.04	0.010–0.150	1.41 ± 0.20	4.45 ± 0.41	1820 ± 138	27.20 ± 15.97
1036–3441	61.5 ± 9.1	9	-4.51 ± 0.13	0.500–10.00	0.97 ± 0.12	5.04 ± 0.37	1368 ± 131	49.24 ± 24.45
1047+2124	94.7 ± 3.81	7	-5.30 ± 0.04	0.500–10.00	0.94 ± 0.16	4.96 ± 0.49	880 ± 76	41.61 ± 26.03
1048–3956	248.08 ± 0.61	31	-3.51 ± 0.00	0.500–10.00	1.07 ± 0.05	5.22 ± 0.11	2307 ± 51	77.00 ± 10.37
1049–3519A	514 ± 26	32	-4.51 ± 0.04	0.500–3.000	1.01 ± 0.07	4.99 ± 0.26	1334 ± 58	43.10 ± 14.99
1049–3519B	514 ± 26	32	-4.61 ± 0.04	0.500–3.000	1.02 ± 0.07	4.95 ± 0.27	1261 ± 55	39.84 ± 15.58
1056+0700	419.1 ± 2.1	17	-3.03 ± 0.00	0.500–10.00	1.56 ± 0.10	5.19 ± 0.05	2517 ± 81	100.70 ± 7.22
1058–1548	57.7 ± 1	6	-3.99 ± 0.02	0.500–10.00	1.00 ± 0.07	5.20 ± 0.19	1809 ± 68	64.24 ± 14.01
1102–3430	18.1 ± 0.5	33	-2.56 ± 0.02	0.008–0.020	2.39 ± 0.14	4.14 ± 0.15	2670 ± 86	35.91 ± 10.71
1110+0116	52.1 ± 1.2	1	-4.97 ± 0.02	0.050–0.120	1.24 ± 0.04	4.15 ± 0.16	926 ± 18	8.98 ± 2.29
1112+3548	46.04 ± 0.9	9	-3.88 ± 0.02	0.080–0.300
1114–2618	179.2 ± 1.4	1	-5.76 ± 0.01	0.500–10.00	0.96 ± 0.16	4.82 ± 0.51	669 ± 55	32.53 ± 21.58
1139–3159	23.82 ± 2.58	34	-2.71 ± 0.09	0.008–0.020	2.20 ± 0.22	4.13 ± 0.16	2552 ± 188	30.05 ± 11.29
1146+2230	36.8 ± 0.8	6	-3.56 ± 0.02	0.500–10.00
1154–3400	25.3 ± 1.7	4	-3.34 ± 0.06	0.010–0.150	1.50 ± 0.26	4.51 ± 0.45	2155 ± 200	36.86 ± 23.01
1155–3727	104.4 ± 4.7	9	-4.01 ± 0.04	0.500–10.00	1.00 ± 0.08	5.19 ± 0.20	1793 ± 80	63.54 ± 14.78
1207–3900	15 ± 3 ^b	4	-3.39 ± 0.18	0.008–0.020	1.71 ± 0.09	4.16 ± 0.10	1961 ± 204	17.28 ± 4.59
1207–3932	19.1 ± 0.4	35	-2.60 ± 0.02	0.008–0.020
1207–3932A	19.1 ± 0.4	35	-2.61 ± 0.02	0.008–0.020	2.33 ± 0.14	4.14 ± 0.15	2637 ± 85	33.43 ± 10.11
1207–3932B	19.1 ± 0.4	35	-4.77 ± 0.07	0.008–0.020	1.36 ± 0.02	3.75 ± 0.10	994 ± 41	4.81 ± 1.38
1217–0311	90.8 ± 2.2	30	-5.29 ± 0.02	0.500–10.00	0.94 ± 0.16	4.97 ± 0.49	885 ± 75	41.70 ± 25.90
1225–2739	75.1 ± 2.5	18	-4.87 ± 0.03	0.500–10.00
1228–1547	49.4 ± 1.9	6	-3.91 ± 0.03	0.500–10.00
1237+6526	96.07 ± 4.78	7	-5.36 ± 0.04	0.500–10.00	0.94 ± 0.16	4.95 ± 0.50	851 ± 74	40.85 ± 25.96
1239+5515	42.4 ± 2.1	1	-3.84 ± 0.04	0.500–10.00
1245–4429	12.66 ± 2.07	34	-2.91 ± 0.15	0.008–0.020	2.00 ± 0.23	4.13 ± 0.15	2391 ± 249	25.41 ± 9.17
1254–0122	84.9 ± 1.9	6	-4.69 ± 0.02	0.500–10.00	0.98 ± 0.15	5.02 ± 0.47	1219 ± 94	47.44 ± 26.78
1300+1221	85.54 ± 1.53	9	-5.54 ± 0.02	0.010–10.00	1.06 ± 0.28	4.44 ± 0.97	721 ± 94	32.10 ± 30.00
1305–2541	52 ± 1.54	3	-3.59 ± 0.03	0.500–10.00
1320+0409	32.3 ± 0.86	2	-3.89 ± 0.03	0.500–10.00	1.01 ± 0.07	5.21 ± 0.17	1913 ± 71	66.94 ± 13.12
1326–0038	49.98 ± 6.33	7	-4.49 ± 0.11	0.500–10.00	0.97 ± 0.11	5.10 ± 0.39	1381 ± 119	51.09 ± 24.90
1346–0031	68.3 ± 2.3	30	-5.06 ± 0.03	0.500–10.00	0.94 ± 0.16	5.01 ± 0.48	1011 ± 86	44.29 ± 26.44
1359–4034	64.2 ± 5.5	9	-4.00 ± 0.07	0.500–10.00	1.00 ± 0.08	5.19 ± 0.20	1799 ± 106	63.44 ± 15.48
1411–2119	26.3 ± 2.9	4	-2.71 ± 0.10	0.010–0.150	1.98 ± 0.44	4.48 ± 0.51	2694 ± 335	69.62 ± 50.83
1416+1348B	109.7 ± 1.3	9	-5.79 ± 0.01	0.500–10.00	0.96 ± 0.16	4.80 ± 0.52	656 ± 54	31.78 ± 21.23
1416+5006	21.9 ± 0.62	9	-4.22 ± 0.03	0.500–10.00	0.99 ± 0.09	5.17 ± 0.23	1595 ± 78	59.02 ± 16.39
1424+0917	31.7 ± 2.5	17	-4.05 ± 0.07	0.500–10.00	1.00 ± 0.08	5.19 ± 0.21	1755 ± 102	62.58 ± 15.57
1425–3650	86.45 ± 0.83	3	-4.04 ± 0.01	0.050–0.120	1.32 ± 0.09	4.43 ± 0.24	1535 ± 55	20.76 ± 7.90
1428+3310	90.8 ± 1.3	18	-3.54 ± 0.01	0.500–10.00	1.06 ± 0.05	5.22 ± 0.11	2275 ± 58	75.98 ± 10.89
1439+1839	28.4 ± 0.7	9	-3.07 ± 0.02	0.500–10.00	1.24 ± 0.04	5.20 ± 0.05	2769 ± 56	98.49 ± 8.49
1439+1929	69.6 ± 0.5	6	-3.69 ± 0.01	0.500–10.00	1.03 ± 0.06	5.22 ± 0.13	2121 ± 61	71.64 ± 11.60
1440+1339	45 ± 1.11	3	-3.17 ± 0.02	0.500–10.00	1.19 ± 0.04	5.21 ± 0.06	2672 ± 57	92.33 ± 8.75
1448+1031	69 ± 4.6	4	-4.19 ± 0.06	0.500–10.00	0.99 ± 0.09	5.17 ± 0.23	1623 ± 91	59.43 ± 16.66
1456–2809	159.2 ± 5.1	16	-3.32 ± 0.03	0.500–10.00	1.12 ± 0.05	5.22 ± 0.08	2511 ± 65	84.02 ± 9.72
1457–2121	171.22 ± 0.94	2	-5.55 ± 0.01	0.500–10.00	0.94 ± 0.16	4.90 ± 0.50	759 ± 63	37.28 ± 24.05
1501+2250	94.4 ± 0.6	6	-3.57 ± 0.01	0.500–10.00	1.05 ± 0.05	5.22 ± 0.11	2242 ± 55	75.07 ± 10.88
1503+2525	157.2 ± 2.2	1	-5.05 ± 0.01	0.500–10.00	0.94 ± 0.16	5.01 ± 0.48	1016 ± 85	44.34 ± 26.30
1504+1027	46.1 ± 1.5	1	-5.09 ± 0.03	0.500–10.00	0.94 ± 0.16	5.00 ± 0.48	992 ± 85	43.97 ± 26.43
1506+1321	70.92 ± 2.5	36	-3.80 ± 0.03	0.500–10.00	1.02 ± 0.07	5.21 ± 0.15	2004 ± 75	68.77 ± 12.85
1507–1627	136.4 ± 0.6	6	-4.21 ± 0.00	0.500–10.00	0.99 ± 0.09	5.18 ± 0.23	1607 ± 70	59.66 ± 15.62

Table 9
Fundamental Parameters of the Sample

1510–0241	61.2 ± 4.7	5	−3.45 ± 0.07	0.500–10.00	1.08 ± 0.06	5.22 ± 0.11	2377 ± 113	78.67 ± 12.15
1511+0607	36.7 ± 6.4	9	−4.31 ± 0.15	0.500–10.00
1515+4847	95.24 ± 2	36	−4.32 ± 0.02	0.500–10.00	0.99 ± 0.10	5.15 ± 0.26	1505 ± 74	56.83 ± 17.52
1523+3014	55.98 ± 0.78	2	−4.60 ± 0.01	0.500–10.00	0.97 ± 0.11	5.09 ± 0.40	1295 ± 76	50.10 ± 24.63
1526+2043	48.5 ± 8.7	9	−4.31 ± 0.16	0.500–10.00	0.98 ± 0.10	5.10 ± 0.31	1518 ± 157	54.39 ± 21.40
1539–0520	64.5 ± 3.4	23	−4.05 ± 0.05	0.500–10.00	1.00 ± 0.08	5.19 ± 0.20	1753 ± 85	62.64 ± 15.14
1546–3325	88 ± 1.9	30	−5.07 ± 0.02	0.500–10.00	0.94 ± 0.16	5.00 ± 0.48	1002 ± 84	44.13 ± 26.34
1552+2948	47.7 ± 0.9	8	−3.55 ± 0.02	0.010–0.150	1.43 ± 0.22	4.48 ± 0.41	1956 ± 148	30.04 ± 17.36
1555–0956	74.53 ± 1.21	3	−3.71 ± 0.01	0.500–10.00	1.03 ± 0.06	5.22 ± 0.14	2102 ± 64	71.12 ± 11.93
1615+1340	68.6 ± 6.4	9	−5.25 ± 0.08	0.500–10.00	0.94 ± 0.16	4.97 ± 0.49	906 ± 87	42.35 ± 26.73
1624+0029	90.9 ± 1.2	30	−5.19 ± 0.01	0.500–10.00	0.94 ± 0.15	4.98 ± 0.48	936 ± 78	42.84 ± 26.06
1626+3925	29.85 ± 1.08	28	−3.71 ± 0.03	0.500–10.00	1.03 ± 0.06	5.22 ± 0.14	2103 ± 75	71.03 ± 12.37
1632+1904	65.6 ± 2.1	6	−4.62 ± 0.03	0.500–10.00	0.97 ± 0.12	5.08 ± 0.41	1279 ± 81	49.46 ± 25.22
1647+5632	116 ± 29	37	−5.31 ± 0.22	0.500–10.00	0.94 ± 0.16	4.89 ± 0.57	875 ± 132	41.07 ± 28.95
1655–0823	155.4 ± 1.33	18	−3.20 ± 0.01	0.500–10.00	1.17 ± 0.03	5.21 ± 0.06	2639 ± 40	90.47 ± 8.00
1658+7026	53.9 ± 0.7	6	−3.63 ± 0.01	0.500–10.00	1.04 ± 0.06	5.22 ± 0.12	2181 ± 62	73.21 ± 11.41
1726+1538	28.6 ± 2.9	8	−3.85 ± 0.09	0.010–0.150	1.40 ± 0.20	4.40 ± 0.42	1668 ± 144	24.06 ± 15.58
1728+3948	41.5 ± 3.26	18	−4.23 ± 0.07	0.500–10.00
1750+1759	36.24 ± 4.53	7	−4.69 ± 0.11	0.500–10.00	0.97 ± 0.16	5.02 ± 0.48	1228 ± 127	47.37 ± 27.39
1828–4849	83.7 ± 7.7	9	−4.97 ± 0.08	0.500–10.00	0.95 ± 0.16	5.01 ± 0.48	1060 ± 103	45.21 ± 27.07
1835+3259	176.5 ± 0.5	38	−3.50 ± 0.00	0.500–10.00	1.07 ± 0.05	5.22 ± 0.11	2316 ± 51	77.28 ± 10.34
1841+3117	23.57 ± 1.89	7	−3.89 ± 0.07	0.500–10.00	1.01 ± 0.07	5.21 ± 0.18	1914 ± 104	66.52 ± 14.30
1843+4040	70.7 ± 0.8	21	−3.11 ± 0.01	0.500–10.00	1.22 ± 0.03	5.20 ± 0.05	2731 ± 40	95.94 ± 7.87
1916+0508	170.1 ± 0.8	21	−3.31 ± 0.00	0.500–10.00	1.13 ± 0.04	5.22 ± 0.08	2531 ± 42	85.15 ± 8.44
2000–7523	31 ± 1 ^b	4	−2.97 ± 0.03	0.012–0.022	1.88 ± 0.11	4.19 ± 0.14	2375 ± 79	24.75 ± 6.06
2047–0718	49.9 ± 7.9	9	−4.86 ± 0.14	0.500–10.00	0.96 ± 0.17	5.00 ± 0.50	1124 ± 134	46.25 ± 27.71
2057–0252	70.1 ± 3.7	9	−3.76 ± 0.05	0.500–10.00	1.02 ± 0.07	5.22 ± 0.15	2044 ± 87	69.56 ± 13.04
2101+1756	30.14 ± 3.42	7	−4.34 ± 0.10	0.500–10.00
2104–1037	53 ± 1.71	3	−3.81 ± 0.03	0.500–10.00	1.02 ± 0.07	5.21 ± 0.16	1994 ± 73	68.59 ± 12.82
2114–2251	40.7 ± 2.4	4	−4.40 ± 0.06	0.012–0.022	1.41 ± 0.03	3.90 ± 0.11	1210 ± 41	7.09 ± 1.98
2126–8140	31.3 ± 2.6	4	−3.85 ± 0.07	0.010–0.150	1.39 ± 0.19	4.40 ± 0.42	1663 ± 135	23.80 ± 15.19
2127–4215	28.9 ± 6.2	16	−3.15 ± 0.19	0.500–10.00	1.21 ± 0.13	5.22 ± 0.08	2676 ± 320	93.91 ± 18.63
2139+0220	101.5 ± 2	39	−4.86 ± 0.02	0.500–10.00	0.96 ± 0.16	5.01 ± 0.49	1123 ± 94	46.29 ± 26.87
2144+1446	55.91 ± 0.45	2	−4.82 ± 0.01	0.100–0.500	1.17 ± 0.05	4.52 ± 0.31	1043 ± 23	20.16 ± 9.42
2148+4003	124.07 ± 0.55	10	−4.39 ± 0.00	0.500–10.00	0.99 ± 0.10	5.13 ± 0.28	1446 ± 72	55.03 ± 18.55
2206–4217	35 ± 0.3 ^b	4	−3.97 ± 0.02	0.050–0.120	1.33 ± 0.10	4.44 ± 0.25	1588 ± 62	21.74 ± 8.52
2208+2921	21.2 ± 0.7	8	−3.70 ± 0.03	0.010–0.150	1.41 ± 0.20	4.44 ± 0.41	1804 ± 132	26.71 ± 15.54
2224–0158	86.2 ± 1.1	1	−4.16 ± 0.01	0.500–10.00	0.99 ± 0.08	5.18 ± 0.22	1646 ± 71	60.57 ± 15.26
2228–4310	94 ± 7	9	−5.28 ± 0.07	0.500–10.00	0.94 ± 0.16	4.97 ± 0.49	891 ± 82	41.97 ± 26.46
2234+4041	37 ± 8	40	−2.94 ± 0.19	0.001–0.010
2237+3922	51.17 ± 1.62	2	−3.64 ± 0.03	0.500–10.00	1.04 ± 0.06	5.22 ± 0.13	2173 ± 72	72.87 ± 11.93
2244+2043	58 ± 0.4 ^b	4	−4.47 ± 0.01	0.050–0.120	1.29 ± 0.03	4.21 ± 0.11	1209 ± 17	11.91 ± 2.79
2306–0502	82.58 ± 2.58	20	−3.28 ± 0.03	0.500–10.00	1.14 ± 0.04	5.22 ± 0.08	2557 ± 64	86.07 ± 9.28
2322–3133	58.6 ± 5.6	9	−3.85 ± 0.08	0.010–0.150	1.39 ± 0.19	4.40 ± 0.42	1665 ± 141	23.93 ± 15.43
2322–6151	22 ± 1 ^b	4	−3.61 ± 0.04	0.010–0.040	1.59 ± 0.05	4.23 ± 0.17	1793 ± 53	17.35 ± 5.44
2351–2537	49 ± 10	4	−3.24 ± 0.18	0.500–10.00	1.16 ± 0.11	5.22 ± 0.09	2590 ± 291	88.31 ± 17.40
2354–3316	44.24 ± 1.78	41	−3.41 ± 0.04	0.500–10.00	1.09 ± 0.05	5.22 ± 0.10	2423 ± 75	80.46 ± 10.73

References. — (1) Dupuy & Liu (2012); (2) van Leeuwen (2007); (3) Dieterich et al. (2014); (4) Faherty et al. in prep; (5) Tinney et al. (1995); (6) Dahn et al. (2002); (7) Vrba et al. (2004); (8) Zapatero Osorio et al. (2014); (9) Faherty et al. (2012); (10) Gizis et al. (2015); (11) Dupuy & Kraus (2013); (12) Marocco et al. (2013); (13) Costa et al. (2005); (14) Naud et al. (2014); (15) Marocco et al. (2010); (16) Tinney (1996); (17) van Altena et al. (1995); (18) Patten et al. (2006); (19) Kirkpatrick et al. (2012); (20) Costa et al. (2006); (21) Monet et al. (1992); (22) Gelino et al. (2014); (23) Andrei et al. (2011); (24) Thorstensen & Kirkpatrick (2003); (25) Leggett et al. (2012); (26) Gatewood & Coban (2009); (27) Artigau et al. (2010); (28) Schilbach et al. (2009); (29) Burgasser et al. (2008c); (30) Tinney et al. (2003); (31) Lurie et al. (2014); (32) Boffin et al. (2013); (33) Teixeira et al. (2008); (34) Weinberger et al. (2012); (35) Ducourant et al. (2008); (36) Cesetti et al. (2013); (37) Kirkpatrick et al. (2011); (38) Reid et al. (2003); (39) Smart et al. (2013); (40) Burgasser (2014); (41) Subasavage et al. (2009).

^a Criteria for age range assumption is described in Section 6

^b Parallax calculated from kinematic distance.

Table 10
Polynomial Relations

P(x) ^a	x ^b	rms ^c	c ₀	c ₁	c ₂	c ₃	c ₄	c ₅	c ₆
M_r FLD	$9.7 < M_H < 15.8$	0.831	-1.209e+01	3.991e+00	-1.269e-01	1.417e-03
M_r YNG	$8.9 < M_H < 16.5$	0.621	-2.487e+01	7.426e+00	-4.107e-01	8.783e-03
M_i FLD	$9.7 < M_H < 18.1$	0.527	6.709e-01	2.447e-01	1.593e-01	-5.333e-03
M_i YNG	$8.9 < M_H < 16.5$	0.419	-2.406e+00	1.127e+00	1.056e-01	-4.964e-03
M_z FLD	$10.3 < M_J < 18.4$	0.334	-3.175e+01	7.899e+00	-4.706e-01	1.085e-02
M_z YNG	$9.6 < M_J < 16.6$	0.314	-3.103e+00	1.277e+00	4.229e-02	-2.371e-03
$M_{[3.6]}$ FLD	$9.2 < M_{W1} < 17.1$	0.164	2.966e+00	3.035e-01	5.349e-02	-1.592e-03
$M_{[3.6]}$ YNG	$8.6 < M_{W1} < 15.7$	0.078	-1.776e+01	5.658e+00	-4.020e-01	1.113e-02
$M_{[4.5]}$ FLD	$9.0 < M_{W2} < 15.6$	0.082	2.924e+00	2.222e-01	6.891e-02	-2.028e-03
$M_{[4.5]}$ YNG	$8.4 < M_{W2} < 13.4$	0.095	-8.286e+00	3.383e+00	-2.274e-01	7.191e-03
$M_{[5.8]}$ FLD	$9.2 < M_{W1} < 16.6$	0.124	-2.113e+01	6.404e+00	-4.482e-01	1.156e-02
$M_{[5.8]}$ YNG	$8.6 < M_{W1} < 14.1$	0.127	-3.504e+01	1.061e+01	-8.595e-01	2.438e-02
$M_{[8]}$ FLD	$9.2 < M_{W1} < 16.6$	0.142	-1.782e+01	5.509e+00	-3.660e-01	8.912e-03
$M_{[8]}$ YNG	$7.7 < M_{W1} < 14.1$	0.240	-5.202e+01	1.511e+01	-1.257e+00	3.590e-02
M_{W1} FLD	$9.0 < M_{[3.6]} < 16.2$	0.179	6.683e+00	-8.159e-01	1.607e-01	-4.335e-03
M_{W1} YNG	$8.4 < M_{[3.6]} < 15.0$	0.079	1.966e+01	-4.326e+00	4.748e-01	-1.361e-02
M_{W2} FLD	$9.0 < M_{[4.5]} < 15.3$	0.085	-2.612e+00	1.664e+00	-5.619e-02	1.578e-03
M_{W2} YNG	$8.4 < M_{[4.5]} < 13.5$	0.094	7.706e+00	-1.172e+00	2.035e-01	-6.329e-03
M_{W3} FLD	$8.9 < M_{[8]} < 13.5$	0.327	-4.795e+01	1.429e+01	-1.203e+00	3.514e-02
M_{W3} YNG	$6.2 < M_{[8]} < 11.8$	0.235	5.845e+00	-1.796e+00	3.927e-01	-1.733e-02
M_u	$17.8 < M_u < 25.6$	1.514	6.510e+01	-8.360e+00	3.930e-01	-5.579e-03
M_g	$16.7 < M_g < 26.7$	0.733	1.442e+02	-1.987e+01	9.532e-01	-1.460e-02
$M_{L'}$	$9.4 < M_{L'} < 15.3$	0.092	1.655e+01	-3.525e+00	4.002e-01	-1.124e-02
M_J	$10.1 < M_{JMKO} < 18.4$	0.114	-5.415e-01	1.054e+00
M_H	$9.6 < M_{HMKO} < 18.8$	0.073	1.167e-01	9.887e-01
M_{Ks}	$9.2 < M_{MKO} < 19.1$	0.300	2.521e-01	9.790e-01
M_J	$6.0 < \text{SpT} < 29.0$	0.402	-8.350e+00	7.157e+00	-1.058e+00	7.771e-02	-2.684e-03	3.478e-05	...
M_{W2}	$6.0 < \text{SpT} < 29.0$	0.398	-5.043e-01	3.032e+00	-3.655e-01	2.283e-02	-6.938e-04	8.190e-06	...
BC_{Ks} FLD	$6.0 < \text{SpT} < 28.0$	0.243	6.815e+00	-1.508e+00	2.204e-01	-1.462e-02	4.549e-04	-5.474e-06	...
BC_{Ks} YNG	$7.0 < \text{SpT} < 28.0$	0.126	-2.174e+00	1.565e+00	-1.759e-01	9.711e-03	-2.633e-04	2.742e-06	...
BC_J FLD	$6.0 < \text{SpT} < 29.0$	0.163	8.842e+00	-2.862e+00	4.566e-01	-3.437e-02	1.200e-03	-1.555e-05	...
BC_J YNG	$7.0 < \text{SpT} < 28.0$	0.189	-7.352e+00	2.899e+00	-3.020e-01	1.165e-02	-1.118e-04	-1.283e-06	...
L_{bol} FLD	$6.0 < \text{SpT} < 29.0$	0.133dex	2.787e+00	-2.310e+00	3.727e-01	-3.207e-02	1.449e-03	-3.220e-05	2.736e-07
T_{eff} FLD	$6.0 < \text{SpT} < 29.0$	113K	4.747e+03	-7.005e+02	1.155e+02	-1.191e+01	6.318e-01	-1.606e-02	1.546e-04
T_{eff} FLD	$9.4 < M_H < 18.1$	29K	-6.108e+04	2.491e+04	-3.690e+03	2.625e+02	-9.131e+00	1.252e-01	...
T_{eff} YNG	$8.6 < M_H < 14.5$	60K	-5.977e+04	2.348e+04	-3.215e+03	1.904e+02	-4.167e+00

^a $P(x) = \sum_{i=0}^n c_i x^i$

^b Polynomials that are a function of spectral type (SpT) accept integers 6-39 corresponding to types M6-T9. Optical spectral types are used for M and L dwarfs and infrared spectral types are used for T dwarfs. All other polynomial ranges are in magnitudes.

^c Units are in magnitudes except where noted.